Inaugural dissertation

for

obtaining the doctoral degree

of the

Combined Faculty of Mathematics, Engineering- and Natural Sciences

of the

Ruprecht - Karls - University

Heidelberg

Presented by

M. Sc. Samantha Lasser

Born in: Freiburg im Breisgau, Germany

Oral Examination: 27.03.2024

MDSC activation mediated by extracellular vesicles-associated microRNA in melanoma

Referees: apl. Prof. Dr. Viktor Umansky

Prof. Dr. Rienk Offringa

SUMMARY

Melanoma progression and immunosuppression in the melanoma microenvironment are significantly fueled by myeloid-derived suppressor cells (MDSCs). MDSC generation in melanoma is mediated by several mediators, including soluble and extracellular vesicles (EV)-associated factors. This study aims to investigate the molecular mechanisms initiated in myeloid cells by melanoma EV-associated microRNA (miR), leading to their conversion to MDSCs, as well as the function of endosomal Toll-like receptors (TLR) in these mechanisms. Using synthetic mimics of miR previously described to be enriched in melanoma EVs, I examined their effects on immature myeloid cells (iMCs) isolated from healthy wild-type mice or TLR-deficient mice. Programmed cell death 1 ligand 1 (PD-L1) was utilized as a marker to identify a MDSC-like phenotype, as it has been shown to be a key immunosuppressive molecule in EV-induced MDSCs. To investigate the involvement of signaling pathways in the regulation of MDSC functions, inhibitors of NF-κB activation or Stat3 activation were utilized. Moreover, I studied the influence of miR mimics on human monocytes isolated from the peripheral blood of healthy donors.

Transfection of iMCs with miR mimics of miR-125a-5p, -125b-5p, or -99b-5p induced the expression of PD-L1 on these cells. A positive correlation was observed between miR-125a-5p levels in the tumor microenvironment (TME) and the tumor progression in the *RET* transgenic mouse model. Furthermore, mimics of miR-125a-5p and the miR cluster 99b/let-7e/125a mediated the upregulation of several MDSC-related factors in iMCs, including IL-6 and reactive oxygen species (ROS). The regulation of PD-L1 expression in iMCs by miR-125a-5p or the miR cluster 99b/let-7e/125a required NF-κB activation, however, it was independent of endosomal TLRs and of STAT3 activation. Similarly, human monocytes did not show clear evidence of STAT3 activation by mimics of miR-125a-5p or the miR cluster 99b/let-7e/125a. Nevertheless, mimics of miR-125a-5p or the miR cluster 99b/let-7e/125a mediated the upregulation of PD-L1 in human monocytes. Additionally, a strong trend of the miR cluster 99b/let-7e/125a to downregulate MHC class II and costimulatory CD86 molecules in human monocytes was observed. Furthermore, human monocytes treated with mimics of the miR cluster 99b/let-7e/125a were able to inhibit proliferation of activated T cells. The finding that miR-125a-5p and the three miRs of the cluster 99b/let-7e/125a showed comparable effects on myeloid cells led to the conclusion that mainly melanoma EV-associated miR-125a-5p could contribute to MDSC generation via NF-κB activation.

ZUSAMMENFASSUNG

Das Fortschreiten des malignen Melanoms und die Immunsuppression in der Tumorumgebung werden in erheblichem Maße durch myeloide Suppressorzellen (MDSCs) unterstützt. Die Bildung von MDSCs beim malignen Melanom wird durch verschiedene Prozesse vermittelt, unter anderem über lösliche und extrazelluläre Vesikel (EV)-assoziierte Faktoren. In dieser Studie sollen die molekularen Mechanismen untersucht werden, die in myeloiden Zellen durch Melanom-EV-assoziierte microRNA (miR) ausgelöst werden und zu ihrer Umwandlung in MDSCs führen, sowie die Beteiligung endosomaler Toll-like-Rezeptoren (TLR) bei jenen Mechanismen. Unter Verwendung synthetischer Mimic-Moleküle von miRs, von denen bekannt ist, dass sie in erhöhter Menge in Melanom-EVs vorhanden sind, wurden die Auswirkungen auf unreife myeloide Zellen (iMCs), die aus gesunden Wildtyp-Mäusen oder TLR-defizienten Mäusen isoliert wurden, nach Transfektion untersucht. Programmed Cell Death 1 Ligand 1 (PD-L1) wurde als Marker zur Identifizierung eines MDSC-ähnlichen Phänotyps verwendet, da es sich als wichtiges immunsuppressives Molekül in EV-induzierten MDSCs erwiesen hat. Um die Beteiligung wichtiger Signalwege an der Regulierung der MDSC-Funktionen zu untersuchen, wurden Inhibitoren der NF-κB-Aktivierung oder der STAT3-Aktivierung eingesetzt. Darüber hinaus wurde die Behandlung humaner Monozyten, die aus mononukleären Zellen des peripheren Blutes gesunder Spender isoliert wurden, mit miR-Mimics mittels Transfektion oder Nanopartikeln untersucht.

Die Transfektion von iMCs mit Mimic-Molekülen von miR-125a-5p, -125b-5p oder -99b-5p induzierte die Expression von PD-L1 in diesen Zellen. Es wurde eine positive Korrelation zwischen miR-125a-5p-Menge in der Tumormikroumgebung und der Tumorprogression im *RET*-transgenen Mausmodell beobachtet. Darüber hinaus vermittelten Mimic-Moleküle von miR-125a-5p und des miR-Clusters 99b/let-7e/125a die Hochregulierung mehrerer MDSC-assoziierter Faktoren in iMCs, einschließlich IL-6 und reaktiver Sauerstoffspezies. Die Regulierung der PD-L1-Expression in iMCs durch miR-125a-5p oder miR-Cluster 99b/let-7e/125a erforderte die Aktivierung von NF-κB, war jedoch unabhängig von endosomalen TLRs sowie von einer STAT3-Aktivierung. Auch humane Monozyten zeigten keinen eindeutigen Nachweis einer Aktivierung von STAT3 durch Mimic-Moleküle von miR-125a-5p oder des miR-Clusters 99b/let-7e/125a. Dennoch vermittelten die Mimic-Moleküle von miR-125a-5p oder des

miR-Clusters 99b/let-7e/125a die Hochregulierung von PD-L1 in humanen Monozyten. Darüber hinaus wurde in humanen Monozyten eine starke Tendenz des miR-Clusters 99b/let-7e/125a zur Herunterregulierung von MHC-Klasse-II-Molekülen und kostimulatorischen CD86-Molekülen beobachtet. Humane Monozyten, die mit Mimic-Molekülen des miR-Clusters 99b/let-7e/125a behandelt wurden, waren außerdem in der Lage, die Proliferation aktivierter T-Zellen zu hemmen. Die Beobachtung, dass miR-125a-5p und die drei miRs des Clusters 99b/let-7e/125a eine vergleichbare Wirkung auf myeloide Zellen zeigten, führte zu der Schlussfolgerung, dass hauptsächlich Melanom-EV-assoziierte miR-125a-5p durch die Aktivierung von NF-κB zur Entwicklung von MDSCs beitragen könnte.

TABLE OF CONTENTS

Page

ABBREVIATIONS

7-AAD	7-aminoactinomycin D
ARG1	arginase 1
BRAF	serine/threonine-protein kinase B-raf
BM	bone marrow
COX2	cyclooxygenase-2
CTLA-4	cytotoxic T lymphocyte-associated antigen 4
Cy3	cyanine3
DCs	dendritic cells
DMSO	dimethyl sulphoxide
EVs	extracellular vesicles
FBS	fetal bovine serum
G-CSF	granulocyte-colony stimulating factor
GM-CSF	granulocyte macrophage-colony stimulating factor
HIF1α	hypoxia-inducible factor 1α
HSP	heat-shock protein
IDO	indoleamine 2,3-dioxygenase
IKKβ	inhibitor of nuclear factor kappa-B kinase subunit β
iMCs	immature myeloid cells
iNOS	inducible nitric oxide synthase
IFN-γ	interferon γ
IKK	inhibitor of nuclear factor kappa-B kinase
IL	interleukin
IRAK1	interleukin-1 receptor-associated kinase 1
LAG3	lymphocyte activation gene 3
M	monocytic

MAPK	mitogen-activated protein kinase
M-CSF	macrophage colony-stimulating factor 1
MDSCs	myeloid-derived suppressor cells
miR	microRNA
NK	natural killer
nt	nucleotide
PBMCs	peripheral blood mononuclear cells
PBS	phosphate-buffered saline
PD-1	programmed cell death protein 1
PD-L1	programmed cell death 1 ligand 1
PGE2	prostaglandin E2
PMN	polymorphonuclear
Pre-miRs	microRNA precursors
Pri-miRs	primary microRNAs
P/S	Penicillin-Streptomycin
RIP1	receptor-interacting serine/threonine-protein kinase 1
RISC	RNA-induced silencing complex
ROS	reactive oxygen species
RT	room temperature
STAT3	signal transducer and activator of transcription 3
TGF-β	transforming growth factor beta
TLRs	Toll-like receptors
TME	tumor microenvironment
TNFα	tumor necrosis factor α
TRAF6	TNF receptor-associated factor 6
VEGF	vascular endothelial growth factor
WT	wild-type

FIGURES

PUBLICATIONS DURING THE DOCTORAL STUDIES

Lasser, S.A., Ozbay Kurt, F.G., Arkhypov, I., Utikal, J., and Umansky, V. (2024). Myeloid-derived suppressor cells in cancer and cancer therapy. Nature Reviews Clinical Oncology. https://doi.org/10.1038/s41571-023-00846-y

Lepper, A., Bitsch, R., Özbay Kurt, F.G., Arkhypov, I., Lasser, S., Utikal, J., and Umansky, V. (2023). Melanoma patients with immune-related adverse events after immune checkpoint inhibitors are characterized by a distinct immunological phenotype of circulating T cells and M-MDSCs. OncoImmunology 12, 2247303.

Ozbay Kurt, F.G., Lasser, S., Arkhypov, I., Utikal, J., and Umansky, V. (2023). Enhancing immunotherapy response in melanoma: myeloid-derived suppressor cells as a therapeutic target. The Journal of Clinical Investigation 133.

Özbay Kurt, F.G., Lepper, A., Gerhards, C., Roemer, M., Lasser, S., Arkhypov, I., Bitsch, R., Bugert, P., Altevogt, P., Gouttefangeas, C., et al. (2022). Booster dose of mRNA vaccine augments waning T cell and antibody responses against SARS-CoV-2. Frontiers in Immunology 13.

Arkhypov, I., Kurt, F.G.Ö., Bitsch, R., Novak, D., Petrova, V., Lasser, S., Hielscher, T., Groth, C., Lepper, A., Hu, X., et al. (2022). HSP90α induces immunosuppressive myeloid cells in melanoma via TLR4 signaling. Journal for ImmunoTherapy of Cancer 10, e005551.

Bitsch, R., Kurzay, A., Özbay Kurt, F., De La Torre, C., Lasser, S., Lepper, A., Siebenmorgen, A., Müller, V., Altevogt, P., Utikal, J., and Umansky, V. (2022). STAT3 inhibitor Napabucasin abrogates MDSC immunosuppressive capacity and prolongs survival of melanoma-bearing mice. Journal for ImmunoTherapy of Cancer 10, e004384.

Groth, C., Weber, R., Lasser, S., Özbay, F.G., Kurzay, A., Petrova, V., Altevogt, P., Utikal, J., and Umansky, V. (2021). Tumor promoting capacity of polymorphonuclear myeloid-derived suppressor cells and their neutralization. International Journal of Cancer 149, 1628-1638.

Groth, C., Arpinati, L., Shaul, M.E., Winkler, N., Diester, K., Gengenbacher, N., Weber, R., Arkhypov, I., Lasser, S., Petrova, V., et al. (2021). Blocking Migration of Polymorphonuclear Myeloid-Derived Suppressor Cells Inhibits Mouse Melanoma Progression. Cancers 13, 726.

Weber, R., Groth, C., Lasser, S., Arkhypov, I., Petrova, V., Altevogt, P., Utikal, J., and Umansky, V. (2021). IL-6 as a major regulator of MDSC activity and possible target for cancer immunotherapy. Cellular Immunology 359, 104254.

Arkhypov, I., Lasser, S., Petrova, V., Weber, R., Groth, C., Utikal, J., Altevogt, P., and Umansky, V. (2020). Myeloid Cell Modulation by Tumor-Derived Extracellular Vesicles. International Journal of Molecular Sciences 21, 6319.

1 INTRODUCTION

1.1 Melanoma

Melanoma is a highly malignant kind of skin cancer that originates from melanocytes. Melanomas on chronically sun-damaged skin often develop in parts of the body that are naturally exposed to ultraviolet radiation, such as the head and neck regions (Castro-Pérez et al., 2023). This tends to occur in people over the age of 55. Melanomas that are not related to chronic sun damage tend to develop in younger people and are typically seen in body locations such as the proximal extremities and the torso (Castro-Pérez et al., 2023). Since melanoma development is often associated with high exposure to mutagens (such as UV radiation), it shows numerous mutations. Over 60 % of all cutaneous melanomas are characterized by an oncogenic mutation in the *BRAF* gene, leading to the hyperactivated mutant protein $BRAF^{V600E}$ (Castro-Pérez et al., 2023). The serine/threonine-protein kinase B-raf (BRAF) is a key enzyme of the mitogen-activated protein kinase (MAPK) pathway. Therefore, targeted therapies designed to inhibit BRAFV600E such as vemurafenib, dabrafenib, and encorafenib or drugs blocking related proteins of the MAPK pathway such as trametinib, cobimetinib, and binimetinib can be very effective for melanoma treatment (Ballantyne and Garnock-Jones, 2013; Chapman et al., 2011; Flaherty et al., 2012; McArthur et al., 2014). However, primary or acquired resistance mechanisms often limit the duration of targeted drugs (Castro-Pérez et al., 2023; Helmbach et al., 2001; Sun et al., 2014). In addition, a high tumor mutational burden increased the likelihood of neoantigen expression, which could be recognized by the immune system. Immunotherapy with immune checkpoint inhibitors to boost the anti-tumor response has substantially improved the median survival of patients with advanced melanoma (Knight et al., 2023). Therapeutic antibodies targeting the programmed cell death protein 1 (PD-1)/programmed cell death 1 ligand 1 (PD-L1) axis (pembrolizumab, nivolumab, atezolizumab), cytotoxic T lymphocyte-associated antigen (CTLA-)4 (ipilimumab), or lymphocyte activation gene 3 (LAG3) protein (relatlimab) have been proven to effectively enhance anti-tumor activity of immune cells (Knight et al., 2023). Yet, melanomas also exhibit primary or acquired resistance to these immunotherapies, limiting their efficacy. The

failure of such therapies may be at least partially attributed to the presence of immunosuppressive cells like myeloid-derived suppressor cells (MDSCs).

1.2 Immunology of melanoma

Multiple findings have led to the conclusion that melanomas are immunogenic tumors, showing spontaneous regression or infiltration by lymphocytes (Mukherji, 2013). Additionally, it has been shown that regressing melanomas demonstrate clonal expansion of T cells that can exert potent cytolytic activity against autologous melanoma cells (Mackensen et al., 1994; Mackensen et al., 1993; Mukherji, 2013). Since melanomas typically do not express MHC class II molecules, T cell responses against melanoma cells are mediated predominantly by CD8 T cells. Nevertheless, melanoma-associated peptides presented by antigen presenting cells can be recognized by CD4 T cells, as the presence of IgG antibodies with specificity against melanoma antigens (for which CD4 T cells are essential) were found (Mukherji, 2013). However, CD4 T cells in melanoma are more likely to be regulatory T cells with immunosuppressive functions (Vence et al., 2007).

Furthermore, melanoma cells were demonstrated to be highly susceptible to natural killer (NK) cells (Carrega et al., 2009). Although CD8 T cells and NK cells possess the ability to provoke an immune response against the tumor, melanoma cells develop mechanisms to escape immune surveillance (Passarelli et al., 2017). For instance, immune evasion can occur through the loss of tumor antigens, alteration or decrease in MHC class I molecules, and impaired antigen presentation, leading to inadequate activation of effector T cells (Passarelli et al., 2017). Furthermore, melanoma cells were reported to express negative immune checkpoint molecules, including CTLA-4, PD-1, LAG3, T-cell immunoglobulin mucin-3, V-type immunoglobulin domain-containing suppressor of T-cell activation, PD-L1, and PD-L2, thereby inhibiting T cell functions (Passarelli et al., 2017). Following prolonged exposure to antigens, T cells may also transit from a state of activation to a state of exhaustion, which is characterized by the expression of additional inhibitory molecules, including LAG3 and T-cell immunoglobulin mucin-3 (Mahmoud et al., 2017). Importantly, melanomas disturb anti-tumor responses by the establishment of an immunosuppressive tumor microenvironment (TME) supported by

transforming growth factor β (TGF-β), interleukin (IL)-6, IL-10, prostaglandin E2 (PGE2), vascular endothelial growth factor (VEGF), indoleamine 2,3-dioxygenase (IDO), and inducible nitric oxide synthase (iNOS) (Passarelli et al., 2017). Such a milieu fosters the generation and recruitment of suppressive, tumor-promoting cells, including regulatory T and B cells, MDSCs, alternatively activated or tumor-associated macrophages, as well as cancer-associated fibroblasts. These regulatory cells not only hinder the immune response against melanoma cells, but also support processes like angiogenesis and metastasis (Lasser et al., 2024).

1.3 Myeloid-derived suppressor cells

1.3.1 Definition and phenotypic characteristics

MDSCs are immune cells of myeloid origin that have an inhibitory effect on other immune cells, like T and NK cells (Gabrilovich et al., 2007). Under pathological conditions such as cancer, MDSCs emerge from aberrant myelopoiesis and impaired maturation of myeloid progenitors in the bone marrow, as well as from conversion of mature myeloid cells in the peripheral organs. Thus, MDSCs are considered as a heterogeneous population of myeloid cells at various phases of maturation. Two main subgroups of MDSCs, polymorphonuclear (PMN) and monocytic (M) MDSCs, have been described in humans and in mice(Movahedi et al., 2008). In humans, PMN-MDSCs are characterized as $CD11b^{+}CD14^{-}CD15^{+}$ or $CD11b^{+}CD14^{-}CD66b^{+}$ cells, while M-MDSCs are $CD11b^{+}CD14^{+}HLA\text{-}DR^{-/lo}CD15^{-}$ cells (Bronte et al., 2016). In mice, PMN-MDSCs are identified as $CD11b^{+}Ly6G^{+}Ly6C^{lo}$ and M-MDSCs as $CD11b^{+}Ly6G^{-}Ly6C^{hi}$ (Bronte et al., 2016). Early MDSCs, a subset of $HLA\text{-}DR^{-}CD33^{+}$ myeloid progenitor lacking the expression of lineage markers (CD3, CD14, CD15, CD19, CD56), have been observed in humans but not in mice (Bronte et al., 2016). Furthermore, $CXCR1^{+}CD15^{-}CD14^{+}HLA\text{-}DR^{-/lo}$ cells were recently reported as monocyte-like progenitors of granulocytes that could differentiate into PMN-MDSCs (Mastio et al., 2019). Importantly, none of the aforementioned surface molecules are exclusively expressed in MDSCs; thus, their immunosuppressive function is the only truly defining characteristic of MDSCs. Several additional markers have been proposed to correlate with MDSC functions. In melanoma, CCR5 expression by MDSCs was found to correlate with their immunosuppressive capacity in both mice and humans

(Blattner et al., 2018). CD84 could serve as a MDSC-specific marker in breast cancer; its potential for identifying MDSCs in other cancer entities is yet unknown (Alshetaiwi et al., 2020). Lectin-like oxidized low-density lipoprotein receptor (LOX) 1 and long-chain fatty acid transport protein (FATP) 2 have been stated as candidates for distinguishing between PMN-MDSCs and classical neutrophils in various cancer types (Condamine et al., 2016; Veglia et al., 2019).

1.3.2 Immunosuppressive mechanisms

MDSCs possess a multitude of mechanisms that aid in evading immune surveillance of tumors, such as inducing T and NK cell exhaustion. MDSCs limit anti-tumor actions of T and NK cells by expressing inhibitory molecules such as PD-L1 (Groth et al., 2019; Hsu et al., 2018; Sun et al., 2020). PD-L1 can interact with the corresponding receptor PD-1 expressed by activated T cells or NK cells, leading to their inhibition. It has been demonstrated in numerous mouse tumor models and cancer patients that tumor-infiltrating MDSCs upregulate PD-L1, which is induced by hypoxic stress as well as tumor-derived soluble or EV-associated molecules (Christiansson et al., 2013; Duraiswamy et al., 2013; Fleming et al., 2019; Iwata et al., 2016; Noman et al., 2014; Prima et al., 2017; Zhang et al., 2013). Lower levels of PD-L1 expressing monocytes were associated with improved survival in melanoma patients (Pico de Coaña et al., 2020), and PMN-MDSCs were shown to highly express PD-L1 in patients not responding to immunotherapy with ipilimumab (Gebhardt et al., 2015), demonstrating a critical role for this mechanism of immunosuppression in melanoma. MDSCs have also been shown to express PD-1 and CTLA-4, albeit with little knowledge of their specific mechanisms (Liu et al., 2009; Strauss et al., 2020).

MDSCs can also cause immunosuppression by expressing enzymes that generate inhibitory molecules. For instance, tumor-derived PGE2 could stimulate the expression of cyclooxygenase-2 (COX2) by MDSCs (Obermajer and Kalinski, 2012; Obermajer et al., 2011). Conversely, COX2 induction can lead to PGE2 production by MDSCs, creating a positive feedback loop. Activation of this mechanism can in turn promote the expression of further enzymes, including IDO1, arginase 1 (ARG1), and iNOS (Obermajer and Kalinski, 2012; Obermajer et al., 2011). Via IDO1 expression, MDSCs can decrease the amount of L-tryptophan in the TME, which is

essential for T cell function (Bilir and Sarisozen, 2017). At the same time, IDO1 activity leads to the accumulation of an immunosuppressive metabolite, namely kynurenine. As a result, MDSCs can cause cell cycle arrest and anergy in T cells, suppress NK cell activity and proliferation, and promote the differentiation of Treg cells via the expression of IDO1 (Chiesa et al., 2006; Frumento et al., 2002; Mezrich et al., 2010; Munn et al., 2005). Notably, promising results (80 % response rate and 43 % complete responses) were seen in a phase 1/2 trial of a vaccination against PD-L1 and IDO as combination therapy with nivolumab for metastatic melanoma, indicating the relevance of IDO1 expression in melanoma patients (Kjeldsen et al., 2021). By expressing ARG1 or iNOS, MDSCs can also mediate the depletion of L-arginine, resulting in altered T cell proliferation and function (Rodríguez and Ochoa, 2008; Rodriguez et al., 2006; Rodriguez et al., 2004b). Moreover, iNOS and NADPH oxidase activity by MDSCs was reported to contribute to excessive production of reactive nitrogen species and reactive oxygen species (ROS) in the TME (Corzo et al., 2009; Fiaschi and Chiarugi, 2012). Reactive nitrogen and oxygen species can reduce T cell migration to the tumor (Gehad et al., 2012; Molon et al., 2011), impair antigen recognition by T cells (Feng et al., 2018; Nagaraj et al., 2007; Tcyganov et al., 2022), suppress T cell proliferation (Bingisser et al., 1998), induce T cell apoptosis (Wang et al., 2010), and inhibit NK cell functions (Stiff et al., 2018). The conversion of extracellular ATP to adenosine via the cell surface ectonucleotidases CD39 and CD73 has been discovered as an additional mechanism by which MDSCs can exert suppressive effects on T cells and NK cells (Li et al., 2017).

Cytokines play a crucial role in regulating immunological activity, and several of them have been associated with immune regulation by MDSCs. One example is the high production of IL-10 by MDSCs in cancer (Hart et al., 2011; Loercher et al., 1999; Sato et al., 2015; Vuk-Pavlović et al., 2010). The induction of T cell anergy, suppression of dendritic cell (DC) functions, and development of Treg cells have all been associated with IL-10 (Hu et al., 2011; Serafini et al., 2006; Sinha et al., 2007; Steinbrink et al., 2002; Steinbrink et al., 1997). Another important example is TGFβ that is able to suppress the cytotoxic activity and infiltration of T cells into tumors (Mariathasan et al., 2018; Thomas and Massagué, 2005). TGFβ has also been shown to impede DC functions and inhibit NK cell cytotoxicity (Kobie et al., 2003; Li et al., 2009; Mao et al., 2014). MDSCs have been shown to secrete TGF-β in melanoma (Filipazzi et al., 2007) and other cancer models (Beury et al., 2014; Chen

et al., 2013; Huang et al., 2006). Despite the release of soluble factors, extracellular vesicles (EVs) appear to serve as additional tool via which MDSCs can regulate the immune system. For instance, MDSC-derived EVs were reported to elicit immunosuppressive characteristics in other myeloid cells or to dampen NK cell-mediated anti-tumor activity (Burke et al., 2014; Tumino et al., 2022).

1.3.3 Expansion and recruitment

Hematopoietic stem cells differentiate into several mature subsets of bone marrow cells, including macrophages, DCs, and granulocytes, under physiological conditions. Myelopoiesis in the bone marrow is facilitated by growth factors including granulocyte macrophage-colony stimulating factor (GM-CSF), granulocyte-colony stimulating factor (G-CSF), and macrophage colony-stimulating factor 1 (M-CSF). However, myeloid cell differentiation can be altered by the constant supply of such growth factors in the setting of a chronic inflammatory milieu, such as cancer, which results in the expansion of MDSCs (Condamine et al., 2015). For instance, dysregulated mTOR signaling in cancer cells has been identified as a key driver of this process via controlling the expression of G-CSF (Welte et al., 2016). Moreover, VEGF produced by cancer cells was found to inhibit the differentiation of immature myeloid cells (iMCs), thereby promoting the accumulation of MDSCs (Gabrilovich et al., 1998; Gabrilovich et al., 1996; Rivera and Bergers, 2015). Several tumor-associated conditions like hypoxia, nutritional deprivation, low pH, and elevated levels of ROS all contribute to endoplasmic reticulum stress, which substantially promotes the generation of MDSCs (Condamine et al., 2015).

The JAK/STAT signaling axis via the transcription factor signal transducer and activator of transcription 3 (STAT3) and the MAPK signaling pathway, which includes CCAAT/enhancer-binding protein-β, are critical in facilitating the development of MDSCs (Condamine et al., 2015). Consequently, factors that activate these pathways like GM-CSF, G-CSF, and IL-6 can stimulate the expansion of MDSCs (Umansky et al., 2016; Weber et al., 2021). Cancer cells as well as stromal cells in the TME can generate those mediators, as well as numerous other cytokines such as IL-1β, IL-4, IL-10, IL-13, TGF-β, tumor necrosis factor (TNFα), and interferon γ (IFN-γ) (Condamine et al., 2015; Umansky et al., 2016). The combined action of such inflammatory mediators may affect myeloid cell

differentiation in a dose- and duration-dependent manner (Umansky et al., 2016). Furthermore, it has been demonstrated that hypoxia-inducible factor 1α (HIF1α), adenosine, COX2, and PGE2 promote MDSC generation (Corzo et al., 2010; Morello et al., 2016; Obermajer et al., 2011).

The recruitment of MDSCs to the tumor site primarily depends on the chemokine receptors CXCR2, CCR2, and CCR5 (Lim et al., 2020). While CXCR2 is highly expressed by PMN-MDSCs and CCR2 is highly expressed by M-MDSCs, CCR5 is found on both subsets of MDSCs (Blattner et al., 2018; Qian et al., 2011; Steele et al., 2016). PMN-MDSCs are therefore predominantly attracted by CXC chemokines such as CXCL1, CXCL2, CXCL5, and CXCL8 (only humans) (Groth et al., 2021; Lim et al., 2020). M-MDSC migration to the tumor is mediated mainly by CCR2 ligands, including CCL2, CCL7, CCL12 (only mice) (Lim et al., 2020). CCR5 ligands, including CCL3, CCL4, and CCL5, can increase the recruitment of both MDSC subpopulations (Blattner et al., 2018).

1.3.4 Regulation of MDSC activity

Numerous mechanisms, including the NF-κB pathway, JAK/STAT pathway, PGE2/COX2 pathway, ER stress response pathway, and metabolic pathways were demonstrated to facilitate immunosuppressive and pro-tumorigenic functions of MDSCs (Condamine et al., 2015; Veglia et al., 2021).

NF-κB signaling

The activation of NF-κB in MDSCs can be triggered by IL-1β and TNFα, as well as by binding of pathogen-associated molecular patterns or damage-associated molecular patterns to pattern recognition receptors like Toll-like receptors (TLRs) (Condamine et al., 2015). In melanoma, heat-shock proteins (HSP), S100 proteins, and HMGB1 have been shown to serve as TLR ligands and activate a signaling cascade via NF-κB, leading to the activation of MDSC immunosuppressive functions (Arkhypov et al., 2022; Fleming et al., 2019; Özbay Kurt, 2023). Such factors can be soluble or EV-associated.

When ligands bind to TLRs, the formation of dimers initiates signaling to MyD88 and/or TRIF, the two main downstream adaptor proteins (Kawasaki and Kawai, 2014). The MyD88-dependent pathway involves activation of interleukin-1 receptor-associated kinase 1 (IRAK1) and TNF receptor-associated factor 6 (TRAF6),

ultimately leading to the activation of inhibitor of nuclear factor kappa-B kinase (IKK) complex, comprising IKKα, IKKβ, and NF-κB essential modulator. The IKK complex then mediates the degradation of the NF-κB inhibitor α, enabling the translocation of NF-κB to the nucleus to exert its function as transcription factor (Kawasaki and Kawai, 2014). The TRIF-dependent pathway transmits the signal via TRAF3 and TRAF6, which recruits the receptor-interacting serine/threonine-protein kinase 1 (RIP1) (Kawasaki and Kawai, 2014). Subsequently, RIP1 facilitates the activation of the IKK complex, resulting in NF-κB translocation. The NF-κB complex can be comprised of different subunits. Depending on the type of stimulus, canonical signaling predominantly via NF-κB subunits p50/p65 or non-canonical signaling predominantly via p52/RelB subunits can occur (Gilmore, 2006).

It has been shown that TLR4 plays an important role in MDSC functions (Arkhypov et al., 2022; Arora et al., 2010; Bunt et al., 2009; Fleming et al., 2019; Özbay Kurt, 2023). Subsequent NF-κB signaling regulates the expression of several MDSC effector molecules, including PD-L1, IDO1, and iNOS, IL-6, and IL-10 (Arkhypov et al., 2022; Fleming et al., 2019; Matsusaka et al., 1993; Saraiva et al., 2005; Simon et al., 2015).

JAK/STAT signaling

IL-6, IL-10, and other ligands in the TME can induce JAK/STAT signaling in MDSCs. The interaction between a cytokine and its receptor induces the formation of a dimer, which allows the activation of tyrosine-protein kinase JAK. The kinase activity leads to phosphorylation of intracellular receptor domains, which allows the binding of STAT molecules (Trikha and Carson, 2014). These STAT molecules are subsequently phosphorylated by JAK, enabling their dimerization and translocation to the nucleus (Trikha and Carson, 2014).

STAT1 activity has been linked to iNOS and ARG1 expression in MDSCs, especially M-MDSCs (Condamine et al., 2015). STAT3 was also shown to regulate iNOS and ARG1 activity, as well as PD-L1, IDO1, and ROS production in MDSCs (Chen et al., 2014; Corzo et al., 2009; Hildebrand et al., 2018; Vasquez-Dunddel et al., 2013; Wölfle et al., 2011). Moreover, STAT6 was reported to promote ARG1 expression and TGFβ production (Condamine et al., 2015).

1.4 Extracellular vesicles

EVs refer to biological nanoparticles that are released by eukaryotic cells, particularly cancer cells and platelets (Colombo et al., 2014; Dvorak et al., 1981; George et al., 1982). They can be found in tissues like cartilage (Anderson 1969), or in biological fluids like plasma (Crawford, 1971). Based on their site and mechanism of biogenesis, EVs are categorized into two main subtypes: exosomes, and ectosomes (van Niel et al., 2022). While ectosomes are produced directly by outward budding of the plasma membrane, exosomes are formed by inward budding of endosomal membranes. This involves the generation of multivesicular endosomes, which can fuse with the plasma membrane and thereby release the exosomes (van Niel et al., 2022; van Niel et al., 2018). As a result, exosomes are small EVs (30 – 150 nm), whereas ectosomes, which include microvesicles and oncosomes, range in diameter from 50 to 10,000 nm (van Niel et al., 2022). Given the challenge of accurately differentiating between numerous subspecies, the term EVs is commonly used.

EVs are important tools to transmit signals as well as functional molecules from one cell to another (Al-Nedawi et al., 2008; Colombo et al., 2014; Raposo et al., 1996; Tkach and Théry, 2016; Zitvogel et al., 1998). Although it is well-known that various cell types can internalize EVs, the mechanisms driving EV entry into recipient cells are incompletely understood (van Niel et al., 2022). Direct interaction with a recipient cell via surface receptors can induce intracellular signaling and/or uptake of the EVs. Endocytosis is thought to be the main mechanism by which EVs are internalized (Mulcahy et al., 2014; Tian et al., 2010; van Niel et al., 2022), although direct fusion with the plasma membrane was also described (Parolini et al., 2009). Following cellular uptake, EVs may become trapped in lysosomes; however, it has been demonstrated that the cargo of EVs is also released into the cytoplasm of the recipient cell (van Niel et al., 2022). Such cargo comprises lipids, membrane proteins, cytosolic proteins and nucleic acids, including functional microRNA (miR) (Théry et al., 2002; Valadi et al., 2007; Zaborowski et al., 2015).

1.5 MicroRNA

MiRs are a group of non-coding RNAs that are highly conserved and have important functions in controlling gene expression at the post-transcriptional level (Bartel, 2018; Lagos-Quintana et al., 2001; Lau et al., 2001; Lee and Ambros, 2001). MiRs play a pivotal role in numerous biological processes and are indispensable for the physiological development (Fu et al., 2013; O'Brien et al., 2018). Dysregulated expression of miRs has been linked to many human disorders (O'Brien et al., 2018; Paul et al., 2018), including cancer (Hayes et al., 2014).

Typically, the size of mature miRs ranges from 19 to 25 nucleotides (nt). However, miRs must undergo a multi-step process before they obtain this mature form, with the transcription of miR genes in the nucleus as its first step (Bartel, 2018; Lee et al., 2004; O'Brien et al., 2018). MiR genes exist in two forms: as individual transcriptional units or as polycistronic transcriptional units, so-called clusters, that give rise to two or more miRs (Lau et al., 2001). Many miR genes are found within the introns of protein-coding genes (Rodriguez et al., 2004a). Other miR genes are part of introns or exons of non-coding RNA genes (Rodriguez et al., 2004a). Also, intergenic miR genes exist, which are controlled by separate promoters and are transcribed independently of another gene.

The DNA-directed RNA polymerase II primarily transcribes miR genes (Bartel, 2018; Cai et al., 2004; Lee et al., 2002; Lee et al., 2004), although there are circumstances where they are transcribed by the DNA-directed RNA polymerase III. The transcripts are referred to as primary miRs (pri-miRs). They can be several kilobases long and are partially organized in hairpin (also known as stem-loop) structures, which serves as a characteristic feature. A protein complex containing the double-stranded RNA-specific endoribonuclease RNase III (also known as Drosha) converts the pri-miRs into shorter, ~70 nt hairpin-shaped molecules called miR precursors (pre-miRs) (Bartel, 2018; Lee et al., 2003; Lee et al., 2002). Prior to further maturation, the pre-miR molecules must be transported from the nucleus to the cytoplasm (Lee et al., 2002). There, the RNase III protein complex Dicer further processes the pre-miRs into miR duplex molecules measuring 19-25 nucleotides in length (Grishok et al., 2001; Hutvágner et al., 2001; Ketting et al., 2001; Knight and Bass, 2001). These duplex molecules interact with argonaute proteins, which are part of the RNA-induced silencing complex (RISC) (Miyoshi et al., 2005; Yoda et al., 2010). The

features of the 5’ terminal region of the miR strands dictate the physics of that interaction and consequently define which one will serve as the mature guide miR in the RISC complex (Kawamata and Tomari, 2010; Leuschner et al., 2006; Miyoshi et al., 2005). The other strand, identified as passenger strand, is typically released from the RISC complex and degraded promptly (Kawamata and Tomari, 2010).

By loading target mRNA in the RISC complex via base pairing, miRs mediate post-transcriptional silencing of gene expression, which is their canonical function. This function is thought to require binding of the 5′ end of the miR with the 3′-UTR of the mRNA as well as endonucleolytic activity of the argonaute proteins. According to the paradigm, the mRNA target will be either degraded, when the miR and mRNA motifs are perfectly complementary, or its translation will be regulated without degradation, when the binding between miR and mRNA motifs occurs only partially (Bartel, 2009; Guo et al., 2010; Hutvágner and Zamore, 2002; Pillai et al., 2005). A mechanism via partial complementary allows a single miR to control numerous mRNA targets (Ying et al., 2008). However, it is important to emphasize that this is a simplified model and that there are various reports of alternative mechanisms and non-canonical miR functions (O'Brien et al., 2018; Santovito and Weber, 2022; Stavast and Erkeland, 2019). For instance, miR-21 and miR-29a have been demonstrated to function as ligands to TLR7 and TLR8 in macrophages, activating a downstream signaling cascade (Fabbri et al., 2012). Importantly, these miRs were delivered to macrophages via cancer cell-derived EVs. As cargo of EVs or bound to argonaute proteins, miRs can be detected in plasma and other biological fluids (O'Brien et al., 2018). In contrast to free intracellular RNA molecules, such extracellular miRs were found to be remarkably stable (Chen et al., 2008; Mitchell et al., 2008; O'Brien et al., 2018).

Melanoma cells, like other tumor cells, were reported to secrete EVs enriched in certain miRNAs, potentially affecting gene expression in recipient cells (Ye et al., 2023). EV-associated miRNA is hypothesized to support melanoma progression by increasing tumorigenic properties (Felicetti et al., 2016; Li et al., 2019; Luan et al., 2021; Pegoraro et al., 2021), promoting metastasis (Chen et al., 2022; Li et al., 2022; Liu et al., 2023; Xiao et al., 2016), stimulating angiogenesis (Zhou et al., 2018a; Zhuang et al., 2012), and fostering a favorable TME (Dror et al., 2016; Gerloff et al., 2020; Shu et al., 2018; Vignard et al., 2020). It has been demonstrated that

melanoma EV-associated miRNA can alter monocyte differentiation, causing their conversion to MDSCs (Huber et al., 2018). The study identified a set of eight miRs as cargo of melanoma-derived EVs: miR-146a, -146b, -155, -125a, -125b, -100, -99b, and let-7e. Transferring those miRs directly into healthy donor-derived monocytes replicated the generation of MDSCs that was observed upon an exposure to melanoma EVs. Also, antagonizing the miRs in monocytes during exposure to melanoma EVs was able to prevent their conversion to MDSCs, indicating that the immunosuppressive properties acquired by melanoma EV-treated monocytes were induced by these miRs (Huber et al., 2018). In addition, miR-125b was reported to be transported to THP-1 macrophages by melanoma EVs in vitro and to aid in the phenotypic changes of THP-1 macrophages towards TAM-like characteristics (Gerloff et al., 2020). While a regulatory mechanism for miR-125b via lysosomal acid lipase A targeting has been suggested (Gerloff et al., 2020), the precise mechanisms through which miR-146a, -146b, -155, -125a, -125b, -100, -99b, and let-7e induce the conversion of primary monocytes remain unknown.

1.6 MicroRNA delivery

Due to their hydrophilic nature and negative charge, miR molecules cannot pass through cellular membranes (Ben-Shushan et al., 2014). Hence, a carrier system is needed to introduce miR into cells. Viral and non-viral methods have been developed for delivering miR, and each of these approaches has different advantages and disadvantages (Yang, 2015). Viral vectors, including retroviral, lentiviral, adenoviral, or adeno-associated viral vectors can efficiently introduce miR genes into cells, allowing their stable expression (Fu et al., 2019; Yang, 2015). Nevertheless, viral delivery systems possess major drawbacks, particularly high immunogenicity (Fu et al., 2019; Yang, 2015). Therefore, non-viral methods, despite their overall lower efficiency, are frequently employed to transfer miRs or miR-expressing vectors (Yang, 2015).

Non-viral delivery technologies can be further categorized into physical and chemical approaches. Physical approaches use mechanical, electrical, ultrasonic, hydrodynamic, or laser-based energy to temporarily weaken the integrity of the cell

membrane, enabling the entry of nucleic acids (Nayerossadat et al., 2012). Among these, electroporation is a frequently used technique, particularly for cells that are resistant to chemical methods. Chemical methods comprise lipid-based, polymer-based, inorganic, and cell-derived carriers (Fu et al., 2019). Cationic amphiphilic lipids often serve as the fundamental component of commercially available transfection reagents that are widely used for miR transfection *in vitro* (Dasgupta and Chatterjee, 2021). Such lipid-based transfection approaches involve the spontaneous formation of complexes between negatively charged RNA molecules and the cationic lipids, allowing cellular uptake (Weisman et al., 2004). Lipoplexes, the lipid-based complexes, can effectively shield the miR from degradation and are thought to be non-immunogenic. However, a significant limitation of lipoplexes is that they can interact non-specifically with proteins, potentially resulting in side effects (Dasgupta and Chatterjee, 2021).

Therefore, the use of nanoparticles for miR transfer, especially for applications *in vivo*, represents a feasible option. Nanoparticles usually range from 1 to 100 nm in size (Ghafouri-Fard et al., 2023) and are comparable to exosomes in this regard. Moreover, intracellular trafficking of nanoparticles was reported to be similar to that of EVs upon internalization (Tian et al., 2010). Different methods have been developed for the preparation of nanoparticles, depending on the composition and desired attributes of the particles (Lee et al., 2019). Emulsion-based preparation of is the most employed technique for the synthesis of miR-loaded particles (Lee et al., 2019). This technique uses ultrasonication, homogenization, and high-speed centrifugation for encapsulating substances into polymer-based nanoparticles (Lamprecht et al., 2000; Lee et al., 2019). Such biodegradable polymers are often polylactic acid-based substances, although natural polymers like chitosan or hyaluronic acid are also used. Other materials utilized for nanoparticles comprise inorganic materials like gold or silica and lipids, including a cationic lipid and helper lipids (e.g. cholesterol, polyethylene glycol) (Hald Albertsen et al., 2022; Lee et al., 2019).

1.7 Aim of the study

Previous studies in our research group demonstrated that EVs derived from Ret mouse melanoma cells induced the conversion of iMCs to immunosuppressive MDSCs, which was accompanied by an upregulation of PD-L1 (Fleming et al., 2019). PD-L1 expression and the immunosuppressive capacity of Ret EV-generated MDSCs were dependent on both HSP90α found on the surface of the EVs and TLR4 on iMCs, suggesting that interactions between TLRs and EV-associated molecules are an important mechanism for the generation of MDSCs in melanoma. Furthermore, EVs derived from human melanoma cells were able to convert $CD14^+$ monocytes isolated from healthy donors to MDSCs in a TLR4-dependent manner (Fleming et al., 2019). Remarkably, certain EV-associated miRs have been reported to interact with endosomal TLRs in macrophages, thereby triggering NF-κB signaling and the acquisition of tumor-promoting functions (Fabbri et al., 2012). EVs isolated from melanoma patients were found to be enriched in miR-146a, miR-155, miR-125b, miR-100, let-7e, miR-125a, miR-146b, and miR-99b, and these miRs appeared to be involved in MDSC generation (Huber et al., 2018). However, the mechanism by which those melanoma EV-associated miRs could mediate the conversion of normal myeloid cells to MDSCs has not been elucidated. Therefore, this study aims to examine the molecular processes that are induced in myeloid cells by melanoma EV-associated miR and to investigate the role of endosomal TLRs in these processes.

2 MATERIAL

2.1 Equipment

	Manufacturer
Balance BP 3100P	Sartorius
Block heater	Peqlab
Cell culture incubator Hera cell 150	Heraeus
Centrifuge Biofuge primo R	Heraeus
Centrifuge Labofuge 400R	Heraeus
Centrifuge MEGAFUGE 40R	Heraeus
Counting chamber Neubauer improved	Brand
Dumont tweezers, curved	Onyx
Dumont tweezers, straight	Onyx
Flow cytometer BD FACSLyric™	BD Biosciences
Flow cytometer CytoFLEX	Beckman Coulter
Freezer (-20 °C)	Liebherr
Freezer (-80 °C)	Heraeus
Graefe forceps, curved	Onyx
Ice machine	Manitowoc
Imaging System Fusion SL4	Viber Lourmat
Laminar flow hood Hera safe	Heraeus
Light microscope DM IL	Leica
MACS® MultiStand	Miltenyi Biotec
Magnetic hotplate stirrer, RCT basic	IKA

Micro dissecting forceps, serrated, curved	Onyx
Micropipette Research® plus, set	Eppendorf
Micropipette Transferpette® S, single-channel, set	Brand
Micropipette Transferpette® S-8, multi-channel	Brand
Microplate reader Tecan infinite M200	Tecan
Mini-PROTEAN® 3 Vertical Electrophoresis Cell	Bio-Rad
N_2 tank BIOSAFE® SC-smart	Cryotherm
Operating scissors, curved	Onyx
Orbital shaker	NeoLab
Pipette controller accu-jet®	Brand
Power supply PowerPac™ HC	Bio-Rad
QuadroMACS™ separator	Miltenyi Biotec
Real-time qPCR machine MX3005	Stratagene
Refrigerator (4 °C)	Liebherr
Semi dry blotting chamber	Bio-Rad
Single-channel micropipette Transferpette® S	Brand
Surgical scissors, straight	Onyx
Thermal cycler DNA Engine®	Bio-Rad
Thermomixer® compact	Eppendorf
TissueLyser	Qiagen
Vortex mixer Mini Sunlab®	NeoLab
Vortex mixer Reax top	Heidolph
Vortex mixer Vortex-Genie 2	Scientific Industries
Water Bath 1008	GFL

2.2 Software

	Company
BD FACSuite™	BD Biosciences
EndNote™ v20 & v21	Clarivate
FlowJo™ v10	FlowJo, LLC / BD Life Sciences
FusionCapt Advance SL4	Vilber Lourmat
GraphPad Prism	GraphPad Software
iControl	Tecan
Kaluza Analysis v2	Beckman Coulter
Microsoft Office 365	Microsoft Corporation
MxPro qPCR	Stratagene

2.3 Consumables

	Manufacturer
4-15% Mini-PROTEAN protein gels	Bio-Rad
Blotting membrane, PVDF	Thermo Fisher Scientific
Cell culture dish, Falcon® 60 mm	Corning
Cell culture plate, 96 well, round base	Sarstedt
Cell strainer 40µM	NeoLab
Cell strainer 100µM	NeoLab
Cryogenic vials, 2 mL	Sarstedt
Culture tubes, 14 mL, round bottom, snap cap	Greiner
Disposable transfer pipette	Sarstedt
Filter tips, sterile	Sarstedt

MACS® LS colums	Miltenyi Biotec
Micro test plate, 96 well, round base	Sarstedt
Needle, Microlance™ 3, 27G, sterile	Becton Dickinson
Pasteur pipettes, glass	Carl Roth
PCR strip of 8 200µL-tubes	Sarstedt
PowerBead Tubes	Qiagen
Round-bottom Polystyrene Tubes, Falcon® 5 mL	Corning
SafeSeal reaction tube, 0.5 mL, sterile	Sarstedt
SafeSeal reaction tube, 1.5 mL, sterile	Sarstedt
SafeSeal reaction tube, 2 mL, sterile	Sarstedt
Serological pipette, plugged, 5 mL, sterile	Sarstedt
Serological pipette, plugged, 10 mL, sterile	Sarstedt
Serological pipette, plugged, 25 mL, sterile	Sarstedt
Screw cap tube, 15 mL, conical base, sterile	Sarstedt
Screw cap tube, 50 mL, conical base, sterile	Sarstedt
Syringe filter, pore size 0.22 µm	Millipore
Syringe, Discardit™ II, 2 mL, sterile	Becton Dickinson
Syringe, Discardit™ II, 10 mL, sterile	Becton Dickinson
Syringe, Discardit™ II, 20 mL, sterile	Becton Dickinson
Syringe, Plastipak™, Luer-Lok™ tip, 50 mL, sterile	Becton Dickinson
Thick blot filter paper, precut	Bio-Rad

2.4 Chemicals, liquids, reagents

	Manufacturer
10x Tris/Glycine Buffer	Bio-Rad
10x Tris/Glycine/SDS	Bio-Rad
10x Tris Buffered Saline (TBS)	Bio-Rad
2-Mercaptoethanol	Sigma-Aldrich
4x NuPAGE™ LDS sample buffer	Thermo Fisher Scientific
7-AAD staining solution	Miltenyi Biotec
BAY 11-7082	Sigma-Aldrich
BOT-64	Abcam
Cell proliferation dye eFluor450	BD Biosciences
CellROX™ Deep Red Reagent	Thermo Fisher Scientific
Chemiluminescent Substrate SuperSignal™ West Pico PLUS	Thermo Fisher Scientific
Chloroform	Carl Roth
Dimethyl sulphoxide (DMSO)	Carl Roth
Dulbecco's phosphate-buffered saline, w/o Ca and Mg, sterile	PAN-Biotech
EDTA, UltraPure™ 0.5 M, pH 8.0	Thermo Fisher Scientific
Ethanol, ≥99,8 %, vergällt	Carl Roth
Ethanol, ≥99,5 %, extra pure	Carl Roth
EveryBlot Blocking Buffer	Bio-Rad
Fixable viability dye 700	BD Biosciences
Fixation/Permeabilization Concentrate	Thermo Fisher Scientific
Fixation/Permeabilization Diluent	Thermo Fisher Scientific

Heat-inactivated fetal bovine serum	Thermo Fisher Scientific
HiPerFect Transfection Reagent	Qiagen
Isopropanol	Carl Roth
L-Arginine, CELLPURE® ≥99 %	Carl Roth
L-Lysine hydrochloride, CELLPURE® ≥98,5 %	Carl Roth
Methanol, ≥99,9 %, Blotting Grade	Carl Roth
Napabucasin	Selleck Chemicals
Opti-MEM™ I Reduced-Serum Medium	Thermo Fisher Scientific
PageRuler Protein ladder prestained	Thermo Fisher Scientific
Pancoll human, density: 1.077 g/ml	PAN-Biotech
Penicillin-Streptomycin (10.000 U/ml)	Thermo Fisher Scientific
Pierce® ECL Western Blotting Substrate	Thermo Fisher Scientific
Pierce® RIPA Buffer	Thermo Fisher Scientific
Ponceau S solution	Sigma-Aldrich
Protease inhibitor cocktail	Promega
RBC Lysis Buffer (10x)	BioLegend
RPMI 1640 Medium for SILAC	Thermo Fisher Scientific
RPMI Medium 1640, GlutaMAX™ Supplement	Thermo Fisher Scientific
RT-PCR Grade Water	Thermo Fisher Scientific
Sodium azide	Carl Roth
Sodium fluoride, 1000x	Jena Bioscience
Sodium orthovanadate, 1M	Jena Bioscience
Trypan blue solution	Sigma Aldrich
Tween® 20	Bio-Rad

2.5 Kits

	Manufacturer
CD14 MicroBeads, human	Miltenyi Biotec
CD3 MicroBeads, human	Miltenyi Biotec
$CD8a^+$ T cell Isolation Kit, mouse	Miltenyi Biotec
EasySep™ Mouse MDSC (CD11b+Gr1+) Isolation Kit	StemCell Technologies
ELISA MAX™ Deluxe Set Mouse IL-6	BioLegend
miRCURY LNA microRNA PCR Starter Kit	Qiagen
miRNeasy Mini Kit	Qiagen
miRNeasy Serum/Plasma Kit	Qiagen
Pierce® BCA Protein Assay Kit	Thermo Fisher Scientific
RNA Spike-In Kit, for RT	Qiagen
RNase-Free DNase Set	Qiagen
RNeasy Mini Kit	Qiagen
SensiFAST™ cDNA Synthesis Kit	Bioline
SensiFAST™ SYBR® Lo-ROX Kit	Bioline

2.6 MicroRNA mimics

All miR mimics were purchased from Qiagen.

miRCURY LNA microRNA Mimic	Catalog No.	Purification
hsa-miR-146a-5p 5'UGAGAACUGAAUUCCAUGGGUU	YM00472124	standard desalted
mmu-miR-155-5p 5'UUAAUGCUAAUUGUGAUAGGGGU	YM00470919	standard desalted
hsa-miR-125b-5p 5'UCCCUGAGACCCUAACUUGUGA	YM00473299	standard desalted
hsa-miR-100-5p 5'AACCCGUAGAUCCGAACUUGUG	YM00472477	standard desalted
hsa-let7e-5p 5'UGAGGUAGGAGGUUGUAUAGUU	YM00471840	standard desalted
hsa-miR-125a-5p 5'UCCCUGAGACCCUUUAACCUGUGA	YM00473474	standard desalted
hsa-miR-146b-5p 5'UGAGAACUGAAUUCCAUAGGCU	YM00472354	standard desalted
hsa-miR-99b-5p 5'CACCCGUAGAACCGACCUUGCG	YM00471551	standard desalted
miRCURY microRNA Mimic Negative Control GAUGCUACGGUCAAUGUCUAAG	YM00479904	standard desalted

2.7 Antibodies

2.7.1 Antibodies for flow cytometry

A test is defined as 2.0 x 10^5 cells in 50 µL of buffer.

Target species	Specificity	Conjugate	Manufacturer	Catalog number	V / test [µL]
Human	Fc receptors	-	Miltenyi Biotec	130-059-901	1.0
Human	CD11b	PC7	Beckman Coulter	A54822	0.6
Human	CD14	APC-A750	Beckman Coulter	B92421	0.6
Human	CD86	PE	BD Biosciences	555658	1.0
Human	HLA-DR	APC	Beckman Coulter	IM3635	0.6
Human	PD-L1 (CD274)	PE-CF594	BD Biosciences	563742	1.0
Human & mouse	pSTAT3 (pY705)	PE	BD Biosciences	562072	1.5
Mouse	Fc receptors	-	BD Biosciences	553141	1.0
Mouse	CD11b	APC-Cy7	BD Biosciences	557657	0.25
Mouse	Gr1	PE-Cy7	BD Biosciences	552985	0.1
Mouse	PD-L1	BV421	BD Biosciences	564716	0.5
	Isotype control	BV421	BD Biosciences	562965	0.5

2.7.2 Functional antibodies for T cell activation

Species reactivity	Specificity	Manufacturer	Catalog number	Final concentration
Human	CD28	Beckman Coulter	IM1376	2 µg/mL
Human	CD3	eBioscience	16-0037-85	1 µg/mL

2.7.3 Primary antibodies for western blotting

Anti-TRIB2 antibodies were kindly provided by Dr. Dagmar Hildebrand (University Hospital Heidelberg).

Species reactivity	Specificity	Manufacturer	Catalog number	Final dilution
Human	IDO1	Cell Signaling Technology	D5J4E	1:1000
Human	TRIB2	Abcam	ab272544	1:1000

2.7.4 Peroxidase-conjugated antibodies for western blotting

Specificity	Manufacturer	Catalog number	Final dilution
Anti-Rabbit IgG	Jackson Immuno Research	115-035-003	1:10,000

2.8 Primers for quantitative RT-PCR

All primers were purchased as oligonucleotides from Metabion.

		Sequence (5’ to 3’)
18S ribosomal RNA	forward	CGC GGT TCT ATT TTG TTG GT
	reverse	AGT CGG CAT CGT TTA TGG TC
Il6	forward	TTC CAT CCA GTT GCC TTC TTG
	reverse	GAA GGC CGT GGT TGT CAC C
Il10	forward	ATA ACT GCA CCC ACT TCC CA
	reverse	GGG CAT CAC TTC TAC CAG GT
CD274	forward	TGG ACA AAC AGT GAC CAC CAA
	reverse	CCC CTC TGT CCG GGA AGT
Nos2	forward	TTGGGTCTTGTTAGCCTAGTC
	reverse	TGTGCAGTCCCAGTGAGGAAC

2.9 Buffers

FACS buffer	1x PBS 2 % (v/v) FBS 2 mM EDTA 0.2 % (w/v) sodium azide
RIPA lysis buffer	1956 µL Pierce® RIPA Buffer (1x) 40 µL Protease inhibitor cocktail (50x) 2 µL Sodium fluoride (1000x) 2 µL Sodium orthovanadate (1M)
Running buffer	100 mL 10x Tris/Glycine/SDS buffer 900 mL deionized water
Separation buffer	1x PBS 1 % (v/v) FBS 2 mM EDTA
TBST buffer	100 mL (1x) 10x Tris buffer 0.1 % (v/v) Tween® 20 900 mL distilled water
Transfer buffer	100 mL 10x Tris/Glycine buffer 200 mL methanol 100 mL deionized water

2.10 Media

Arginine-low medium	RPMI 1640 Medium for SILAC 10 % (v/v) FBS 1 % (v/v) P/S 0.04 mg/mL L-Lysine hydrochloride 0.15 mM L-Arginine
RPMI complete medium	RPMI Medium 1640, GlutaMAX™ 10 % (v/v) FBS 1 % (v/v) P/S 10 mM HEPES 1 mM Sodium Pyruvate 1 mM MEM non-essential amino acids
Transfection medium	RPMI Medium 1640, GlutaMAX™ 10 % (v/v) FBS

2.11 Mice

RET transgenic mice with C57BL/6 background were originally provided by Dr. Nakashima (Chubu University, Aichi, Japan) (Kato et al., 1998). The *RET* transgenic mouse strain was bred at the animal facility of the German Cancer Research Center (DKFZ) in Heidelberg. C57BL/6 wild-type (WT) mice were provided as non-transgenic litter mates by the DKFZ animal facility. Femurs and tibias of TLR7-deficient ($TLR7^{-/-}$) mice were kindly provided by Dr. Martina Seiffert (DKFZ Heidelberg). Femurs and tibias of TLR8-deficient ($TLR8^{-/-}$) mice were kindly provided by Dr. Lena Alexopolou (Centre d'Immunologie de Marseille-Luminy). Femurs and tibias of TLR3/7/9-deficient ($TLR3^{-/-}TLR7^{-/-}TLR9^{-/-}$) mice, MyD88-deficient ($MyD88^{-/-}$) mice, and MyD88/TRIF-deficient ($MyD88^{-/-}TRIF^{-/-}$) mice were kindly provided by Dr. Carsten Kirschning (University Hospital Essen). The bones were kept in cold RPMI medium and shipped overnight.

3 METHODS

3.1 *RET* transgenic mice

3.1.1 Breeding and care standards

Mice were bred and kept under specific pathogen-free conditions in the animal facilities of the German Cancer Research Center and the Medical Faculty Mannheim of Heidelberg University, in compliance with governmental and institutional standards and regulations (approval number G-40/19). For blood and tumor sample collection, *RET* transgenic mice were sacrificed by CO_2 asphyxia. WT animals that were produced during the breeding process were used to obtain bone marrow (BM). For this, the mice were sacrificed by cervical dislocation.

3.1.2 Blood sample collection

Following CO_2 asphyxia, cardiac puncture was used to obtain 0.5 mL of blood. For this, a thoracotomy was performed. The blood sample was collected with a syringe and a needle that had been rinsed with 0.5 M EDTA solution before. The blood sample was then transferred into a 1.5 mL reaction tube filled with 50 µL of the 0.5 M EDTA solution and centrifuged at 1900 x g and 4 °C for 10 min. 200 – 300 µL of plasma was subsequently transferred into a 1.5 mL reaction tube and snap frozen. Plasma samples were then stored at -80 °C.

3.1.3 Tumor sample collection

Spontaneous tumor growth of *RET* transgenic mice was evaluated by macroscopic examination. Skin tumors were surgically removed and transferred into a 1.5 mL reaction tube. The tumor mass was measured. Subsequently, the tumor samples were snap frozen and stored at -80 °C.

3.2 Cell culture

3.2.1 Cell counting

The cell concentration was determined by diluting 10 µL of single cell suspension at a 1:10 ratio using trypan blue solution. 10 µL of the diluted single cell suspension

were used to count the cells using a Neubauer improved counting chamber. Only trypan blue-negative cells, referred to as living cells, were counted. The following equation was used to determine the total number of living cells per mL:

$$cell\ concentration\ [cells/mL] = \frac{\text{number of cells} \times 10\ \text{(dilution factor)} \times 10^4\text{(volume factor)}}{\text{number of squares}}$$

3.2.2 Isolation of mouse cells

Isolation of BM cells

Femurs and tibias of C57BL/6 WT mice were isolated using surgical instruments, cleansed with an ethanol-soaked tissue, and placed into a sterile cell culture dish containing RPMI complete medium. Isolation of TLR-deficient cells was performed together with Lennart Fritz. Under aseptic conditions, both ends of femurs and tibias were cut with sharp scissors. A 10 mL syringe with a 27G needle was used to flush out the bone marrow with phosphate-buffered saline (PBS). A 40 µm cell strainer was placed on top of a 50 mL conical tube, and the bone marrow suspension was transferred onto the cell strainer using a sterile disposable transfer pipette. With the plunger from the 10 mL syringe, the bone marrow was gently mashed through the cell strainer. The plunger end and the cell strainer were rinsed with PBS. The cell suspension was then centrifuged at 300 x *g* for 5 min at room temperature (RT).

Isolation of immature myeloid cells (iMCs) from bone marrow cells

To isolate iMCs using immunomagnetic negative selection, BM cells were resuspended in separation buffer, and the cell number was determined. IMCs were isolated using the Mouse MDSC (CD11b+Gr1+) Isolation Kit (Stemcell Technologies) according to the manufacturer's instructions. The elimination of undesired cell populations was achieved by using biotinylated antibodies that specifically bind to non-iMCs in combination with streptavidin-coated magnetic particles. For this, BM cells (1.0×10^8 cells/mL) were incubated with FcR blocking solution (40 µL/mL) and the antibody cocktail (50 µL/mL) in a 5 mL round-bottom tube for 10 min at RT. Then, the streptavidin-coated magnetic particles (75 µL/mL) were added. The samples were mixed and incubated for 5 min at RT. The volume was then increased to 2.5 mL with separation buffer. Subsequently, the tube was

placed into an EasyEights™ magnet. Following a 3-min incubation period, the enriched iMC suspension was carefully pipetted into a new tube.

Isolation of T cells from spleens

Under aseptic conditions, the spleen of a C57BL/6 mouse was isolated using surgical instruments and placed into a sterile cell culture dish containing PBS. The spleen was cut into small pieces with a scalpel, and the spleen fragments were transferred with a sterile disposable transfer pipette onto a 40 µm cell strainer positioned on a 50 mL conical tube. With a plunger of a syringe, the splenocytes were gently pressed through the cell strainer. Cold PBS was added to wash the splenocytes through the cell strainer. The cells were then centrifuged at 400 x *g* for 5 min at 4 °C and resuspended in 2 mL of cold RBC lysis buffer (1x). Following an incubation for 5 min at 4 °C, the cell suspension was washed with 10 mL of cold PBS and centrifuged at 400 x *g* for 5 min at 4 °C. The cell pellet was resuspended in separation buffer and $CD8^+$ T cells were isolated using the $CD8a^+$ T cell Isolation Kit, mouse (Miltenyi Biotec). The protocol provided by the manufacturer was followed. In brief, a mix of biotin-conjugated antibodies targeting CD4, CD11b, CD11c, CD19, CD45R, CD49b, CD105, MHC-II, Ter-119, and TCRγ/δ was used to negatively select $CD8^+$ T cells via magnetic separation.

3.2.3 Isolation of primary human cells

Isolation of peripheral blood mononuclear cells (PBMCs) from buffy coats

Under aseptic conditions, the buffy coat blood was transferred into 50 mL conical tubes and diluted 1:1 with sterile PBS. 30 mL of the diluted buffy coat blood was slowly layered onto 15 mL of Pancoll separating solution using a serological pipette. The cells were subsequently separated by centrifugation at 400 x *g* for 30 min at RT without applying brakes. The PBMC layer was harvested using a sterile disposable transfer pipette and transferred into a 50 mL conical tube. PBMCs were washed by adding PBS and subsequent centrifugation at 400 x *g* for 5 min. PBMCs were resuspended in 20 mL PBS for counting. Prior to further isolation steps, the cell suspension was centrifuged again at 400 x *g* for 5 min.

Isolation of monocytes from buffy coat-derived PBMCs

$CD14^+$ monocytes were isolated by positive selection with CD14 MicroBeads (Miltenyi Technologies) following the instructions provided by the manufacturer. The PBMC cell pellet was resuspended in 80 µL of separation buffer per 10^7 cells and 20 µL of CD14 MicroBeads per 10^7 cells was added. The cell suspension was mixed and incubated for 15 minutes at 4 °C. The cells were then washed by adding 10 mL MACS buffer and centrifuged at 300 x *g* for 5 min. The supernatant was aspirated, and the cell pellet was resuspended in 1 mL of separation buffer. An LS column was placed in the QuadroMACS™ separator and rinsed with 3 mL of the separation buffer. The cell suspension was then applied onto the LS column. The column was washed three times with 3 mL of separation buffer. Then, the column was removed from the separator and placed on top of a 15 mL conical tube. 5 mL of separation buffer were used to flush the $CD14^+$ monocytes out of the column.

Isolation of T cells from buffy coat-derived PBMCs

$CD3^+$ T cells were isolated by positive selection with CD3 MicroBeads (Miltenyi Biotec), according to the instructions provided by the manufacturer. Either the whole PBMC population or the $CD14^-$ fraction was used. The cells were resuspended in 80 µL of separation buffer per 10^7 cells and 20 µL of CD3 MicroBeads per 10^7 cells were added. The sample was mixed and incubated for 15 min at 4 °C. The cells were washed with 10 mL separation buffer and pelleted at 300 x *g* for 5 min. The pellet was resuspended in 1 mL of separation buffer. After placing an LS column into the QuadroMACS™ separator, it was rinsed with 3 mL of separation buffer. Subsequently, the cell suspension was loaded onto the column. The column was washed three times with 3 mL of separation buffer. The column was then removed from the separator and transferred to a 15 mL conical tube. 5 mL of separation buffer were used to flush the $CD3^+$ T cells into the tube.

3.2.4 Culture conditions

Cells were maintained at 37 °C in 5 % CO_2.

3.3 MicroRNA delivery

3.3.1 Transfection

A total of 5.0×10^5 cells were seeded in a 14 mL culture tube with 100 µL of transfection medium. For the short time until transfection, the cells were incubated under standard culture conditions. 30 pmol miR mimics (Qiagen) were diluted in 100 µL of Opti-MEM™ medium, and then 1 µL of HiPerFect transfection reagent was added to the diluted miR mimics. This mixture was shortly vortexed and incubated for 5 – 10 min at room temperature to allow the assembly of transfection complexes. Subsequently, the Opti-MEM™ medium containing the miR transfection complexes was added drop-wise to the cell solution. The tubes were gently swirled prior to incubating the cells with the transfection complexes for 3 h. Next, 400 µL of RPMI complete medium was added, resulting in a final miR concentration of 50 nM. Until analysis, the cells were kept in standard culture conditions.

3.3.2 Nanoparticles

All experiments involving the delivery of miRs via nanoparticles were carried out in the frame of a research stay at the laboratory of Prof. Licia Rivoltini (Fondazione IRCCS Istituto Nazionale dei Tumori, Milan, Italy). Empty nanoparticles as well as nanoparticles loaded with miR mimics were kindly provided. The amount of incorporated miR was measured by Alessandro Mereu, using a Qubit fluorometer (Thermo Fisher Scientific). The amount of nanoparticle solution required for a final miR concentration of 50 nM was then added for treatment of 1.0×10^6 human monocytes in 500 µL of RPMI complete medium. Accordingly, equal amounts of empty nanoparticles were used as a control. The cells were incubated for 48 h under standard culture conditions. All experiments were performed in collaboration with Alessandro Mereu and Nicola Cerioli under the supervision of Prof. Licia Rivoltini.

3.4 T cell suppression assay

The test was conducted in accordance with the established, standardized protocol (Cassetta et al., 2020). Each well of a 96-well cell culture plate (round-bottom) was coated with 1 µg/mL of anti-CD3 antibodies and 2 µg/mL of anti-CD28 antibodies (see 2.7.2 Functional antibodies for T cell activation) in 100 µL of PBS either for

3 hours at 37 °C or overnight at 4 °C. CD3 T cells were isolated from PBMCs obtained from healthy donors, as described above. Subsequently, T cells were labeled with 10 µM of Cell Proliferation Dye eFluor™ 450 (Thermo Fisher Scientific) in 500 µL of PBS, in accordance with the instructions provided by the manufacturer. CD3 T cells were washed with RPMI medium and resuspended in arginine-low medium. The coating solution was removed from the wells of a 96-well plate and 3.0×10^4 T cells in 50 µL of arginine-low medium were added per well. Human monocytes that were treated with miR mimics for 48 hours were centrifuged and resuspended in arginine-low medium. 6.0×10^4 monocytes per well in 50 µL of arginine-low medium were added to the T cell suspension.

The cells were co-cultured for 96 hours under standard culture conditions. Then, the plate was centrifuged at 300 x *g* for 5 minutes. The cell pellets were resuspended in 100 µL of FACS buffer, and the proliferation of T cells was evaluated by measuring the proliferation dye intensity per cell, using a BD FACSLyric™ flow cytometer or a CytoFLEX flow cytometer. FlowJo™ v10 was used for evaluation of the data. T cells that have not been activated with anti-CD3 and anti-CD28 as well as activated T cells in the absence of monocytes were used as controls. If the baseline proliferation of activated T cells obtained from different donors varied greatly, the proliferation values were normalized to untreated controls. To calculate the division index, the number of T cells per generation was first determined by defining each generation according to the signal intensity of the proliferation dye (viewed as one peak in the histogram). The statistics function of FlowJo™ v10 was used for determining the number of T cells. Then, the total number of divisions was calculated as follows:

$$No.\,of\ div. = \left(\frac{number\ of\ cells\ in\ generation\ 1}{2}\right) \times 1\ \left(\frac{number\ of\ cells\ in\ generation\ 2}{4}\right) \times 2 + \cdots$$

The total number of divisions was then divided by the total number of T cells analyzed.

3.5 Flow cytometry

3.5.1 Surface staining of mouse immature myeloid cells

2.0×10^5 cells were transferred into a well of a 96-well micro test plate (round-bottom), washed with FACS buffer, and pelleted for 5 min at 300 x g and 4 °C. The cell pellet was then resuspended in 50 µL of FACS buffer containing FcR blocking

reagent. Following a 5-min incubation period at 4 °C, 50 µL of FACS buffer containing the conjugated antibodies that specifically target the surface markers of interest were added (see 2.7.1 Antibodies for flow cytometry). The cells were incubated in the antibody mix for 20 min at 4 °C in the dark. Unbound antibodies were washed out with FACS buffer, and the cells were centrifuged for 5 min at 300 x *g* and 4 °C. The cell pellet was resuspended in 100 µL of PBS containing 7-aminoactinomycin D (7-AAD) staining solution. Following a 5-min incubation period at RT in the dark, the cells were analyzed with the BD FACSLyric™ flow cytometer. FlowJo™ v10 was used for evaluation of the data.

3.5.2 Staining of ROS

2.0×10^5 cells were transferred into a well of a 96-well micro test plate (round-bottom). CellROX® Deep Red reagent was added to the cells at a final concentration of 5 µM in RPMI medium. The cells were incubated for 30 min at 37 °C, pelleted for 5 min at 300 x *g* to remove the medium, and washed with PBS. The cells were finally resuspended in 100 µL of PBS for immediate analysis on a BD FACSLyric™ flow cytometer. FlowJo™ v10 was used for evaluation of the data.

3.5.3 Surface staining of human monocytes

Surface staining of nanoparticles-treated monocytes was performed in collaboration with Alessandro Mereu and Nicola Cerioli under the supervision of Prof. Licia Rivoltini. $2.0 - 5.0 \times 10^5$ cells were transferred into a 5 mL round-bottom tube and centrifuged for 10 min at 300 x *g* at RT. The supernatant was poured off, and the cells were resuspended in the remaining medium. FcR blocking reagent was added to the cells, which were then incubated for 10 min at RT in the dark. Next, conjugated antibodies (see 2.7.1 Antibodies for flow cytometry) were added to the cell suspension. Following a 20-min incubation period at RT in the dark, the cells were washed with PBS. The cell suspension was centrifuged for 10 min at 300 x *g* and RT, and the cell pellet was resuspended in 100 µL PBS. Analysis was performed on a CytoFLEX flow cytometer. Kaluza Analysis v2 was used for evaluation of the data.

3.5.4 Intracellular staining of human monocytes

Intracellular staining of transfected human monocytes was performed, using the BD Phosflow™ Fix buffer I and the BD Phosflow™ Perm buffer III. Prior to use, the BD Phosflow™ Fix buffer I was warmed to 37 °C, and the BD Phosflow™ Perm buffer III was chilled to -20 °C. 5.0×10^5 cells were fixed in 100 µL of the BD Phosflow™ Fix buffer I for 10 min at 37 °C. Subsequently, the cells were washed with FACS buffer and centrifuged for 10 min at 400 x *g*. Permeabilization was performed by incubating the cells in 200 µL of BD Phosflow™ Perm buffer III for 20 min on ice. The cells were then washed twice with FACS buffer before being resuspended in 100 µL containing conjugated anti-pSTAT3 antibodies. Following a 30-minutes incubation period at RT and in the dark, cells were washed and resuspended in 100 µL of FACS buffer for analysis on a BD FACSLyric™ flow cytometer. FlowJo™ v10 was used for evaluation of the data.

Intracellular staining of nanoparticles-treated monocytes was performed in collaboration with Alessandro Mereu and Nicola Cerioli under the supervision of Prof. Licia Rivoltini. Fixation/Permeabilization Concentrate (Thermo Fisher Scientific) was diluted with Fixation/Permeabilization Diluent (Thermo Fisher Scientific) according to the manufacturer's instructions. The solution was then filtered through a 0.22 µm syringe filter. Following extracellular staining, 5.0×10^5 monocytes were washed with PBS and centrifuged for 10 min at 300 x *g* and RT. The cell pellet was resuspended in 0.5 mL of Fixation/Permeabilization buffer and incubated for 40 min on ice. Then, the cells were washed with FACS buffer and resuspended in 100 µL of FACS buffer. Following a 30-min incubation period with conjugated antibodies targeting pSTAT3 (pY705) on ice, the cells were washed with FACS buffer and resuspendend in 100 µL of FACS buffer for analysis on a CytoFLEX flow cytometer. Kaluza Analysis v2 was used for evaluation of the data.

3.6 RNA isolation

3.6.1 Total RNA >200 nucleotides

3.0×10^6 iMCs were harvested for total RNA isolation using the RNeasy Mini Kit (Qiagen) according to the manufacturer's instructions. In brief, cells were lysed and homogenized, and the lysis product was loaded onto a silica-based membrane. An

on-column DNAse digestion with the RNAse-free DNase set (Qiagen) was performed. Contaminants were washed away, and the RNA was eluted with 30 µL nuclease-free water. RNA samples were stored at -80 °C.

3.6.2 Total RNA including smaller RNA species

For microRNA isolation from tumor samples, the miRNeasy Mini Kit (Qiagen) was used. 50 mg flash-frozen tumor tissue was thawed and placed into 700 µL of QIAzol lysis reagent (Qiagen). The tissue was disrupted and homogenized using a TissueLyser (Qiagen) and appropriate tubes containing a stainless-steel bead. Chloroform was added to the homogenate, and phase separation was accomplished by centrifugation according to the manufacturer's instructions. The aqueous phase was mixed with ethanol, the sample was transferred to a RNeasy Mini spin column, and the RNA was isolated by following the protocol provided by the manufacturer. 30 µL RNase-free water was used to elute the RNA. RNA samples were stored at -80 °C.

For microRNA isolation from plasma samples, the miRNeasy Serum/Plasma Kit (Qiagen) was used. Flash-frozen plasma was thawed at RT and centrifuged for 5 min at 1600 x *g* and 4 °C. 200 µL of the supernatant were used for RNA isolation according to the manufacturer's instructions. 14 µL RNase-free water were used to elute the RNA. RNA samples were stored at -80 °C.

3.7 Reverse transcription and qPCR

3.7.1 Quantification of mRNA

The concentration of RNA samples was determined using the Infinite M200 microplate reader (Tecan) with a NanoQuant Plate™. 500 ng of RNA was used for reverse transcription using the SensiFAST™ cDNA synthesis kit (Bioline) according to the manufacturer's instructions. The following controls were employed: a "no RT" control containing RNA but no reverse transcriptase and a "no template" control containing reverse transcriptase but no RNA. Quantitative PCR was performed using the SensiFAST™ SYBR® Lo-ROX Kit (Bioline) and the real-time PCR system MX3005 (Stratagene).

3.7.2 Quantification of microRNA

Reverse transcription reactions for miR quantification were set up with the miRCURY LNA RT Kit (Qiagen). RNA samples from tumor tissues were measured, using the Infinite M200 microplate reader (Tecan) with a NanoQuant Plate™, and adjusted to 5 ng/µL. The protocol “miRCURY LNA microRNA PCR assays” was followed for reverse transcription. A synthetic RNA-spike in control (Qiagen) was used according to the instructions of the manufacturer. For RNA isolated from plasma, 1.12 µL eluate (equivalent to the RNA amount isolated from 16 µL of plasma sample) were used, and the protocol “miRCURY LNA Focus PCR Panel – serum/plasma” was followed. A synthetic RNA-spike in control (Qiagen) was used according to the instructions of the manufacturer.

Analysis of miR from tumor tissue was performed using the miRCURY LNA SYBR® Green PCR Kit (Qiagen) according to the “miRCURY® LNA® microRNA SYBR® Green PCR Handbook”. Analysis of miR from plasma samples was performed using the miRCURY LNA SYBR® Green PCR Kit (Qiagen) according to “miRCURY® LNA® microRNA SYBR® Green PCR – Exosomes, Serum/Plasma, and Other Biofluid Samples Handbook”.

3.8 Gene expression analysis

RNA samples were submitted to the Microarray Core Facility at the DKFZ, Heidelberg. The Affymetrix GeneChip™ Mouse Gene 2.0 ST Array (Thermo Fisher Scientific) was used for the analysis. Raw data were submitted to Dr. Carolina De La Torre (NGS Core Facility, Medical Faculty Mannheim, Heidelberg University) for bioinformatic and statistical analysis. A log2 transformation was used, and a quantile normalization and robust multiarray analysis (RMA) was performed for background correction. A previously described empirical Bayes approach was used to identify differentially expressed genes (Smyth, 2004), which was implemented in the R/Bioconductor software package *limma* (Ritchie et al., 2015). Furthermore, gene set enrichment analysis (GSEA) (Subramanian et al., 2005) and Kyoto Encyclopedia of Genes and Genomes (KEGG) functions analysis (Kanehisa and Goto, 2000) were performed.

3.9 ELISA

The Mouse IL-6 ELISA MAX Deluxe Set (Biolegend) was used according to the manufacturer's instructions to measure the IL-6 concentration in cell culture supernatant. Samples were diluted 1:1 in PBS. All standards and samples were run in triplicate.

3.10 Western Blotting

Western blotting of samples obtained from transfected monocytes was performed together with Nina Gutzeit.

3.10.1 Protein isolation

2.5×10^6 monocytes were harvested 48 hours after transfection. The cells were washed with PBS and centrifuged for 10 min at 400 x *g* and 4 °C. The cell pellet was resuspended in 300 µL of cold RIPA buffer and incubated for 30 min on ice. In between, the samples were vortexed carefully. The lysates were centrifuged for 15 min at 16,000 x *g*. The supernatant containing proteins was transferred to a new tube.

3.10.2 Bicinchoninic acid (BCA) assay

Pierce® BCA Protein Assay Kit (Thermo Fisher Scientific) was used for determining the protein concentration of the lysates. The protocol provided by the manufacturer was followed. The albumin standard was diluted to the following concentrations: 2000, 1500, 1000, 750, 250, 125, and 25 µg/mL in PBS. The samples were diluted 1:1 in PBS. All standards and samples were run in triplicate. The absorbance was measured using the Infinite M200 microplate reader (Tecan).

3.10.3 Gel electrophoresis

The lysate was diluted 3:1 in 4x NuPAGE™ LDS sample buffer (Thermo Fisher Scientific) containing 5 % 2-mercaptoethanol. The sample was boiled for 5 min at 95 °C in a block heater. 4-15% Mini-PROTEAN protein gels (Bio-Rad) were placed in a Mini-PROTEAN® 3 Vertical Electrophoresis Cell (Bio-Rad), filled with running buffer. Equal amounts of total protein (different lysate volumes) were loaded. 7 µL

of PageRuler Protein ladder prestained (Thermo Fisher Scientific) was used as molecular weight markers. The gel was run at 70 V for 10 min, then the voltage was increased to 100 V for approximately 60 min (until the tracking dye reached the bottom of the gel). Ponceau S staining was performed to determine total protein levels.

3.10.4 Blotting and immunostaining

A semi-dry transfer method was used for blotting the protein samples. The protein gel was equilibrated in transfer buffer, while a membrane and gel-sized filter papers were prepared. A polyvinylidene-difluoride (PVDF) blotting membrane was incubated in methanol for 1 min. Subsequently, the membrane was rinsed with water and placed in a container filled with transfer buffer. Filter papers were soaked with transfer buffer and placed on the plate electrode of a semi-dry blotting chamber. The membrane was placed on top of the filter paper stack, followed by the protein gel. Another stack of filter papers was placed on top of the gel. Air bubbles were carefully removed by rolling a serological pipette over the filter paper on top. The second plate electrode was placed onto the transfer sandwich, and the transfer was run at 60 mA/gel for 90 min.

Following the electroblotting, the membrane was incubated in 12 mL of EveryBlot Blocking Buffer (Bio-Rad) for 5 min with agitation. The membrane was next incubated in 12 mL of blocking buffer containing the primary antibody (see 2.7.3 Primary antibodies for western blotting) at 4 °C overnight. The antibody solution was removed, and the membrane was washed three times with TBST buffer for 10 min on an orbital shaker. The membrane was next incubated in blocking buffer containing the secondary antibody for 1 h at RT with agitation. The antibody solution was removed, and the membrane was washed three times with TBST buffer for 10 min on an orbital shaker. Finally, the membrane was incubated in ECL substrate according to the manufacturer's instructions, and chemiluminescent signals were measured using the imaging system Fusion SL4 and the FusionCapt Advance SL4 software.

3.11 Statistical analysis

A statistical analysis of the data was conducted on a minimum of three biological replicates. The GraphPad Prism software was used for data analysis. Two experimental groups were compared with paired two-tailed Student's t test assuming a Gaussian distribution of the data. More than two experimental groups were compared by analysis of variance (ANOVA), followed by multiple comparison of each experimental group with every other experimental group. For correlation analysis, Pearson correlation coefficient was calculated.

4 RESULTS

4.1 Optimizing microRNA transfection of iMCs

The lipid-based transfection method was established to deliver miR mimics into myeloid cells, serving as a model system for studying the effects of exogenous introduced miR on MDSC generation. This approach was favored over alternative transfection methods for delivering small RNA molecules into myeloid cells due to its superior efficiency and low toxicity (Ng et al., 2012).

$CD11b^{+}Gr1^{+}$ iMCs isolated from the BM of healthy mice were used as a source of myeloid cells due to their potential to be pathologically activated and to acquire MDSC characteristics. The viability of iMCs following a 20-h exposure to different volumes of the HiPerFect transfection reagent (Qiagen) was verified by 7-AAD exclusion using flow cytometry (Fig. 1). 7-AAD negative cells were selected based on the fluorescence intensity of unstained cells (Fig. 1A). 7-AAD negative cells were defined as viable cells. Untreated iMCs and treated iMCs with up to 6 µL of the transfection reagent showed 90 – 91 % 7-AAD negative cells (Fig. 1B). Nevertheless, relatively high amounts of cell debris were observed (Fig. 1A). Importantly, there was also only minor variation in the amount of cell debris across the conditions. Following the incubation period, untreated cells showed equal proportions of cell debris, while this was not observed in samples of the freshly isolated iMCs (Fig. 1C). Therefore, this effect could be attributed to the cultivation process of the cells.

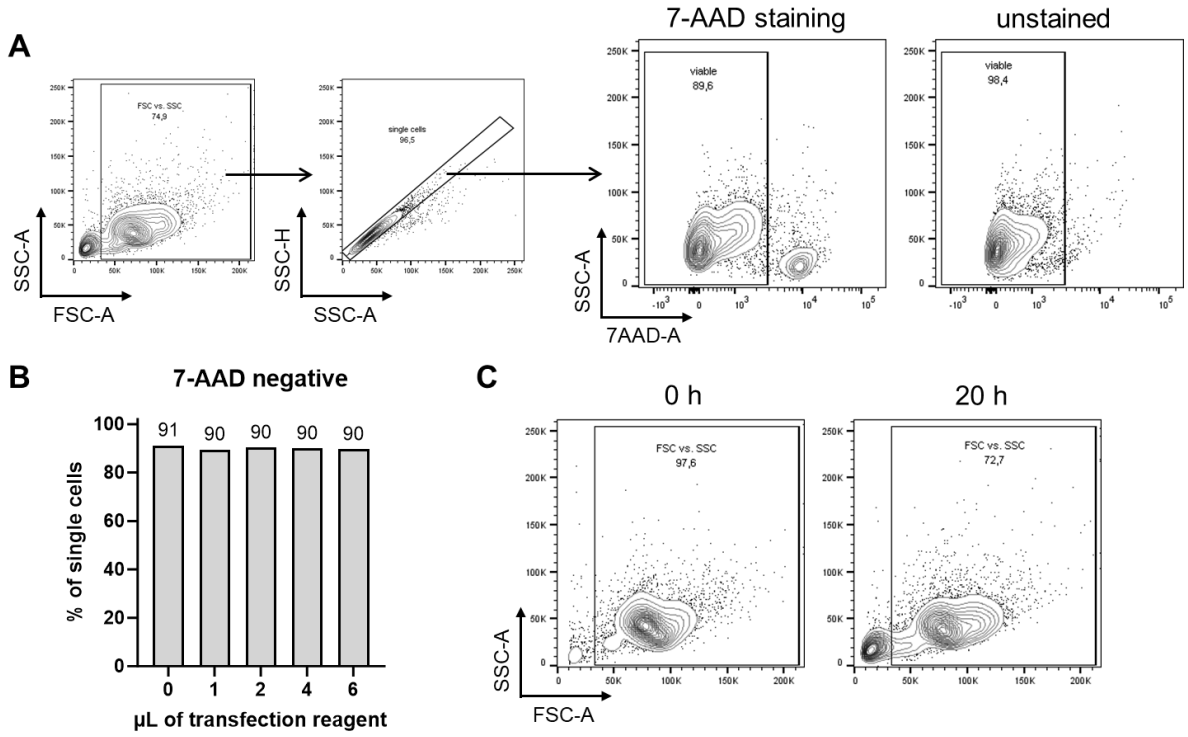

Figure 1: Viability of iMCs upon exposure to HiPerFect transfection reagent. IMCs were isolated from the BM of healthy mice based on co-expression of CD11b and Gr1 following treatment with different volumes of HiPerFect transfection reagent for 20 hours. The impact of the HiPerFect transfection reagent treatment on the viability of iMCs was assessed using flow cytometry. **A** The gating strategy to determine the frequency of viable cells (defined as 7-AAD negative cells) is shown for iMCs following exposure to 6 µL of HiPerFect transfection reagent as an example. **B** The frequencies of 7-AAD negative iMCs upon 20-hour exposure to different volumes of HiPerFect transfection reagent is shown. **C** The accumulation of cell debris after 20-hour incubation of untreated iMCs is shown in comparison to freshly isolated iMCs.

Since PD-L1 was utilized as an MDSC-related marker, the effect of different transfection reagent volumes on PD-L1 expression was investigated (Fig. 2). Flow cytometric analysis was performed by gating the population of viable cells (Fig. 1A), selecting iMCs based on CD11b and Gr1 co-expression, and distinguishing PD-L1 expressing cells using an isotype control (Fig. 2A). When compared to untreated iMCs, exposure to 1 µL of the transfection had no substantial effect on PD-L1 expression, while exposure to 2 – 6 µL of the transfection reagent resulted in an upregulation of PD-L1 (Fig. 2B-C).

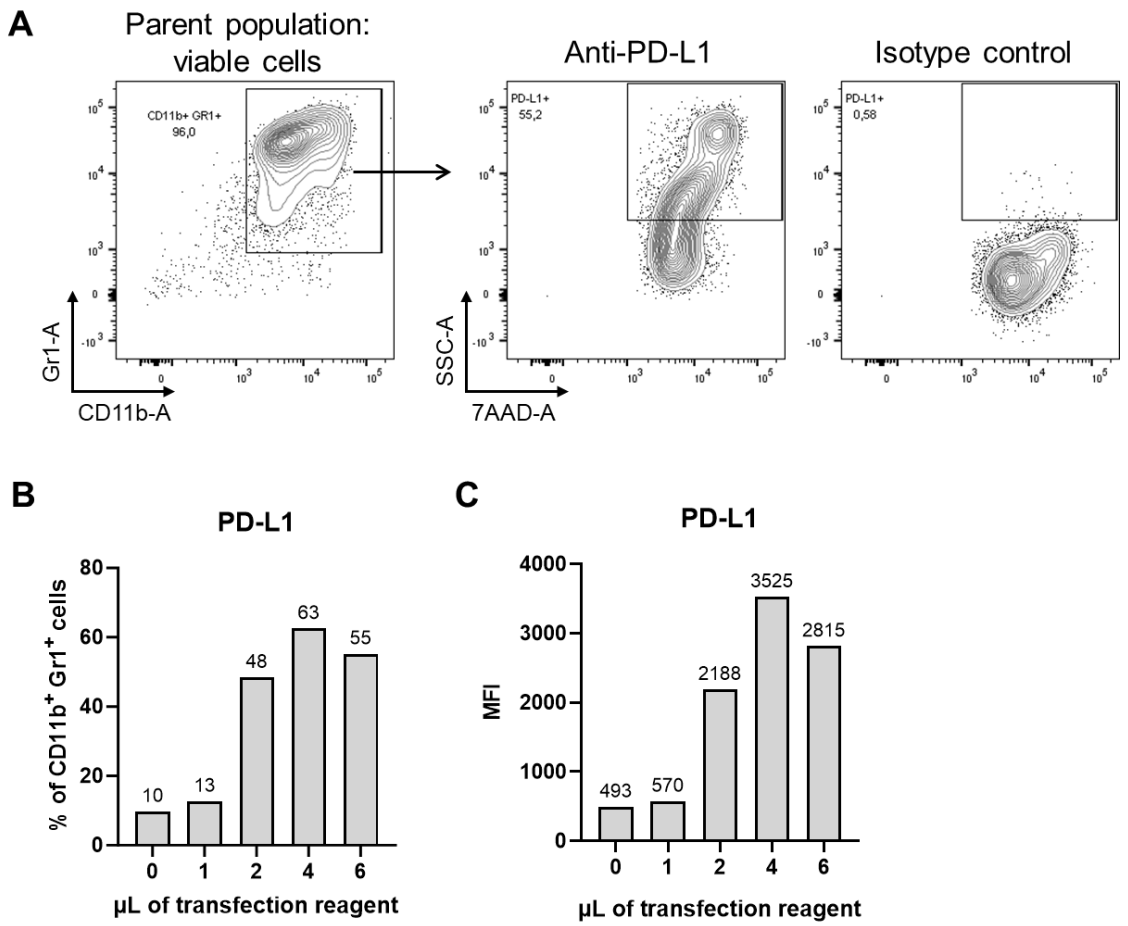

Figure 2: PD-L1 expression in iMCs treated with HiPerFect transfection reagent. IMCs from healthy mice were treated with different volumes of HiPerFect transfection reagent for 20 h. PD-L1 expression in iMCs was assessed using flow cytometry. **A** Viable cells were gated as shown before. IMCs were then identified as CD11b and Gr1 co-expressing cells. The gating of PD-L1 expressing iMCs in comparison to an isotype control is shown exemplary for iMCs treated with 6 µL of HiPerFect transfection reagent. **B** The frequencies of 7-AAD negative iMCs upon 20-h exposure to different volumes of HiPerFect transfection reagent is shown. **C** The accumulation of cell debris after the incubation of untreated iMCs for 20 h is shown in comparison to freshly isolated iMCs.

The transfection efficiency of a Cyanine3 (Cy3)-labeled miR mimic was assessed for different amounts of the transfection reagent (Fig. 3). The proportion of Cy3-positive iMCs exceeded 90% when 1 µL of the transfection reagent was used; it further increased to 99% as the transfection reagent volume increased (Fig. 3A). The maximum MFI of Cy3 was seen when 2 µL of the transfection reagent was used (Fig. 3B). Overall, even with minimal transfection reagent amount, it was possible to to introduce similar amounts of labeled miR into the cells. Nevertheless, it is important to point out that this evaluation was conducted with the premise that the fluorescence signal directly correlated with the quantity of miR taken up by the cells. However, the used technique was unable to directly track the cellular localization of the molecules.

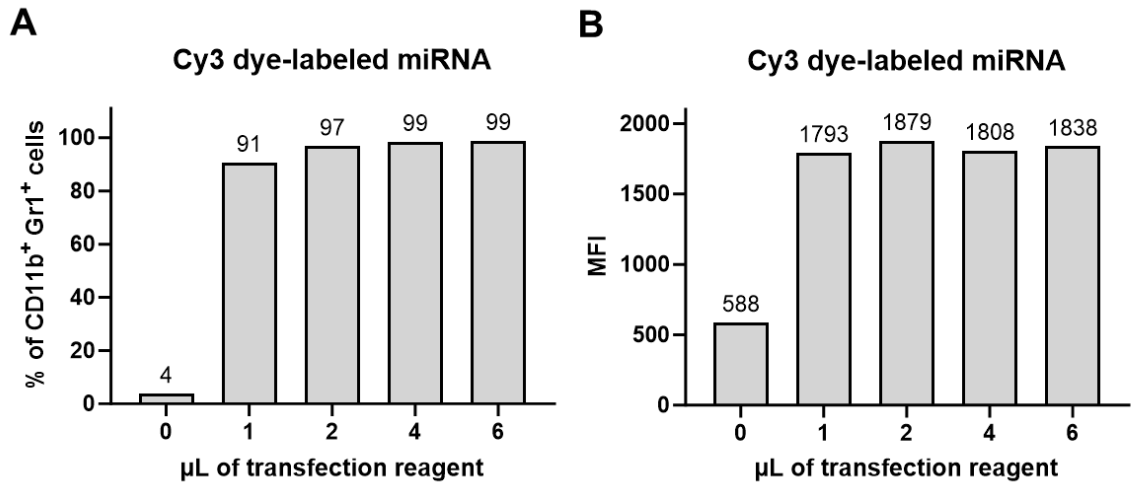

Figure 3: Efficiency of the transfection of iMCs with a Cyanine3-labeled microRNA mimic. IMCs from healthy mice were transfected with Cyanine3 (Cy3)-labeled miR mimics (50 nM), using different volumes of HiPerFect transfection reagent, as indicated on the x-axis. The fluorescent signal of the cells through Cy3-labeled miR uptake was measured by flow cytometry. **A** The frequencies of Cy3-positive iMCs 20 h after transfection with different volumes of HiPerFect transfection reagent is shown. **C** The median fluorescence intensity (MFI) of iMCs 20 h after transfection with different volumes of HiPerFect transfection reagent is shown.

Since 1 µL of the transfection reagent alone did not stimulate PD-L1 expression in iMCs and appeared to effectively deliver miR mimics, I decided to continue using this amount for transfecting the cells.

4.2 Effects of melanoma EV-associated miRs on PD-L1 expression in mouse iMCs

MiR-146a, -146b, -155, -125a, -125b, -100, -99b, and let-7e (MDSC-miR set) have been reported to be enriched in plasma EVs, in peripheral blood monocytes, and in tumors of melanoma patients (Huber et al., 2018). In addition, this study revealed that the MDSC-miR set was pivotal in the conversion of classical $CD14^+$ human monocytes to MDSCs driven by melanoma EVs. The MDSC-miR set was also demonstrated to trigger MDSC characteristics, including PD-L1 expression, upon transfection (Huber et al., 2018). To get a better understanding of the different miRs comprising the MDSC-miR set, I first sought to elucidate their specific roles in the pathological activation of normal myeloid cells. For this purpose, iMCs were transfected with individual mimics of the MDSC-miR set and analyzed after 20 h of incubation. I utilized PD-L1 as a marker to identify a MDSC-like phenotype, as it has

been shown to be a key immunosuppressive molecule in EV-induced MDSCs (Fleming et al., 2019).

Transfecting iMCs with mimics of miR-125a-5p, -125b-5p, or -99b-5p led to an increase in PD-L1 expressing iMCs (Fig. 4). Transfection of miR-125a-5p or miR-125b-5p mimics had a strong impact on iMCs, with upregulation of PD-L1 in 68 % and 65 % of iMCs, respectively. Stimulation with mimics of miR-99b-5p resulted in a weaker induction of PD-L1 expression: an average of 41 % of iMCs expressed PD-L1 after transfection. MiR mimic negative control (mimic NC) and mimics of miR-146a-5p, -146b-5p, -155-5p, -100-5p, or let-7e-5p did not have significant effects on PD-L1 expression in iMCs.

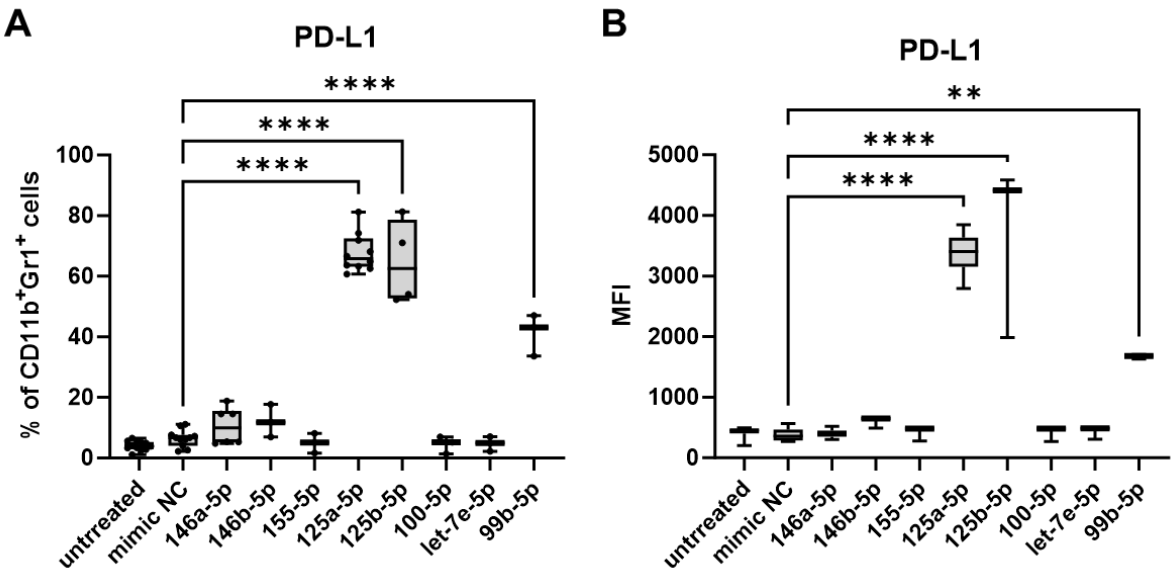

Figure 4: Expression of PD-L1 in iMCs upon transfection with mimics of various melanoma-associated microRNAs. Immature myeloid cells (iMCs) from healthy mice were transfected with different miR mimics (each 50 nM) as indicated on the x-axis. Untreated iMCs and iMCs transfected with 50 nM miR mimic negative control molecules (mimic NC) were used as controls. **A** The frequencies of PD-L1 positive iMCs 20 h after transfection with different miR mimics is shown. **B** The median fluorescence intensity (MFI) of iMCs 20 h after transfection with different miR mimics is shown. Box-and-whiskers plots: min to max; all data points are shown; the horizontal line is plotted at the median. N = 3-10. Analysis of variance and multiple comparisons were performed (**p<0.01, ****p<0.0001).

It was particularly intriguing that miR-125a-5p exerted a very potent effect on the cells, given that previous research in our group identified miR-125a-5p as one of the most prevalent miRs in EVs derived from the *RET* melanoma cell line (Fleming, unpublished data). Moreover, miR-125a-5p was highly elevated in iMCs that had been exposed to *RET* melanoma cell-derived EVs *in vitro* (Fleming, 2018) as well

as in MDSCs isolated from the tumors of *RET* transgenic mice (Hu, unpublished data). Taken together, these findings suggested that miR-125a-5p might substantially contribute to the EV-mediated generation of MDSCs in melanoma. Thus, the effects caused by miR-125a-5p and their underlying mechanism became the main focus of my research.

4.3 Expression of miR-125a-5p in the mouse melanoma microenvironment

To further validate the relevance of miR-125a-5p in melanoma, I determined the quantity of miR-125a-5p in the TME as well as in the circulation of melanoma-bearing mice. For this purpose, I collected tumor and plasma samples from *RET* transgenic mice, which spontaneously develop tumors resembling melanoma (Kato et al., 1998). Using a miR-125a-5p PCR assay, an endogenous miR control PCR assay as well as a spike-in control PCR assay, relative expression of miR-125a-5p was measured by qPCR and its association with the skin tumor weight (as an indicator of melanoma progression) was analyzed. Interestingly, a positive correlation between miR-125a-5p abundance in the TME and tumor progression could be observed (Fig. 5A). In contrast, there was no association between the amount of miR-125a-5p in the plasma and the tumor progression (Fig. 5B).

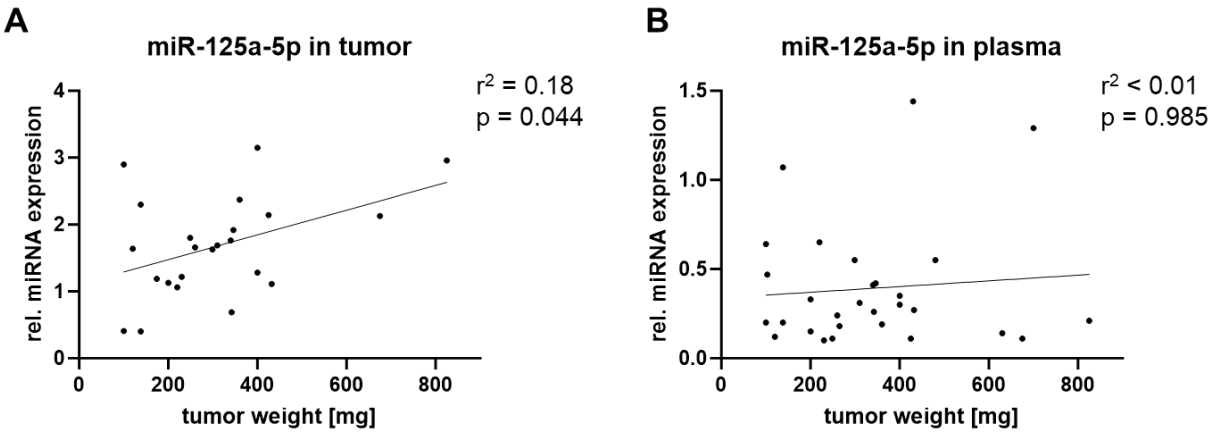

Figure 5: Expression of miR-125a-5p in tumor-bearing *RET* transgenic mice. Tumor and plasma samples were collected from *RET* transgenic mice. MiR-125a-5p was measured by qRT-PCR. UniSp6 (spike-in control) and miR-103 (endogenous microRNA control) were used to calculate relative (rel.) expression levels. The correlation between the tumor progression and the rel. expression levels of miR-125a-5p in the tumor (**A**) and in the plasma (**B**) is shown. Pearson correlation analysis of tumor weight vs. rel. expression of miR-125a-5p was performed with ΔCT values (n = 23-29).

4.4 Effects of exogenous miR-125a-5p on mouse iMCs

4.4.1 Transcriptional profiling of mouse iMCs transfected with miR-125a-5p mimics

Next, I studied how miR-125a-5p could alter polarization and function of myeloid cells. Using microarray analysis, differences in gene expression between iMCs transfected with mimics of miR-125a-5p or mimic negative control were assessed (Fig. 6). IMCs treated with miR-125a-5p mimics displayed increased gene expression levels of factors known to be associated with MDSC function or recruitment, including *Cd274* (encodes PD-L1), *Nos2* (encodes iNOS), *Mmp13*, *Il10*, *Il6*, *Ccl2*, *Ccl7*, and *Ccl12* (Fig. 6A). Expression of *Slamf6* and *Slamf9* was also increased in miR-125a-5p mimic-treated iMCs.

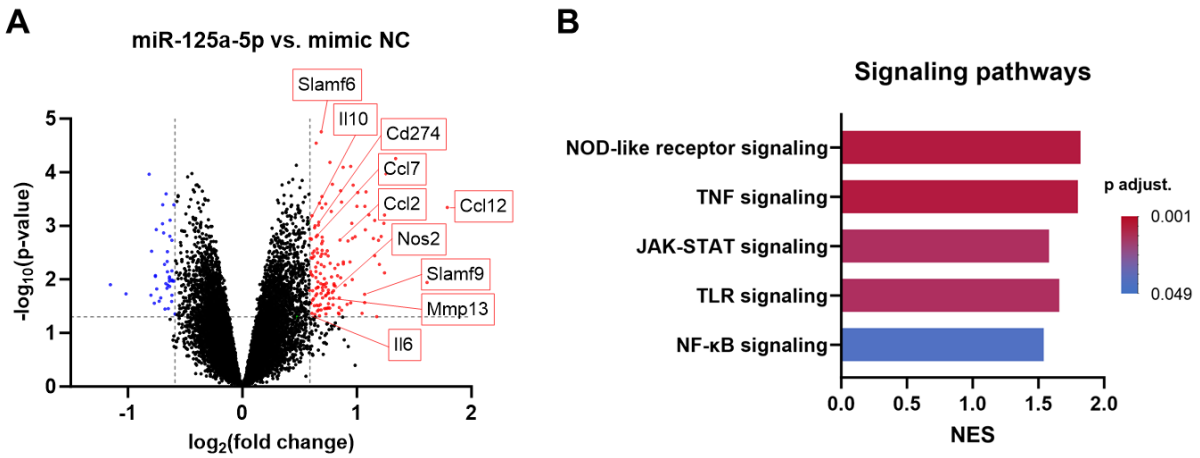

Figure 6: Transcriptional analysis of iMCs transfected with miR-125a-5p mimics. IMCs from healthy mice were transfected with miR-125a-5p mimics or with miR mimic negative control molecules (mimic NC). Differences in gene expression between miR-125a-5p-treated iMCs and mimic NC-treated iMCs after 20 h were analyzed. **A** Gene expression in miR-125a-5p-treated iMCs compared to gene expression in mimic NC-treated iMCs is shown in a volcano plot. MDSC-related genes are labeled. Blue dots show expression values downregulated in miR-125a-5p-treated iMCs compared to mimic NC-treated iMCs. Red dots show expression values upregulated in miR-125a-5p-treated iMCs compared to mimic NC-treated iMCs. **B** Normalized enrichment scores (NES) for signaling pathways associated with changes in miR-125a-5p-treated iMCs identified by gene set enrichment analysis are shown. The color of the bars implies the adjusted p-value (p adjust., n = 3).

A gene set enrichment analysis was used to further evaluate the microarray data and acquire insights into biological processes induced by miR-125a-5p mimic in iMCs. Particularly, annotated signaling pathways were screened to obtain information about the molecular mechanisms by which miR-125a-5p could act on iMCs. Gene sets that can be assigned to NOD-like receptor signaling, TNF

signaling, JAK-STAT signaling, TLR signaling, or NF-κB signaling were significantly enriched in the miR-125a-5p mimic group versus the mimic NC group (Fig. 6B).

4.4.2 Expression of MDSC-related factors in mouse iMCs induced by exogenous miR-125a-5p

I evaluated the upregulation of genes associated with MDSC functions by qPCR. Transcriptional analysis showed a significant increase in the expression of *Cd274*, *Il6*, *Il10*, and *Nos2* in iMCs transfected with miR-125a-5p compared to mimic NC-treated iMCs (Fig. 7A). Moreover, IL-6 protein levels were markedly increased: the average IL-6 concentration was elevated 7.5-fold in conditioned medium of miR-125a-5p mimic-treated iMCs compared to mimic NC-treated iMCs (Fig. 7B). In mouse bone marrow cells, IL-6 was demonstrated to increase the production of ROS, acting as a factor associated with immunosuppressive capacity by MDSCs (Weber et al., 2020). Therefore, I tested the impact of miR-125a-5p mimics on the production of ROS in iMCs. ROS levels were also found to be increased in iMCs transfected with miR-125a-5p compared to mimic NC-treated iMCs (Fig. 7C).

In sum, these results indicated that iMCs polarized towards MDSC-like cells upon exposure to miR-125a-5p mimics. IMCs stimulated with exogenous miR-125a-5p produced factors that are closely related to MDSC functions, including PD-L1, IL-6, and ROS.

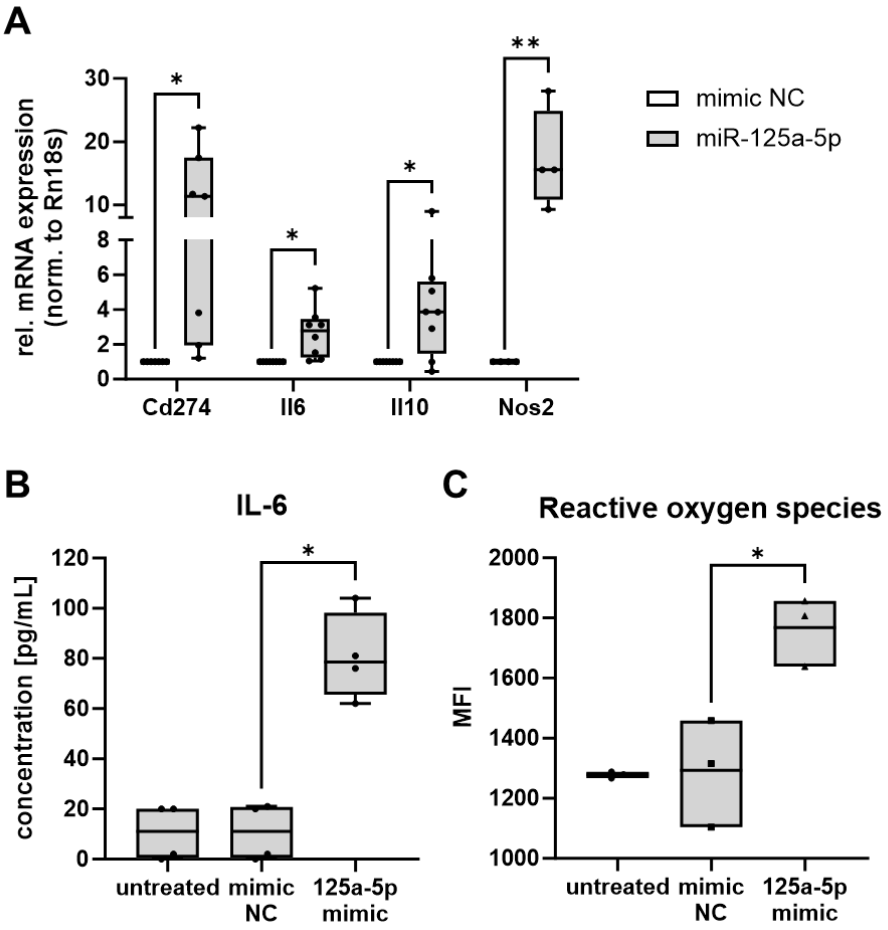

Figure 7: Expression of MDSC-related factors in iMCs upon transfection with miR-125a-5p mimics. IMCs from healthy mice were transfected with miR-125a-5p mimics or with miR mimic negative control molecules (mimic NC) and incubated for 20 h. Untreated iMCs were used as additional control **A** Expression of the genes indicated on the x-axis were analyzed in miR-125a-5p mimic-treated iMCs relative (rel.) to mimic NC-treated iMCs after 20 h. Expression data of *Rn18s* were used for normalization. Paired two-tailed student's t test was performed with ΔCT values (norm., n = 4-8, *p<0.05, **p<0.01). **B** Concentration of IL-6 in the conditioned medium of iMCs transfected with miR-125a-5p mimics or mimic NC, as well as untreated iMCs, was measured after 20 h by ELISA. Analysis of variance and multiple comparisons were performed (n = 4, *p<0.05). **C** Production of ROS in iMCs transfected with miR-125a-5p mimics or mimic NC, as well as untreated iMCs, was determined by flow cytometry, using the CellROX deep red reagent. Median fluorescence intensity of iMCs incubated for 20 h is shown. Analysis of variance and multiple comparisons were performed (n = 3-8, *p<0.05). **A-C** Box-and-whiskers plots: min to max; all data points are shown; the horizontal line is plotted at the median.

4.5 Investigation of mechanisms underlying miR-125a-5p-mediated effects in mouse iMCs

4.5.1 Exogenous miR-125a-5p mediates the upregulation of PD-L1 via NF-κB activation in mouse iMCs

The NF-κB signaling pathway serves as an essential mechanism in the activation of MDSCs, especially of the M-MDSC subset (Condamine et al., 2015). Hence, I investigated its role in the regulation of iMCs by miR-125a-5p. BAY-11-7082 and BOT-64 are inhibitors of IKKβ, a key component of the NF-κB activation cascade (Kim et al., 2008; Lee et al., 2012). Both inhibitors of IKKβ were tested for their effects on PD-L1 expression in iMCs, which was used as a marker for MDSC-like polarization (Fig. 8). To examine the effect of NF-κB blockage, transfected iMCs were incubated either in the presence of DMSO or in the presence of the inhibitor in DMSO. Importantly, the applied concentrations of the inhibitors did not induce a substantial reduction in the viability of the cells. In the miR-125a-5p-transfected and DMSO-treated group, an average of 39 % of iMCs expressed PD-L1 (Fig. 8). In the presence of BAY-11-7082 or BOT-64, an average of 13 – 14 % of iMCs expressed PD-L1 upon miR-125a-5p transfection.

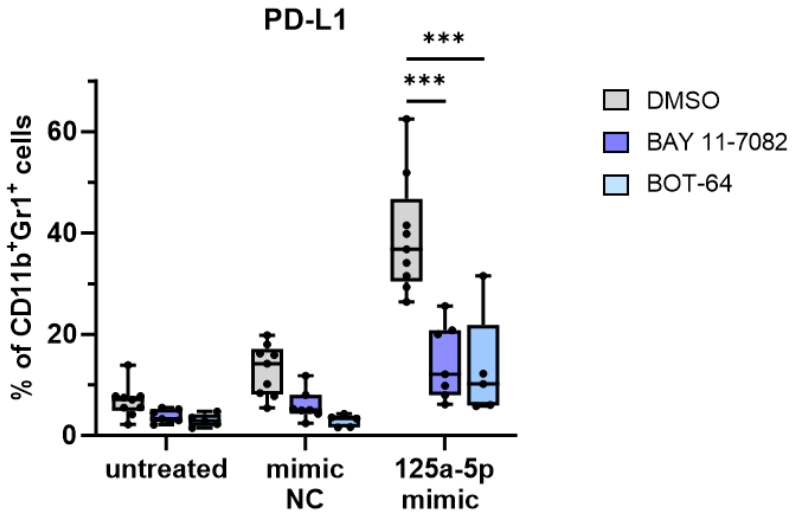

Figure 8: Expression of PD-L1 in miR-125a-5p mimic-treated iMCs in the presence or absence of NF-κB activation inhibitors. IMCs from healthy mice were treated with dimethyl sulfoxide (DMSO, solvent control), NF-κB inhibitors BAY 11-7082 (1 µM) or BOT-64 (5 µM) and transfected with miR-125a-5p mimics or miR mimic negative control molecules (mimic NC). Untransfected (untreated) iMCs were used as an additional control. Following 20 h of incubation, the expression of PD-L1 in iMCs was measured by flow cytometry. **A** The frequencies of PD-L1 expressing cells are shown. **B** The median fluorescence intensities (MFI) are shown. **A&B** Box-and-whiskers plots: min to max; all data points are shown; the horizontal line is plotted at the median. Analysis of variance and multiple comparisons were performed (n = 5-9, ***p<0.001).

4.5.2 Endosomal TLRs are not required for miR-125a-5p-mediated upregulation of PD-L1 in mouse iMCs

Certain tumor-derived miRs have been shown to directly interact with endosomal TLRs of macrophages, resulting in the activation of NF-κB and the secretion of IL-6 and TNF-α (Fabbri et al., 2012). Therefore, I aimed to examine whether the miR-125a-5p-mediated effects on iMCs could be induced through a mechanism involving endosomal TLRs. The PD-L1 expression was measured to assess the response of iMCs to miR-125a-5p in the presence or absence of endosomal TLRs (Fig. 9). IMCs isolated from TLR7$^{-/-}$, TLR8$^{-/-}$, or TLR3$^{-/-}$TLR7$^{-/-}$TLR9$^{-/-}$ mice responded to miR-125a-5p stimulation to a similar extent as iMCs obtained from WT mice (Fig. 9A-C). Due to the unavailability of cells lacking all endosomal TLRs, iMCs from mice deficient in the adapter molecules MyD88 and TRIF, which are crucial for TLR downstream signaling (Kawasaki and Kawai, 2014), were utilized. PD-L1 upregulation was comparable in MyD88-deficient iMCs stimulated with miR-125a-5p mimics to that in WT-iMCs (Fig. 9D). However, iMCs lacking both MyD88 and TRIF showed a modest reduction in miR-125a-5p-induced PD-L1 expression (Fig. 9D).

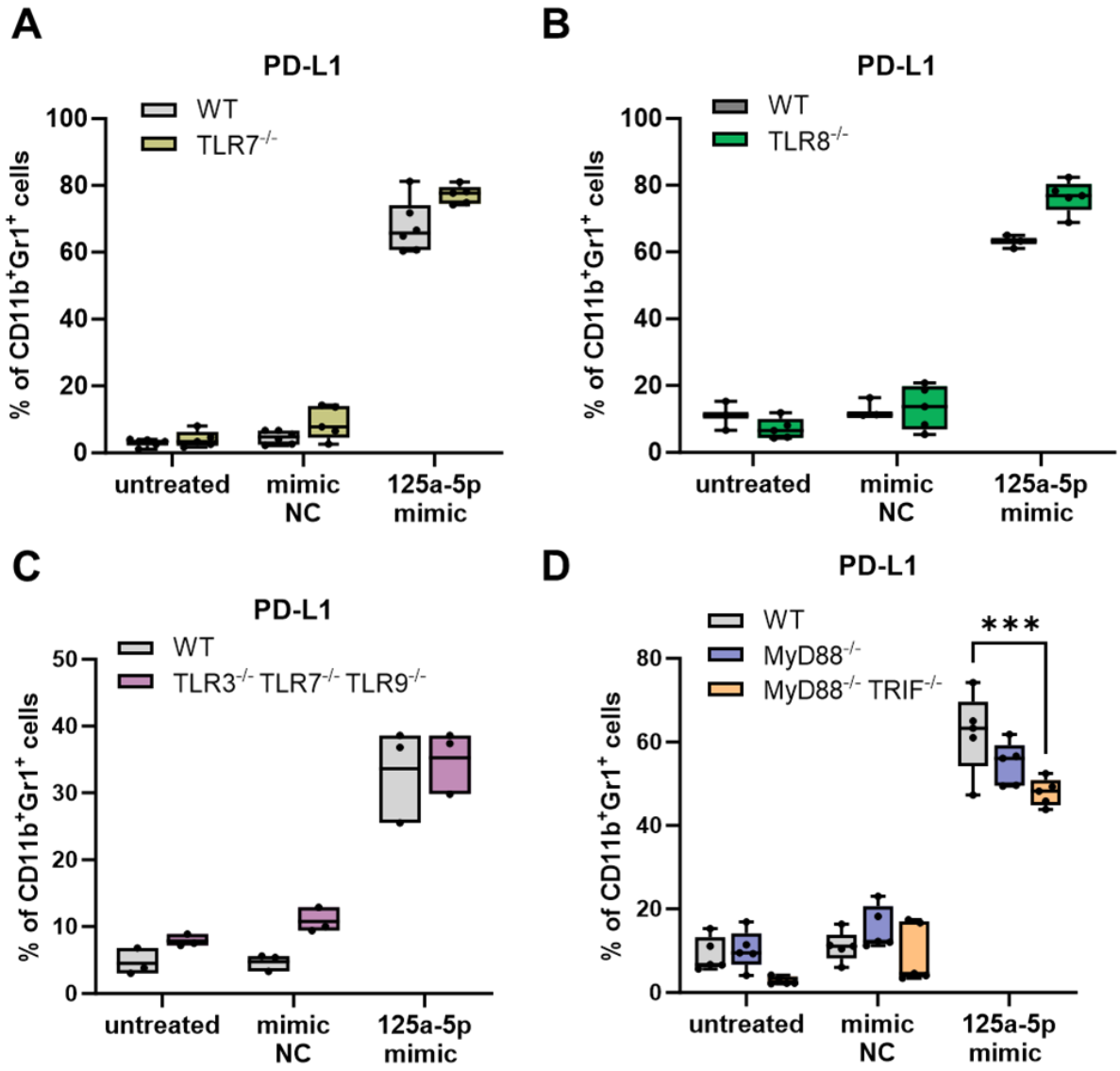

Figure 9: Expression of PD-L1 in miR-125a-5p mimic-treated iMCs in the presence or absence of TLRs and downstream adapter molecules. IMCs from healthy wild-type (WT) mice or different knock-out mice were transfected with miR-125a-5p mimics or miR mimic negative control molecules (mimic NC). Untreated iMCs were used as additional controls. PD-L1 expression in iMCs was measured after 20 h of incubation by flow cytometry. **A** The frequencies of PD-L1 expressing cells in WT iMCs and in TLR7-deficient ($TLR7^{-/-}$) iMCs are shown (n = 5-6). **B** The frequencies of PD-L1 expressing cells in WT iMCs and in TLR8-deficient ($TLR8^{-/-}$) iMCs are shown (n = 3-5). **C** The frequencies of PD-L1 expressing cells in WT iMCs and in iMCs lacking TLR3, TLR7, and TLR9 ($TLR3^{-/-}TLR7^{-/-}TLR9^{-/-}$) are shown (n = 3). **D** The frequencies of PD-L1 expressing cells in WT iMCs, in MyD88-deficient iMCs ($MyD88^{-/-}$), and in iMCs lacking MyD88 and TRIF ($MyD88^{-/-}TRIF^{-/-}$) are shown (n = 5). **A-D** Box-and-whiskers plots: min to max; all data points are shown; the horizontal line is plotted at the median. Analysis of variance and multiple comparisons were performed (***p<0.001).

4.5.3 STAT3 activation is not required for miR-125a-5p-mediated upregulation of PD-L1 in mouse iMCs

Since miR-125a-5p mimics could induce the secretion of IL-6 by iMCs and the IL-6/STAT3 axis has been demonstrated to be an important stimulator of MDSC generation (Weber et al., 2021), I wanted to test the involvement of STAT3 activation in the miR-125a-5p-mediated effects. A potent inhibitor of STAT3 activation, napabucasin, was used to investigate the involvement of STAT3 signaling. However, no effect of napabucasin on the induction of PD-L1 expression in iMCs by miR-125a-5p could be observed (Fig. 10). The expression of PD-L1 in transfected iMCs was comparable between DMSO- and napabucasin-treated iMCs.

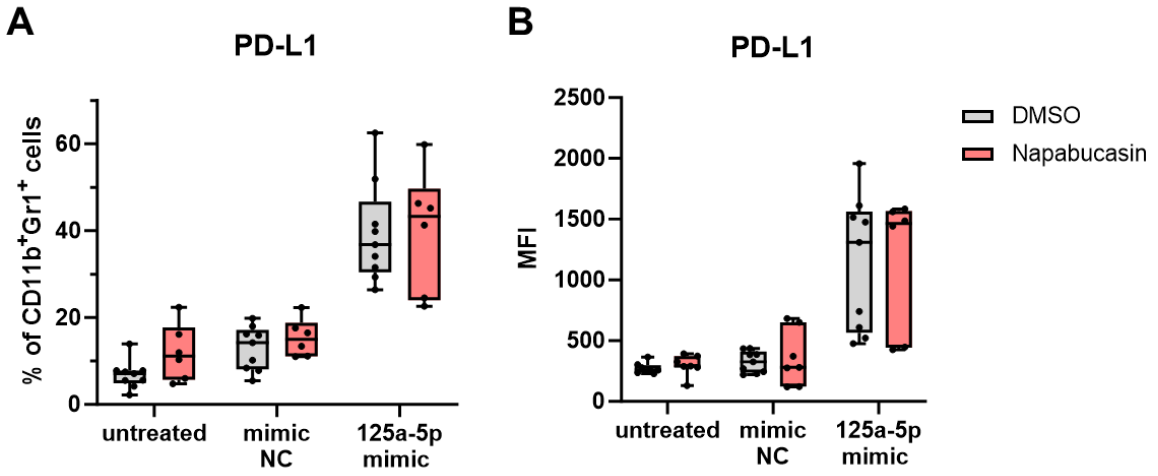

Figure 10: Expression of PD-L1 in miR-125a-5p mimic-treated iMCs in the presence or absence of a STAT3 inhibitor. IMCs from healthy mice were treated with dimethyl sulfoxide (DMSO, solvent control) or 1 µM napabucasin (STAT3 inhibitor) and transfected with miR-125a-5p mimics or miR mimic negative control molecules (mimic NC). Untransfected (untreated) iMCs were used as additional controls. The expression of PD-L1 in iMCs was measured after 20 h of incubation by flow cytometry. **A** The frequencies of PD-L1 expressing cells are shown. **B** The median fluorescence intensities (MFI) are shown. **A&B** Box-and-whiskers plots: min to max; all data points are shown; the horizontal line is plotted at the median (n = 6-9). Analysis of variance and multiple comparisons were performed.

4.6 Investigation of mechanisms of miR cluster 99b/let-7e/125a effects on mouse iMCs

It was described that human monocyte-derived DCs demonstrated an upregulation of the miR cluster 99b/let-7e/125a upon prolonged TLR stimulation, leading to the activation of a STAT3-dependent pathway (Hildebrand et al., 2018). Considering that miR-99b-5p and let-7e-5p were also found to be present in melanoma-derived

EVs, I studied the effect of all three miRs together. Furthermore, miRs in one cluster are thought to function collaboratively in repressing target genes (Wang et al., 2016); therefore, it was reasonable that the presence of all three miRs in the cluster might result in additive effects on the same pathway. It was plausible that the direct transfer of the miR cluster 99b/let-7e/125a might bypass the interaction between TLRs and TLR ligands and could directly regulate a NF-κB/STAT3 axis in myeloid cells, resulting in their pathological activation. To test this possibility, I first evaluated the effects of mimics of miR-125a-5p, miR-99b-5p, and let-7e-5p ("cluster mimics") on iMCs when co-transfected (Fig. 11).

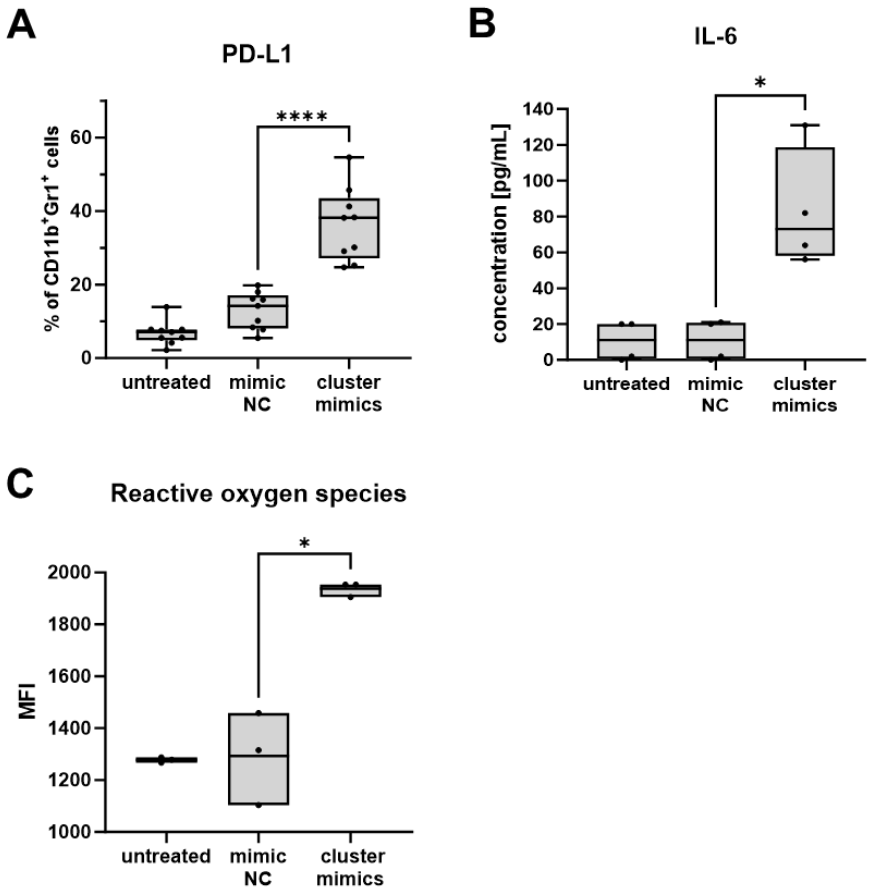

Figure 11: Expression of MDSC-related factors in iMCs upon transfection with mimics of the miR cluster 99b/let-7e/125a. IMCs from healthy mice were transfected with mimics of miR-125a-5p, miR-99b-5p, and let-7e-5p (cluster mimics) or with miR mimic negative control molecules (mimic NC) and incubated for 20 h. Untreated iMCs were used as an additional control **A** Frequencies of PD-L1 expressing iMCs, measured 20 h after transfection by flow cytometry are shown (n = 9). **B** Concentration of IL-6 in the conditioned medium of iMCs transfected with cluster mimics or mimic NC, as well as untreated iMCs, was measured after 20 h by ELISA (n = 4,).**C** Production of ROS in iMCs transfected with cluster mimics or mimic NC, as well as untreated iMCs, was determined by flow cytometry, using the CellROX deep red reagent. Median fluorescence intensity of iMCs incubated for 20 h is shown (n = 3). **A-C** Box-and-whiskers plots: min to max; all data points are shown; the horizontal line is plotted at the median. Analysis of variance and multiple comparisons were performed (*p<0.05, ****p<0.0001).

IMCs stimulated with cluster mimics showed an upregulation of PD-L1 expression (Fig. 11A), elevated production of IL-6 (Fig. 11B), and increased levels of ROS (Fig. 11C). Unexpectedly, the observations were very similar to those mediated by miR-125a-5p alone, indicating that the effects were mainly mediated by miR-125a-5p, and that the miRs 99b/let-7e/125a in cluster did not show synergistic effects in mouse iMCs.

When NF-κB activation was blocked by addition of either BAY 11-7082 or BOT-64 during transfection, PD-L1 expression was significantly reduced (Fig. 12A). However, inhibition of STAT3 activation by napabucasin did not impair the upregulation of PD-L1 by the miR mimics (Fig. 12B).

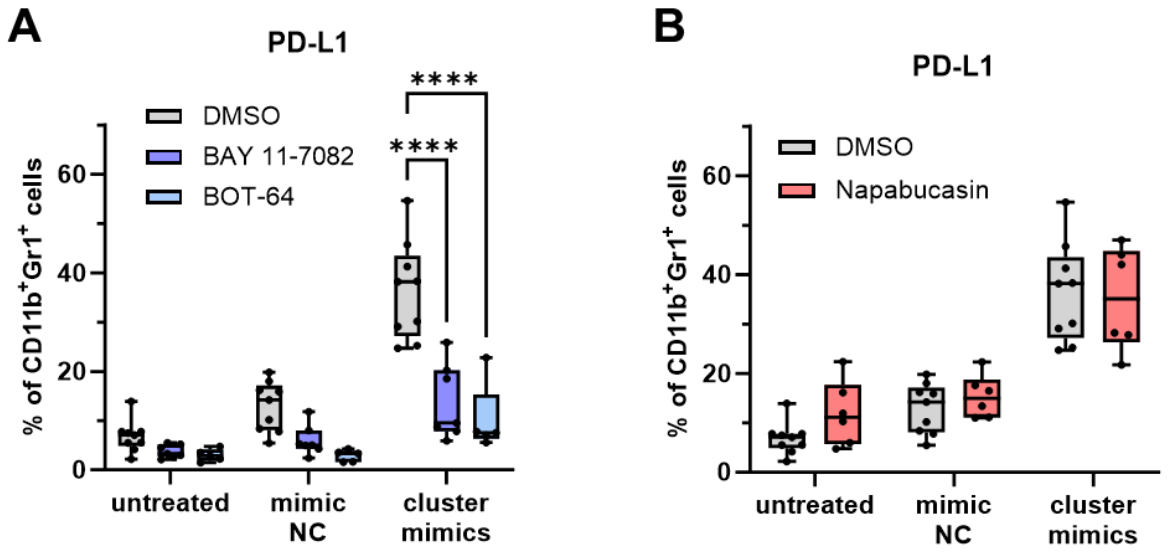

Figure 12: Expression of PD-L1 in iMCs transfected with mimics of the miR cluster 99b/let-7e/125a in the presence or absence of NF-κB and STAT3 inhibitors. IMCs from healthy mice were treated with dimethyl sulfoxide (DMSO, solvent control), 1 µM BAY 11-7082 (NF-κB activation inhibitor), 5 µM BOT-64 (NF-κB activation inhibitor), or 1 µM napabucasin (STAT3 inhibitor). Subsequently, the iMCs were transfected with mimics of miR-125a-5p, miR-99b-5p, and let-7e-5p (cluster mimics) or miR mimic negative control molecules (mimic NC). Untransfected (untreated) iMCs were used as additional controls. The expression of PD-L1 in iMCs was measured after 20 h of incubation by flow cytometry. **A** The frequencies of PD-L1 expressing cells in DMSO-, BAY 11-7082-, and BOT-64-treated iMCs upon transfection are shown (n = 5-9). **B** The frequencies of PD-L1 expressing cells in DMSO- and napabucasin-treated iMCs upon transfection are shown (n = 6-9). **A&B** Box-and-whiskers plots: min to max; all data points are shown; the horizontal line is plotted at the median. Analysis of variance and multiple comparisons were performed (****p<0.0001).

4.7 Study of mechanisms of miR cluster 99b/let-7e/125a effects on human monocytes

As the mechanism of MDSC generation via STAT3 mediated by the miR cluster 99b/let-7e/125a was characterized in alternatively activated human monocyte-derived DCs (Hildebrand et al., 2018), I investigated if the mediators that were altered by endogenous overexpression of the miR cluster 99b/let-7e/125a would also be modified in human monocytes transfected with mimics of this cluster. The first component in the mechanism outlined by Hildebrand et al. (2018) is TRIB2, which controls the activation of MAPK and is diminished in the presence of the miR cluster 99b/let-7e/125a. Human monocytes derived from healthy donors were transfected with miR mimics, and the expression of TRIB2 in monocytes was determined by western blotting after 48 hours. In our model, however, TRIB2 was not clearly reduced in human monocytes upon introduction of the cluster mimics (Fig. 13). The impact of the miR transfection on TRIB2 expression varied greatly among the different biological replicates, with only some of them showing a decrease in TRIB2 expression upon treatment with cluster mimics (Fig. 13A). Surprisingly, monocytes treated with miR-125a-5p mimics alone displayed slightly lower TRIB2 expression compared to monocytes treated with the cluster mimics (Fig. 13B).

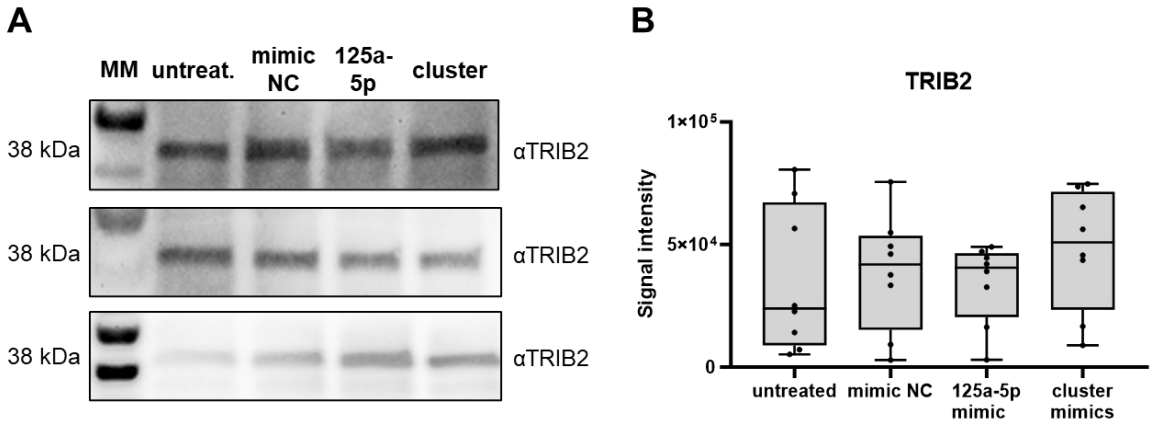

Figure 13: Expression of TRIB2 in monocytes transfected with mimics of the miR cluster 99b/let-7e/125a. Human monocytes from healthy donors were transfected with mimics of miR-125a-5p, miR-99b-5p, and let-7e-5p (cluster), miR-125a-5p mimics alone (125a-5p), or miR mimic negative control molecules (mimic NC). Untreated (untreat.) monocytes were used as additional controls. The expression of TRIB2 in monocytes was measured after 48 hours of incubation by western blotting. **A** Representative TRIB2 blots are shown for 3 biological replicates. **B** The signal intensity of TRIB2 staining normalized to the total amount of protein loaded is shown. Box-and-whiskers plots: min to max; all data points are shown; the horizontal line is plotted at the median. Analysis of variance and multiple comparisons were performed (n = 8).

According to Hildebrand et al. (2018), MAPK activity leads to IL-6 production, which in turn activates STAT3 in the human monocyte-derived DCs. Therefore, I investigated the activation of STAT3 by transfecting human monocytes with the miR cluster 99b/let-7e/125a and staining for intracellular phosphorylated STAT3 (pSTAT3). There was no increase in pSTAT3 levels in human monocytes transfected with mimics of the miR cluster 99b/let-7e/125a (Fig. 14A). In contrast, transfection of mimic negative control molecules caused a slight increase in pSTAT3 compared to untreated cells, suggesting unspecific effects in this model. Thus, a different approach for miR delivery was used. Human monocytes were treated with nanoparticles containing mimics of the miR cluster 99b/let-7e/125a to test their effect on STAT3 phosphorylation. Using this method, I observed a tendency of the cluster mimics to elevate pSTAT3 levels in comparison to empty nanoparticles (Fig. 14B). Unexpectedly, the abundance of intracellular pSTAT3 in untreated monocytes varied greatly among the biological replicates (Fig. 14B).

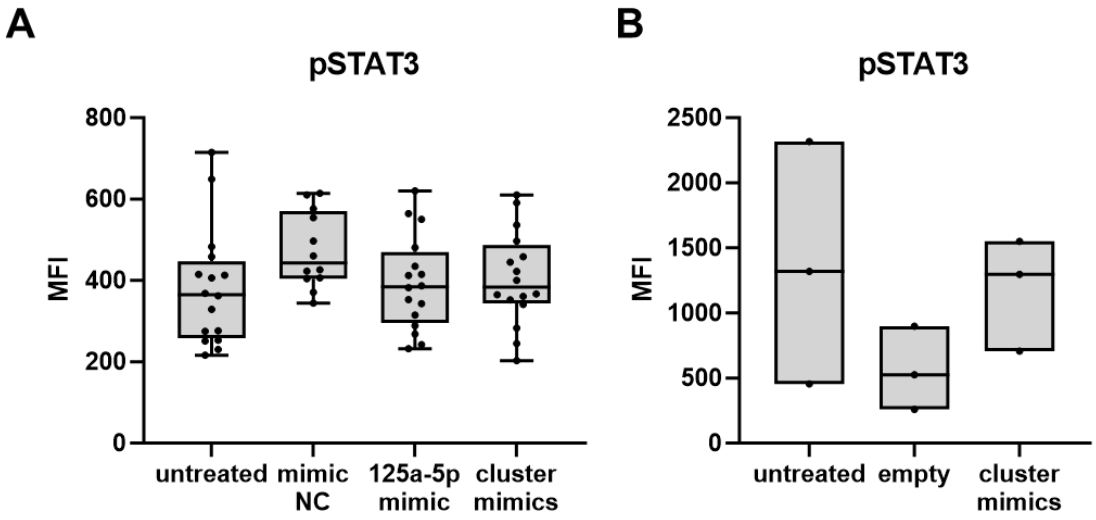

Figure 14: Levels of intracellular phosphorylated STAT3 in monocytes transfected with mimics of the miR cluster 99b/let-7e/125a. A Human monocytes obtained from healthy donors were transfected with mimics of miR-125a-5p, miR-99b-5p, and let-7e-5p (cluster mimics), miR-125a-5p mimics alone (125a-5p), or miR mimic negative control molecules (mimic NC). Untreated monocytes were used as additional controls (n = 16). **B** Human monocytes from healthy donors were treated with nanoparticles loaded with cluster mimics or with empty nanoparticles (empty). Untreated monocytes were used as additional controls (n = 3). **A&B** The levels of phosphorylated STAT3 (pSTAT3) in monocytes was measured after 48 h of incubation by flow cytometry. The median fluorescence intensity (MFI) of the monocytes is shown. Box-and-whiskers plots: min to max; all data points are shown; the horizontal line is plotted at the median. Analysis of variance and multiple comparisons were performed.

Enhanced IDO1 activity was an important aspect of the acquisition of immunosuppressive features induced by IL-6/STAT3 signaling following endogenous upregulation of the miR cluster 99b/let-7e/125a (Hildebrand et al., 2018). Hence, the effect of introducing mimics of the miR cluster 99b/let-7e/125a to human monocytes on IDO1 expression was tested. Transfection with mimic negative control molecules seemed to have a minor effect on IDO1 expression (Fig. 15), which could be expected due to slightly increased pSTAT3 levels (Fig. 14A). Still, there was a notable tendency for the transfection with the cluster mimics to cause an upregulation of IDO1 expression (Fig. 15B). A weak tendency was also seen when miR-125a-5p mimics were used but the trend was more pronounced in the cluster mimics-treated monocytes.

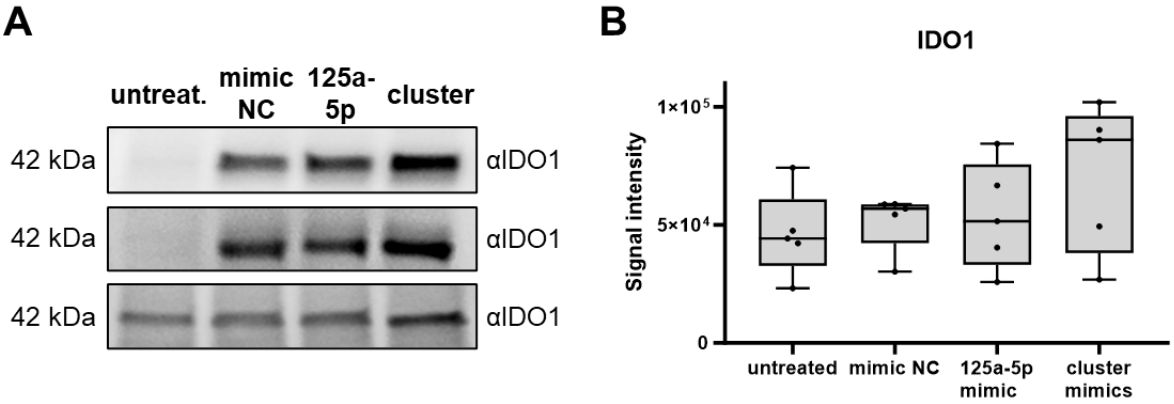

Figure 15: Expression of IDO1 in monocytes transfected with mimics of the miR cluster 99b/let-7e/125a. Human monocytes from healthy donors were transfected with mimics of miR-125a-5p, miR-99b-5p, and let-7e-5p (cluster), miR-125a-5p mimics alone (125a-5p), or miR mimic negative control molecules (mimic NC). Untreated (untreat.) monocytes were used as additional control. The expression of IDO1 in monocytes was measured after 48 h of incubation by western blotting. **A** Representative IDO1 blots are shown for 3 biological replicates. **B** The signal intensity of IDO1 staining normalized to the total amount of protein loaded is shown. Box-and-whiskers plots: min to max; all data points are shown; the horizontal line is plotted at the median. Analysis of variance and multiple comparisons were performed (n = 5).

Given that PD-L1 plays an important role in the immunosuppressive functions of pathologically activated myeloid cells, and the treatment of iMCs with mimics of the miR cluster 99b/let-7e/125a led to an increase in PD-L1 expression, the effect of cluster mimics on PD-L1 expression was investigated also in human monocytes. Treatment with cluster mimics resulted in an upregulation of PD-L1 expression in monocytes (Fig. 16). Interestingly, the impact of the miRs on PD-L1 expression appeared to be less potent as compared to the findings in mouse iMCs.

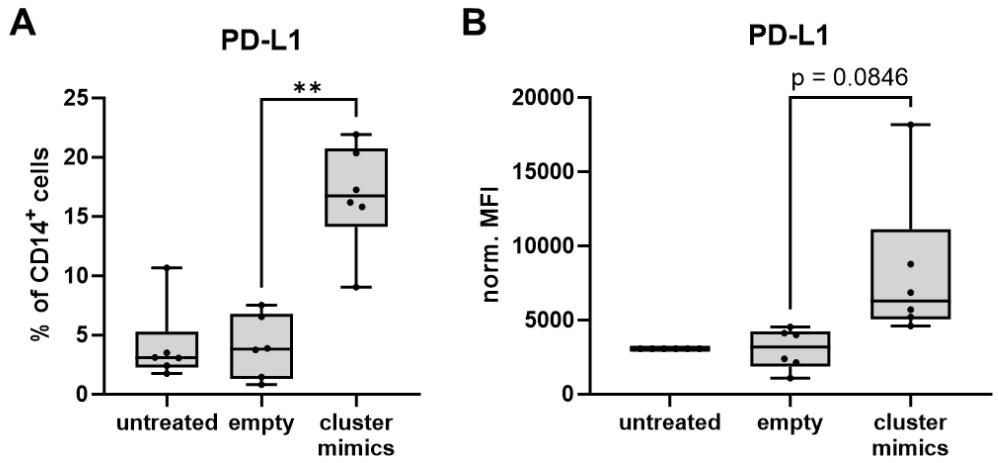

Figure 16: Expression of PD-L1 in monocytes treated with mimics of the miR cluster 99b/let-7e/125a via nanoparticles. Human monocytes were treated with nanoparticles loaded with cluster mimics or with empty nanoparticles. Untreated monocytes were used as additional control. PD-L1 expression in monocytes was measured after 48 hours of incubation by flow cytometry. **A** The frequencies of PD-L1 expressing monocytes are shown. **B** The PD-L1 median fluorescence intensity (MFI) of treated monocytes normalized to the MFI of the corresponding untreated monocytes is shown. Statistical analysis was performed with paired raw values. Box-and-whiskers plots: min to max; all data points are shown; the horizontal line is plotted at the median. Analysis of variance and multiple comparisons were performed (n = 6, **p<0.01).

Despite increased expression of suppressive molecules, the downregulation of immunostimulatory markers can also contribute to the inhibitory activity of MDSCs. In this regard, I analyzed the expression of HLA-DR and CD86 in human monocytes after the treatment with mimics of the miR cluster 99b/let-7e/125a. The monocytes that were treated with cluster mimics tended to lose (Fig. 17A) or downregulate (Fig. 17B) the expression of HLA-DR. Furthermore, CD86 expressing monocytes were reduced in the cluster mimics-treated group (Fig. 17C).

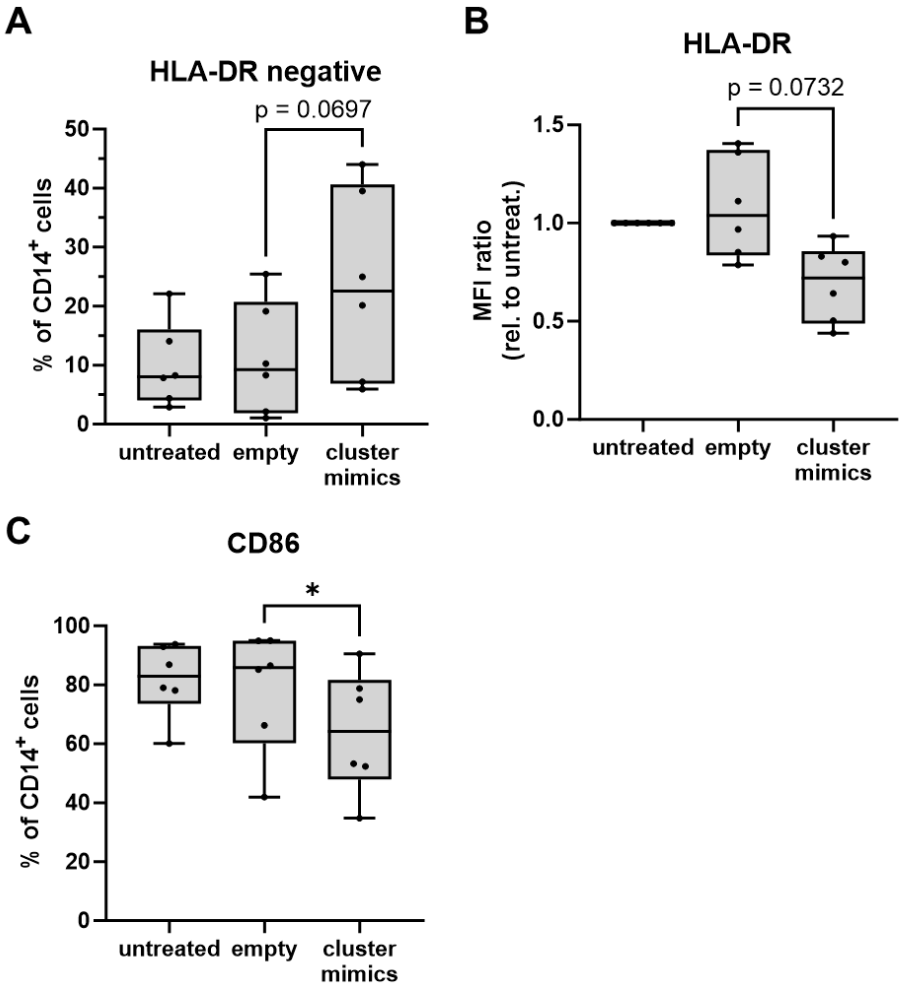

Figure 17: Expression of T cell stimulating molecules in monocytes treated with mimics of the miR cluster 99b/let-7e/125a via nanoparticles. Human monocytes from healthy donors were treated with nanoparticles loaded with cluster mimics or with empty nanoparticles (empty). Untreated monocytes were used as additional controls. Expression of molecules important for T cell stimulation was measured by flow cytometry after 48 h. **A** Frequencies of monocytes lacking HLA-DR expression are shown (n = 6). **B** The HLA-DR median fluorescence intensity (MFI) of treated monocytes is shown normalized to the MFI of the corresponding untreated monocytes. Statistical analysis was performed with paired raw values (n = 6). **C** Frequencies of CD86 expressing monocytes are shown (n = 6). Box-and-whiskers plots: min to max; all data points are shown; the horizontal line is plotted at the median. Analysis of variance and multiple comparisons were performed (*p<0.05).

Next, the effect of human monocytes treated with mimics of the miR cluster 99b/let-7e/125a on T cell proliferation was examined to test whether the identified phenotypic alterations translated into immunosuppressive functions. For this, autologous human T cells labeled with a fluorescent dye were co-cultured with cluster mimics-treated or control monocytes for 96 h. By flow cytometry analysis, the successfully labeled T cells were gated (Fig. 18A) and the proliferation was determined based on the dilution of the fluorescent signal by the dye (Fig. 18B). Human monocytes transfected with cluster mimics modestly reduced the frequency of human T cells that had undergone proliferation (Fig. 18C). In addition, the

average number of divisions of T cells was decreased when co-cultured with cluster mimics-transfected monocytes (Fig. 18D). MiR-125a-5p-transfected monocytes also showed a tendency to decrease T cell proliferation, however, the impact varied greatly across the different donors of human monocytes. Moreover, co-culture with monocytes treated with the mimic NC resulted in a slight reduction in T cell proliferation, indicating that the transfection process partially induced immunosuppressive effects through a non-specific mechanism.

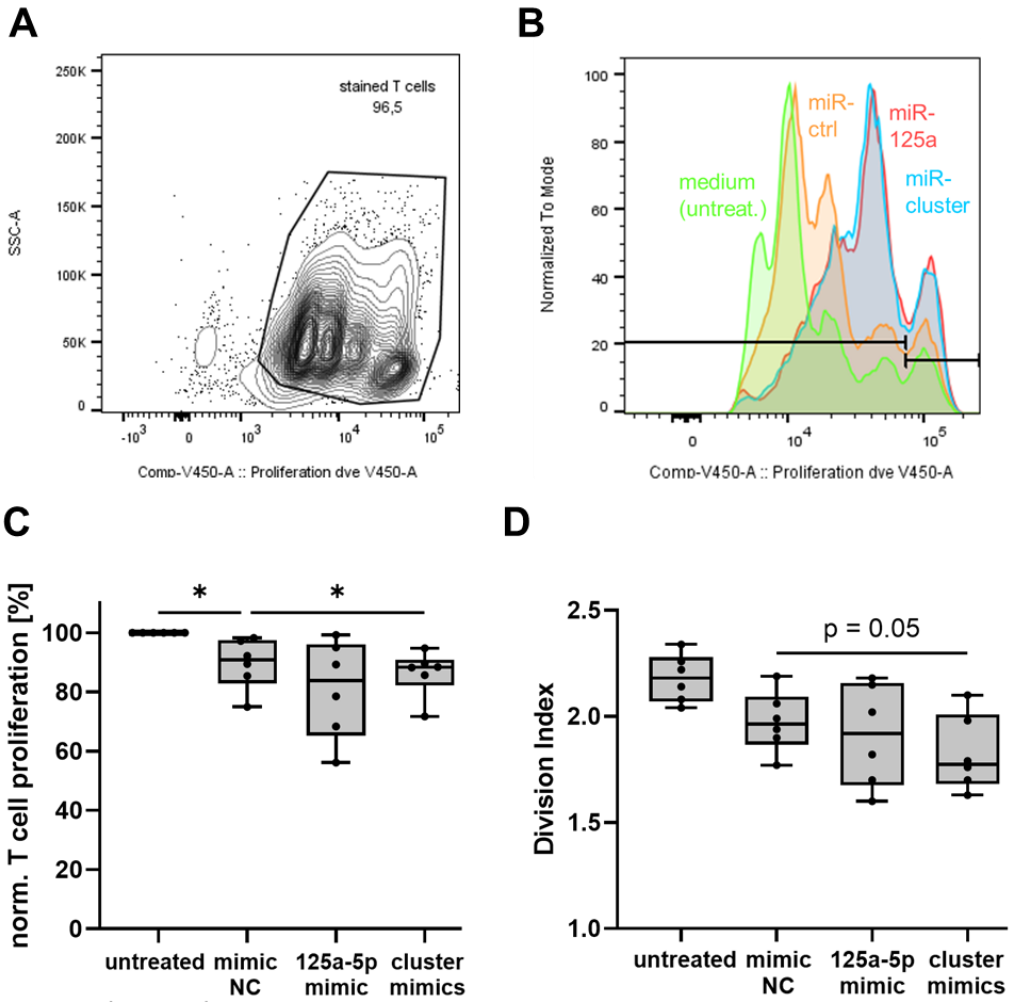

Figure 18: Impact of monocytes transfected with mimics of the miR cluster 99b/let-7e/125a on T cell proliferation. Human monocytes from healthy donors were transfected with mimics of miR-125a-5p, miR-99b-5p, and let-7e-5p (cluster mimics), miR-125a-5p mimics alone, or miR mimic negative control molecules (mimic NC). Untreated monocytes were used as additional controls. Following 48 h of monocyte incubation, T cells were labeled with a proliferation dye and co-cultured with the transfected monocytes for 96 h. T cell proliferation was determined by flow cytometry. **A** Unlabeled cells and cell debris were excluded from the analysis as shown in this representative plot. **B** The proliferation was assessed based on the dilution of the proliferation dye as shown in this representative histogram. Each peak was defined as one generation. **C** The frequency of T cells that had undergone proliferation was determined and normalized to the corresponding value of the co-culture with untreated monocytes (n = 6). **D** The average number of divisions per T cell was calculated (n = 6). Box-and-whiskers plots: min to max; all data points are shown; the horizontal line is plotted at the median. Analysis of variance and multiple comparisons were performed (*p<0.05).

Next, human monocytes were also exposed to nanoparticles carrying mimics of the miR cluster 99b/let-7e/125a to further evaluate the specific suppressive capacity of the cells. Human monocytes treated with cluster mimics via nanoparticles showed an inhibitory effect on T cell proliferation (Fig. 19). Both the percentage of T cells that underwent proliferation (Fig. 19A) and the average number of divisions per T cell (Fig. 19B) were significantly decreased in the presence of cluster mimics-treated monocytes compared to monocytes treated with empty nanoparticles.

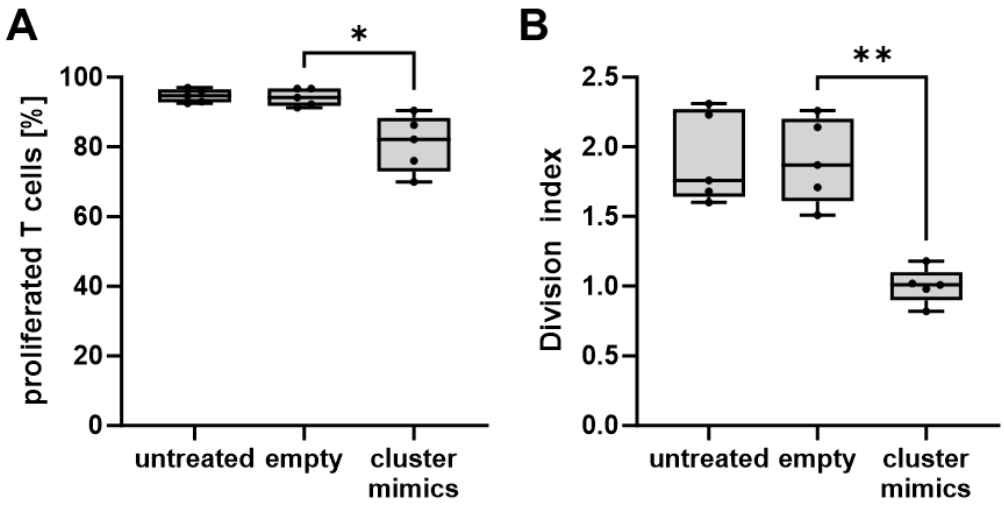

Figure 19: Impact of monocytes treated with nanoparticles containing mimics of the miR cluster 99b/let-7e/125a on T cell proliferation. Human monocytes from healthy donors were treated with nanoparticles loaded with mimics of miR-125a-5p, miR-99b-5p, and let-7e-5p (cluster mimics), with empty nanoparticles, or kept untreated. Following 48 h of monocyte incubation, T cells were labeled with a proliferation dye and co-cultured with the treated or untreated monocytes for 96 h. T cell proliferation was determined by flow cytometry. **A** The frequency of T cells that had undergone proliferation was determined (n = 6). **B** The average number of divisions per T cell was calculated (n = 6). Box-and-whiskers plots: min to max; all data points are shown; the horizontal line is plotted at the median. Analysis of variance and multiple comparisons were performed (*$p<0.05$, **$p<0.01$).

5 DISCUSSION

Myeloid cells exhibit a spectrum of characteristics and activation mechanisms in response to different environmental stimuli. Thus, the function of myeloid cells in melanoma as well as in cancer in general can be altered depending on the factors to which they are exposed. MiRs derived from melanoma cells have been shown to be transferred to myeloid cells as cargo of EVs, inducing an MDSC phenotype and function in normal myeloid cells (Gerloff et al., 2020; Huber et al., 2018). MDSC differentiation and activation is regulated by multifaceted signaling and metabolic pathways. The present study aims to better understand the mechanisms by which melanoma cell-derived miRs could participate in this regulation.

5.1 Lipid-based miR delivery

The HiPerFect transfection reagent, a mixture of cationic and neutral lipids, was used for miR transfection. As a result of electrostatic interactions, cationic lipids spontaneously assemble with negatively charged nucleic acids, thereby forming so-called lipoplexes (Pedroso de Lima et al., 2001). The surface of these lipoplexes is positively charged, which enhances their ability to interact with the negatively charged cell surface (Pedroso de Lima et al., 2001). Endocytosis is thought to be the primary mechanism for lipoplex uptake, with the release of the nucleic acid cargo facilitated by disruption of the lipoplex structure in the acidic milieu (Pedroso de Lima et al., 2001; Zuhorn and Hoekstra, 2002). Importantly, most experimental data, especially for myeloid cells, also indicate that EVs are typically internalized into endosomal compartments via endocytosis (Mulcahy et al., 2014). Given that the information obtained from miR transfection studies was aimed to provide insights about the mechanism activated by EV-associated miR, it was essential that the miR would enter the cells through a very similar route.

The physical characteristics of the lipoplexes can be modified by addition of a helper lipid, leading to improved uptake of the complexes and release of the nucleic acid content (Zuhorn and Hoekstra, 2002). Since no specific information on the lipids present in the HiPerFect transfection reagent is provided, it can only be presumed that the neutral lipid component matches the function of a helper lipid. According to

the manufacturer, the lipid mixture of the HiPerFect transfection reagent yields effective transfection of primary cells while maintaining high viability. The transfection reagent did not seem to affect the cell survival over the 20 h incubation period (Fig. 1B). The cultivation of iMCs without growth factor supplementation, on the other hand, appeared to restrict cell integrity (Fig. 1C). Growth factors were omitted because they can activate MDSC-like features in iMCs (Weber, 2020), potentially interfering with the response of iMCs to the miR. It was crucial to ensure that the technique did not influence the activation state and phenotype of the cells. Therefore, the effect of the HiPerFect transfection reagent on PD-L1 expression in iMCs was tested. While 1 µL of the transfection reagent had no impact on PD-L1 expression, higher doses induced a substantial upregulation of PD-L1 (Fig. 2B-C). Consequently, the volume of transfection reagent utilized to examine the effects of exogenous miR on iMCs was reduced to 1 µL.

In the investigated settings, uptake of transfection complexes occurred in more than 90 % of iMCs using the HiPerFect transfection reagent (Fig. 3A). This was assessed based on the fluorescence signal of labeled miR mimics, therefore it was not possible to make any conclusions regarding the release of the miR molecules within the cells. Higher amounts of the transfection reagent increased the transfection performance up to 99 % (Fig. 3A). However, the dosage of miR delivered into the cells did not increase proportionally with the amount of transfection reagent applied (Fig. 3B). Remarkably, it has also been reported that using miR concentrations ranging from 10 to 100 nM to form transfection complexes with a lipid-based reagent resulted in nearly equivalent quantities of this miR within primary fibroblasts (Pop and Almquist, 2021). The authors conclude that, while the technique efficiently transfects miR, the amount of miR that becomes functionally accessible in the cytosol is at least partially a stochastic phenomenon.

5.2 PD-L1 as a functional MDSC marker

To analyze the effects mediated by the individual miRs of the described MDSC-miR set, PD-L1 was selected as a marker for the conversion of iMCs to a MDSC-like state. Research in our group previously demonstrated that PD-L1 was a crucial molecule for the immunosuppressive activity of iMC-derived MDSCs induced by EVs (Fleming, 2018). Furthermore, PD-L1 expression was found to be higher in

tumor-infiltrating MDSCs compared to splenic counterparts in a mouse model of melanoma (Noman et al., 2014). Blocking PD-L1 under hypoxic conditions greatly reduced their immunosuppressive capacity (Noman et al., 2014). PD-L1 has also been used in an immune monitoring study of advanced melanoma patients as an indicator of the activation program and immunosuppressive potential (Pico de Coaña et al., 2020). This study demonstrated that lower levels of PD-L1 expressing monocytes were associated with improved survival outcomes, suggesting that these cells indeed have a tumor-promoting role in melanoma. A screening of essential MDSC markers was conducted by analyzing PBMCs from advanced melanoma patients and comparing them to PBMCs from healthy donors (Huber et al., 2021). The percentage of $CD14^+$ $PD\text{-}L1^+$ cells was one of the four variables together defined as the myeloid index score, which could reliably serve as a prognostic factor in melanoma (Huber et al., 2021).

Although PD-L1 can consequently be considered as an important functional MDSC marker, other functional mediators exist. MDSCs can produce a variety of immunosuppressive factors, depending on the specific subtype and the surrounding conditions. Thus, MDSC functions might also occur independently of PD-L1 expression. For instance, inhibition of PD-L1 had no effect on the immunosuppressive functions of MDSCs induced by cervical cancer cell conditioned medium, but reprogramming these MDSCs with all-trans retinoic acid (ATRA), which has been shown to stimulate the maturation of myeloid cells (Kusmartsev et al., 2003; Mirza et al., 2006), was successful (Liang et al., 2022).

In order to evaluate the significance of the individual melanoma EV-associated miRs, I used only PD-L1, and analyzed the total iMC population without distinguishing between MDSC subtypes. These circumstances represent notable limitations. Nevertheless, given the substantial role of PD-L1 expressing cells in the setting of melanoma, the impact of miRs on PD-L1 was considered of particular importance for studying the underlying mechanisms.

5.3 Effects of melanoma EV-associated miRs on myeloid cells

5.3.1 MiR-125 family

Studying the frequency of PD-L1$^+$ iMCs following transfection with the single miRs that comprise the MDSC-miR set (Huber et al., 2018), mimics of miR-125a-5p and miR-125b-5p were found to trigger PD-L1 expression in a particularly high percentage of iMCs (Fig. 4). The results suggested that miR-125a-5p and miR-125b-5p could have the capacity to modify the functional state of myeloid cells. This is supported by a study showing that alternatively activated macrophages, generated from mouse BM cells *in vitro*, displayed higher levels of miR-125a-5p and miR-125b-5p compared to classically activated macrophages (Banerjee et al., 2013). The authors reported a particularly high expression of miR-125a-5p in the alternatively activated macrophages. This finding is consistent with results obtained by our research group, which also showed a substantial upregulation of miR-125a-5p expression in MDSC-like iMCs that were exposed to *RET* melanoma cell-derived EVs *in vitro* (Fleming, 2018) as well as in MDSCs isolated from tumors of *RET* transgenic mice (Hu, unpublished data). In addition, the abundance of miR-125a-5p in the TME was shown to be associated with the tumor progression (indicated by the tumor weight) in *RET* transgenic mice (Fig. 5A). There was no association between miR-125a-5p levels in the plasma and the tumor progression in these mice (Fig. 5B). Such results indicate that miR-125a-5p could have a more important role in activating MDSCs within the TME, while its influence on the generation of MDSCs in the periphery might be lower.

Banerjee et al. (2013) demonstrated that miR-125a-5p is augmented by TLR2 or TLR4 activation in BM-derived mouse macrophages, but this effect was only observed after 24 h (in comparison, *Tnf* expression was significantly upregulated after 4 h). Transfection of the BM-derived mouse macrophages with miR-125a-5p resulted in reduced production of TNF-α, IL-12, and iNOS, as well as the suppression of bactericidal functions, which the authors considered as the features of classically activated macrophages (Banerjee et al., 2013). In addition to PD-L1 upregulation, increased expression of *Il6*, *Il10*, and *Nos2*, as well as elevated production of IL-6 and ROS was observed in iMCs transfected with miR-125a-5p mimics (Fig. 7). Upregulated expression of *Il6* and *Il10* has also been seen in iMCs

treated with EVs derived from RET mouse melanoma cells as well as in human monocytes treated with EVs derived from HT-144 human melanoma cells (Fleming et al., 2019). According to various publications, MDSCs generate large amounts of IL-6, IL-10, NO, and ROS (Chalmin et al., 2010; Liu et al., 2015; Loercher et al., 1999; Raber et al., 2014). Moreover, the transcriptional analysis of miR-125a-5p-treated iMCs revealed an increased expression of *Slamf6* and *Slamf9* (Fig. 6A). Interestingly, expression of *Slamf6* and *Slamf9* was reported to be elevated in tumor-associated myeloid cells (Dollt et al., 2018; Meng et al., 2022). Collectively, the data strengthen the hypothesis that miR-125a-5p could play an important regulatory role in myeloid cell differentiation and function, potentially promoting the generation of immunosuppressive, tumor-promoting MDSCs when transported via EVs. Consistent with this, I observed a tendency of miR-125a-5p-transfected human monocytes to reduce the proliferation of activated human T cells (Fig. 18).

In contrast, stimulatory effects on T cell proliferation were reported for BM-derived macrophages that were transfected with miR-125a mimics and treated with LPS and IFN-γ (Zhao et al., 2016). However, the authors did not specify the sequence of the miR-125a mimic used in this study. Additionally, Zhao et al. (2016) applied different stimuli in their experiments, which might account for the discrepant results. In human monocyte-derived macrophages, the classical activation pattern was associated with miR-125a-3p rather than miR-125a-5p expression (Graff et al., 2012). The same study also showed that IFN-γ antagonized LPS-induced miR-125a-5p expression in THP-1 cells.

Unlike miR-125a-5p, miR-125b-5p has been demonstrated to be downregulated in mouse macrophages by LPS-mediated TLR4 activation (Androulidaki et al., 2009; Banerjee et al., 2013; Tili et al., 2007). Interestingly, the transfection of THP-1 macrophages with miR-125b-5p was found to induce a phenotypic switch, partially overlapping with effects induced by melanoma EVs, resulting in the phenotype associated with tumor-associated macrophages (Gerloff et al., 2020). Similarly, miR-125b was demonstrated to be transported to macrophages by EVs produced from ovarian cancer cells and promotes tumor-promoting polarization in macrophages (Chen et al., 2018). In the myeloid cell line Mono Mac 6, miR-125b-5p was shown to target and suppress 5-lipoxygenase, a key enzyme in the synthesis of leukotrienes which are inflammatory mediators (Busch et al., 2015). However, the

authors did not discuss the functional consequences for the myeloid cells. Several studies reported a downregulation of TNF-α in monocytes/macrophages by miR-125b (Huang et al., 2012; Rajaram et al., 2011; Tili et al., 2007). On the other hand, Duroux-Richard et al. (2016) described a modulating role for miR-125b in the mitochondrial metabolism of human monocytes/macrophages, triggering their classical activation. Furthermore, BM-derived mouse macrophages transduced with miR-125b encoding vectors were shown to stimulate CD8 T cells *in vitro* and exert anti-tumor effects *in vivo* (Chaudhuri et al., 2011). Although miR-125b has been associated with diverse effects on myeloid cells, its role in the context of tumors, especially as EV-delivered miR, appears to be focused on tumor-supporting differentiation. The observed increase in PD-L1 in iMCs upon miR-125b-5p transfection (Fig. 4) may also point to an immunosuppressive function of the cells. This, however, has not been investigated at the functional level.

5.3.2 MiR cluster 99b/let-7e/125a

MiR-99b, let-7e, and miR-125a originate from one miR cluster positioned on chromosome 19 in humans (Potenza et al., 2017). In the mouse genome, a homologous miR cluster is located on chromosome 17 (Gerrits et al., 2012). MiRs of a cluster are transcribed concomitantly, resulting in similar expression rates. Evidence suggests that miRs of a cluster act cooperatively to suppress target genes (Wang et al., 2016). Notably, the expression of the miR cluster 99b/let-7e/miR-125a was found to be regulated by the transcription factor Zinc finger E-box-binding homeobox 1 (ZEB1) (Ma et al., 2017), which appears to be crucial for the pathological activation of macrophages with tumor-promoting features (Cortés et al., 2017). In human monocytes, expression of the miR cluster 99b/let-7e/miR-125a was inducible by LPS stimulation (Bazzoni et al., 2009). However, human neutrophils did not display an induction of these miRs in response to LPS stimulation (Bazzoni et al., 2009).

Further research found that the LPS-mediated induction of the miR cluster 99b/let-7e/miR-125a occured with a delayed kinetic compared to other LPS-induced miRs, and was associated with a shift to an anti-inflammatory function (Curtale et al., 2018). In agreement with this, Hildebrand et al. (2018) demonstrated that sustained TLR7/8 activation enhanced the expression of the miR cluster 99b/let-7e/miR-125a

in human monocyte-derived dendritic cells. Such cells have previously been shown to upregulate the expression of negative immune checkpoint molecules (such as PD-L1), to downregulate HLA-DR expression, and to produce high amounts of cytokines, including IL-6 and IL-10 (Wölfle et al., 2011). Furthermore, this study found that such alternatively activated myeloid cells suppressed T cell proliferation. Introducing mimics of miR-99b.5p, let-7e-5p, and miR-125a-5p directly to mouse iMCs or human monocytes, I observed very similar effects dealing with the upregulation of PD-L1 expression as well as the production of IL-6 and ROS (Fig. 11). Human monocytes treated with mimics of the miR cluster 99b/let-7e/125a also showed an increase in the frequency of PD-L1 expressing cells (Fig. 16) as well as a tendency to downregulate the expression of HLA-DR and CD86 (Fig. 17), which have an important role in T cell activation. Taken together, these observations strongly suggested that the transfer of the miR cluster 99b/let-7e/miR-125a via EVs could elicit similar effects as the upregulation of the endogenous miRs by inflammatory stimuli, ultimately leading to the generation of immunosuppressive MDSCs.

5.3.3 MiR-146 family

Due to minimal, non-significant alterations in PD-L1 expression seen in iMCs transfected with miR-146a-5p or miR-146b-5p mimics (Fig. 4), the role of these miRs in MDSC generation was not further studied. Nevertheless, miR-146a and miR-146b have been proposed to function as negative feedback regulators of TLR signaling in human monocytic cells by targeting TRAF6 and IRAK1 (Daveri et al., 2020; Taganov et al., 2006). Another research article highlighted an important role of miR-146a in the regulation of immune cell activation (Daveri et al., 2020). Furthermore, in the melanoma microenvironment, miR-146a has been described as a pivotal negative regulator of the STAT1-IFN-γ axis; blocking miR-146a combined with anti-PD1 therapy benefited the survival of melanoma-bearing mice (Mastroianni et al., 2019). MiR-146a has also been linked to the development of tumor-promoting macrophages in endometrial cancer (Zhou et al., 2018b). In addition, miR-146b has been shown to affect macrophage polarization by targeting IRF5, which has an important role in the classical activation of macrophage functions (Peng et al., 2016).

5.4 Mechanisms of miR-mediated MDSC generation

5.4.1 MiR-125a-5p

To get an insight into the mechanism of the modification of myeloid cell polarization by miR-125a-5p, gene expression data were analyzed for patterns of changes in genes linked to certain signaling pathways. The miR-125a-5p treated samples showed a substantial enrichment of gene sets related to NOD-like receptor signaling, TNF signaling, JAK-STAT signaling, TLR signaling, and NF-κB signaling, in comparison to the control samples (Fig. 6B). As the NF-κB signaling pathway appears to be very important in the activation phase of MDSC generation (Condamine et al., 2015), I examined whether its inhibition would affect the response to miR-125a-5p. Indeed, blocking the NF-κB signaling pathway prevented the increase in PD-L1 expressing iMCs by miR-125a-5p (Fig. 8), indicating that NF-κB activation is a key event facilitated by miR-125a-5p in iMCs.

Not only PD-L1 is regulated by NF-κB, but also other factors upregulated in miR-125a-5p-stimulated iMCs, including *Il6*, *Il10*, and *Nos2* (Fig. 7A), can be induced by NF-κB (Libermann and Baltimore, 1990; Saraiva et al., 2005; Xie et al., 1994). Interestingly, NF-κB is reported to be a redox-sensitive signaling factor, which can be activated by ROS in myeloid cells (Kaul et al., 1998; Nakajima and Kitamura, 2013; Takada et al., 2003). MiR-125a-5p-treated iMCs produced high levels of ROS (Fig. 7C), suggesting that miR-125a-5p mediated accumulation of ROS could contribute the activation of the NF-κB signaling pathway. MiR-125a-5p was also proposed to target tumor necrosis factor alpha-induced protein 3 (TNFAIP3, also known as A20) in THP-1 macrophages, which functions as a negative regulator of NF-κB signaling (Graff et al., 2012). Further studies have reported TNFAIP3 targeting by miR-125 in different cell types and conditions (de la Rica et al., 2015; Hsu et al., 2017; Kim et al., 2012).

TLR ligands are among the inflammatory stimuli that can activate the NF-κB pathway in MDSCs. The transport of tumor-derived miR-21 and miR-29a through EVs has been shown to result in a direct interaction with TLR7 and TLR8 in mouse macrophages, leading to the activation of NF-κB signaling (Fabbri et al., 2012). Notably, the changes in gene expression induced by miR-125a-5p mimic transfection of iMCs were associated with the TLR signaling pathway (Fig. 6B).

Hence, I investigated whether miR-125a-5p could also act as ligand of endosomal TLRs. For this, I tested the responsiveness of TLR-deficient iMCs to miR-125a-5p mimics. However, iMCs lacking TLR7, TLR8, or the combination of TLR3, TLR7, and TLR9 did not show an impaired response to miR-125a-5p mimics, as measured by PD-L1 expression (Fig. 9A-C). Moreover, there was no reduction in PD-L1 response by iMCs deficient in the critical downstream adaptor molecule MyD88 (Fig. 9D). Among the conditions that were evaluated, only the MyD88$^{-/-}$TRIF$^{-/-}$ iMCs showed a slightly decreased response to miR-125a-5p transfection (Fig. 9D). These results strongly indicated that miR-125a-5p does not trigger TLR signaling, and subsequently NF-κB activation, via a direct interaction with the endosomal receptors.

The NOD-like receptor pathway was another mechanism linked to the alterations in gene expression caused by miR-125a-5p transfection (Fig. 6B). NOD-like receptors are a class of cytosolic PAMP-sensing receptors. Notably, the downstream signaling events triggered by NOD-like receptors have substantial overlaps to those triggered by TLRs as well as TNF receptors. Importantly, TNFAIP3 has a crucial role in limiting TNF receptor-induced, TLR-induced as well as NOD-like receptor induced NF-κB activity (Boone et al., 2004; Hitotsumatsu et al., 2008; Lee et al., 2000). Taken together, it appears reasonable that the delivery of exogenous miR-125a-5p to myeloid cells might bypass the stimulation of such immune receptors by targeting the expression of TNFAIP3, resulting in the activation of NF-κB.

Based on the increased IL-6 production caused by miR-125a-5p transfection (Fig. 7B) and transcriptional analysis, which provided evidence of a change in the JAK/STAT pathway (Fig. 6B), I investigated the involvement of STAT3 in the miR-125a-5p-induced effects. The IL-6/STAT3 axis has already been identified to contribute to the accumulation and activation of MDSCs (Condamine and Gabrilovich, 2011); IL-6 was shown to be associated with higher MDSC frequency in different cancer entities, including malignant melanoma (Bjoern et al., 2016; Tobin et al., 2019). Notably, there have also been reports of an interaction between STAT3 and NF-κB, potentially facilitating transcriptional synergy (Grivennikov and Karin, 2010). The collaboration between the STAT3 and NF-κB pathways may be necessary for the induction of a particular gene subset (Grivennikov and Karin, 2010). Nevertheless, the presence of the STAT3 inhibitor napabucasin during

transfection of iMCs with miR-125-5p mimics had no effect on the upregulation of PD-L1 expression (Fig. 10), indicating that STAT3 is not required for the miR-125a-5p-mediated changes in iMC polarization. However, PD-L1 might potentially be increased by NF-κB activation without the involvement of STAT3, whereas STAT3 might impact other factors important for the generation of MDSCs that have not been explored in our experiments.

5.4.2 MiR cluster 99b/let-7e/125a

The miR cluster 99b/let-7e/125a has been proven to have a crucial function for regulating the suppressive phenotype of pathologically activated human monocyte-derived DCs at several levels (Hildebrand et al., 2018). Considering the potential combinatorial effects of the three miRs, which cannot be evident when testing miR-125a-5p alone, I studied the mechanism of their joint actions upon direct delivery to myeloid cells. In mouse iMCs, which comprised both polymorphonuclear and monocytic cells, distinct processes in each subset could potentially have an influence on the overall effect by the miRs. Additionally, mouse and human myeloid cells may respond differently. Thus, I studied the effects mediated by the miR cluster 99b/let-7e/125a also in human monocytes.

Hildebrand et al. (2018) showed that the miR cluster 99b/let-7e/125a was highly expressed upon TLR stimulation in their model, subsequently targeting TRIB2 to modulate MAPK signaling. Therefore, I tested whether transfection of human monocytes with mimics of the miR cluster 99b/let-7e/125a would also reduce TRIB2 protein levels. However, the impact of the miR cluster 99b/let-7e/125a on TRIB2 expression varied greatly across the samples obtained from different donors, and also the baseline expression of TRIB2 fluctuated among the replicates (Fig. 13). Overall, the data did not provide evidence of any reduction in TRIB2 levels caused by the miR cluster 99b/let-7e/125a.

Importantly, the mechanism of immunosuppressive function activation by endogenous miRs of the cluster 99b/let-7e/125a in human monocyte-derived DCs described by Hildebrand et al. (2018) involved phosphorylation of STAT3. In their model, the inhibition of TRIB2 led to increased activity of MAPK, which was associated with a high level of IL-6 and IL-10. Especially the high supply of IL-6 was argued to be responsible for the activation of STAT3 (Giesbrecht et al., 2017;

Hildebrand et al., 2018). In contrast, transfecting human monocytes with mimics of the miR cluster 99b/let-7e/125a failed to increase STAT3 phosphorylation in our experiments (Fig. 14A). Furthermore, non-specific effects of the transfection were observed. Therefore, nanoparticles loaded with cluster mimics were used as an alternative method for the miR delivery. Due to the restricted availability of the nanoparticles, only one experiment could be conducted, which showed a trend of enhanced STAT3 activity in monocytes treated with nanoparticles containing mimics of the miR cluster 99b/let-7e/125a compared to monocytes treated with empty nanoparticles (Fig. 14B). The levels of STAT3 in untreated monocytes, however, were unexpectedly high. Nevertheless, this spontaneous phosphorylation of STAT3 did not appear to be sufficient to cause downstream effects since neither phenotype nor function were affected in these untreated monocytes. Overall, I could not observe a similar upregulation of STAT3 activity by the mimics of the miR cluster 99b/let-7e/125a as was reported for the alternatively activated monocyte-derived DCs by Hildebrand et al. (2018).

Although a modulation of TRIB2 and STAT3 by the mimics of the miR cluster 99b/let-7e/125a was not found in our model, similar trends in their impact on immunosuppressive factors, as was described for the alternatively activated monocyte-derived DCs (Hildebrand et al., 2018) were observed. The cluster mimics-treated monocytes showed an increase in PD-L1 expression as well as a tendency to increase the expression of IDO1 (Fig. 15). In addition, molecules important for T cell activation, including HLA-DR and CD86, appeared to be negatively affected in human monocytes by the direct transfer of miR cluster 99b/let-7e/125a mimics (Fig. 17).

5.5 Conclusions

In summary, this study suggests a key role of miR-125a-5p in the generation of MDSCs via melanoma EV-associated microRNA through activation of NF-κB. Melanoma EVs have been demonstrated to activate NF-κB signaling in mature myeloid cells via a direct interaction HSP cargo molecules and TLRs (Fleming et al., 2019; Shen et al., 2017), resulting in the acquisition of tumor-promoting properties. My data indicate that melanoma EVs could induce similar NF-κB-mediated effects in myeloid cells, including PD-L1 upregulation, via a TLR-independent mechanism

caused by miR-125a-5p delivery. MiR-125a-5p-induced production of ROS and IL-6 could potentially amplify the conversion of myeloid cells to immunosuppressive MDSCs. However, an involvement of STAT3, which could be expected to be activated by IL-6, was not observed. Thus, it appears that TNFAIP3 targeting by miR-125a-5p is the most plausible driver of dysregulated NF-κB activity in this system. The observation that the miR-125a-5p and the three miRs of the cluster 99b/let-7e/125a had similar effects on the myeloid cells supports the conclusion that miR-125a-5p is mainly responsible for shifting the myeloid cell polarization towards MDSCs.

6 REFERENCES

Al-Nedawi, K., Meehan, B., Micallef, J., Lhotak, V., May, L., Guha, A., and Rak, J. (2008). Intercellular transfer of the oncogenic receptor EGFRvIII by microvesicles derived from tumour cells. Nature Cell Biology *10*, 619-624.

Alshetaiwi, H., Pervolarakis, N., McIntyre, L.L., Ma, D., Nguyen, Q., Rath, J.A., Nee, K., Hernandez, G., Evans, K., Torosian, L.*, et al.* (2020). Defining the emergence of myeloid-derived suppressor cells in breast cancer using single-cell transcriptomics. Science Immunology *5*, eaay6017.

Anderson , H.C. (1969). VESICLES ASSOCIATED WITH CALCIFICATION IN THE MATRIX OF EPIPHYSEAL CARTILAGE. Journal of Cell Biology *41*, 59-72.

Androulidaki, A., Iliopoulos, D., Arranz, A., Doxaki, C., Schworer, S., Zacharioudaki, V., Margioris, A.N., Tsichlis, P.N., and Tsatsanis, C. (2009). The Kinase Akt1 Controls Macrophage Response to Lipopolysaccharide by Regulating MicroRNAs. Immunity *31*, 220-231.

Arkhypov, I., Kurt, F.G.Ö., Bitsch, R., Novak, D., Petrova, V., Lasser, S., Hielscher, T., Groth, C., Lepper, A., Hu, X.*, et al.* (2022). HSP90α induces immunosuppressive myeloid cells in melanoma via TLR4 signaling. Journal for ImmunoTherapy of Cancer *10*, e005551.

Arora, M., Poe, S.L., Oriss, T.B., Krishnamoorthy, N., Yarlagadda, M., Wenzel, S.E., Billiar, T.R., Ray, A., and Ray, P. (2010). TLR4/MyD88-induced CD11b+Gr-1intF4/80+ non-migratory myeloid cells suppress Th2 effector function in the lung. Mucosal Immunology *3*, 578-593.

Ballantyne, A.D., and Garnock-Jones, K.P. (2013). Dabrafenib: First Global Approval. Drugs *73*, 1367-1376.

Banerjee, S., Cui, H., Xie, N., Tan, Z., Yang, S., Icyuz, M., Thannickal, V.J., Abraham, E., and Liu, G. (2013). miR-125a-5p Regulates Differential Activation of Macrophages and Inflammation. Journal of Biological Chemistry *288*, 35428-35436.

Bartel, D.P. (2009). MicroRNAs: Target Recognition and Regulatory Functions. Cell *136*, 215-233.

Bartel, D.P. (2018). Metazoan MicroRNAs. Cell *173*, 20-51.

Bazzoni, F., Rossato, M., Fabbri, M., Gaudiosi, D., Mirolo, M., Mori, L., Tamassia, N., Mantovani, A., Cassatella, M.A., and Locati, M. (2009). Induction and regulatory function of miR-9 in human monocytes and neutrophils exposed to proinflammatory signals. Proceedings of the National Academy of Sciences *106*, 5282-5287.

Ben-Shushan, D., Markovsky, E., Gibori, H., Tiram, G., Scomparin, A., and Satchi-Fainaro, R. (2014). Overcoming obstacles in microRNA delivery towards improved cancer therapy. Drug Delivery and Translational Research *4*, 38-49.

Beury, D.W., Parker, K.H., Nyandjo, M., Sinha, P., Carter, K.A., and Ostrand-Rosenberg, S. (2014). Cross-talk among myeloid-derived suppressor cells, macrophages, and tumor cells impacts the inflammatory milieu of solid tumors. Journal of Leukocyte Biology *96*, 1109-1118.

Bilir, C., and Sarisozen, C. (2017). Indoleamine 2,3-dioxygenase (IDO): Only an enzyme or a checkpoint controller? Journal of Oncological Sciences *3*, 52-56.

Bingisser, R.M., Tilbrook, P.A., Holt, P.G., and Kees, U.R. (1998). Macrophage-derived nitric oxide regulates T cell activation via reversible disruption of the Jak3/STAT5 signaling pathway. J Immunol *160*, 5729-5734.

Bjoern, J., Juul Nitschke, N., Zeeberg Iversen, T., Schmidt, H., Fode, K., and Svane, I.M. (2016). Immunological correlates of treatment and response in stage IV malignant melanoma patients treated with Ipilimumab. OncoImmunology *5*, e1100788.

Blattner, C., Fleming, V., Weber, R., Himmelhan, B., Altevogt, P., Gebhardt, C., Schulze, T.J., Razon, H., Hawila, E., Wildbaum, G.*, et al.* (2018). CCR5+ Myeloid-Derived Suppressor Cells Are Enriched and Activated in Melanoma Lesions. Cancer Research *78*, 157-167.

Boone, D.L., Turer, E.E., Lee, E.G., Ahmad, R.-C., Wheeler, M.T., Tsui, C., Hurley, P., Chien, M., Chai, S., Hitotsumatsu, O.*, et al.* (2004). The ubiquitin-modifying enzyme A20 is required for termination of Toll-like receptor responses. Nature Immunology *5*, 1052-1060.

Bronte, V., Brandau, S., Chen, S.-H., Colombo, M.P., Frey, A.B., Greten, T.F., Mandruzzato, S., Murray, P.J., Ochoa, A., Ostrand-Rosenberg, S.*, et al.* (2016). Recommendations for myeloid-derived suppressor cell nomenclature and characterization standards. Nature Communications *7*, 12150.

Bunt, S.K., Clements, V.K., Hanson, E.M., Sinha, P., and Ostrand-Rosenberg, S. (2009). Inflammation enhances myeloid-derived suppressor cell cross-talk by signaling through Toll-like receptor 4. Journal of Leukocyte Biology *85*, 996-1004.

Burke, M., Choksawangkarn, W., Edwards, N., Ostrand-Rosenberg, S., and Fenselau, C. (2014). Exosomes from Myeloid-Derived Suppressor Cells Carry Biologically Active Proteins. Journal of Proteome Research *13*, 836-843.

Busch, S., Auth, E., Scholl, F., Huenecke, S., Koehl, U., Suess, B., and Steinhilber, D. (2015). 5-Lipoxygenase Is a Direct Target of miR-19a-3p and miR-125b-5p. The Journal of Immunology *194*, 1646-1653.

Cai, X., Hagedorn, C.H., and Cullen, B.R. (2004). Human microRNAs are processed from capped, polyadenylated transcripts that can also function as mRNAs. RNA *10*, 1957-1966.

Carrega, P., Pezzino, G., Queirolo, P., Bonaccorsi, I., Falco, M., Vita, G., Pende, D., Misefari, A., Moretta, A., Mingari, M.C.*, et al.* (2009). Susceptibility of Human Melanoma Cells to Autologous Natural Killer (NK) Cell Killing: HLA-Related Effector Mechanisms and Role of Unlicensed NK Cells. PLOS ONE *4*, e8132.

Cassetta, L., Bruderek, K., Skrzeczynska-Moncznik, J., Osiecka, O., Hu, X., Rundgren, I.M., Lin, A., Santegoets, K., Horzum, U., Godinho-Santos, A.*, et al.* (2020). Differential expansion of circulating human MDSC subsets in patients with cancer, infection and inflammation. Journal for ImmunoTherapy of Cancer *8*, e001223.

Castro-Pérez, E., Singh, M., Sadangi, S., Mela-Sánchez, C., and Setaluri, V. (2023). Connecting the dots: Melanoma cell of origin, tumor cell plasticity, trans-differentiation, and drug resistance. Pigment Cell & Melanoma Research *36*, 330-347.

Chalmin, F., Ladoire, S., Mignot, G., Vincent, J., Bruchard, M., Remy-Martin, J.-P., Boireau, W., Rouleau, A., Simon, B., Lanneau, D.*, et al.* (2010). Membrane-associated Hsp72 from tumor-derived exosomes mediates STAT3-dependent immunosuppressive function of mouse and human myeloid-derived suppressor cells. The Journal of Clinical Investigation *120*, 457-471.

Chapman, P.B., Hauschild, A., Robert, C., Haanen, J.B., Ascierto, P., Larkin, J., Dummer, R., Garbe, C., Testori, A., Maio, M.*, et al.* (2011). Improved Survival with Vemurafenib in Melanoma with BRAF V600E Mutation. New England Journal of Medicine *364*, 2507-2516.

Chaudhuri, A.A., So, A.Y.-L., Sinha, N., Gibson, W.S.J., Taganov, K.D., O'Connell, R.M., and Baltimore, D. (2011). MicroRNA-125b Potentiates Macrophage Activation. The Journal of Immunology *187*, 5062-5068.

Chen, H., Zeng, B., Li, X., Zhao, Q., Liu, D., Chen, Y., Zhang, Y., Wang, J., and Xing, H.R. (2022). High-Metastatic Melanoma Cells Promote the Metastatic Capability of Low-Metastatic Melanoma Cells via Exosomal Transfer of miR-411-5p. Frontiers in Oncology *12*.

Chen, M.-F., Kuan, F.-C., Yen, T.-C., Lu, M.-S., Lin, P.-Y., Chung, Y.-H., Chen, W.-C., and Lee, K.-D. (2014). IL-6-stimulated CD11b + CD14 + HLA-DR − myeloid-derived suppressor cells, are associated with progression and poor prognosis in squamous cell carcinoma of the esophagus. Oncotarget *5*.

Chen, X., Ba, Y., Ma, L., Cai, X., Yin, Y., Wang, K., Guo, J., Zhang, Y., Chen, J., Guo, X.*, et al.* (2008). Characterization of microRNAs in serum: a novel class of biomarkers for diagnosis of cancer and other diseases. Cell Research *18*, 997-1006.

Chen, X., Eksioglu, E.A., Zhou, J., Zhang, L., Djeu, J., Fortenbery, N., Epling-Burnette, P., Van Bijnen, S., Dolstra, H., Cannon, J.*, et al.* (2013). Induction of myelodysplasia by myeloid-derived suppressor cells. The Journal of Clinical Investigation *123*, 4595-4611.

Chen, X., Zhou, J., Li, X., Wang, X., Lin, Y., and Wang, X. (2018). Exosomes derived from hypoxic epithelial ovarian cancer cells deliver microRNAs to macrophages and elicit a tumor-promoted phenotype. Cancer Letters *435*, 80-91.

Chiesa, M.D., Carlomagno, S., Frumento, G., Balsamo, M., Cantoni, C., Conte, R., Moretta, L., Moretta, A., and Vitale, M. (2006). The tryptophan catabolite l-

kynurenine inhibits the surface expression of NKp46- and NKG2D-activating receptors and regulates NK-cell function. Blood *108*, 4118-4125.

Christiansson, L., Soderlund, S., Svensson, E., Mustjoki, S., Bengtsson, M., Simonsson, B., Olsson-Stromberg, U., and Loskog, A.S. (2013). Increased level of myeloid-derived suppressor cells, programmed death receptor ligand 1/programmed death receptor 1, and soluble CD25 in Sokal high risk chronic myeloid leukemia. PLoS One *8*, e55818.

Colombo, M., Raposo, G., and Théry, C. (2014). Biogenesis, Secretion, and Intercellular Interactions of Exosomes and Other Extracellular Vesicles. Annual Review of Cell and Developmental Biology *30*, 255-289.

Condamine, T., Dominguez, G.A., Youn, J.-I., Kossenkov, A.V., Mony, S., Alicea-Torres, K., Tcyganov, E., Hashimoto, A., Nefedova, Y., Lin, C*., et al.* (2016). Lectin-type oxidized LDL receptor-1 distinguishes population of human polymorphonuclear myeloid-derived suppressor cells in cancer patients. Science Immunology *1*, aaf8943-aaf8943.

Condamine, T., and Gabrilovich, D.I. (2011). Molecular mechanisms regulating myeloid-derived suppressor cell differentiation and function. Trends in Immunology *32*, 19-25.

Condamine, T., Mastio, J., and Gabrilovich, D.I. (2015). Transcriptional regulation of myeloid-derived suppressor cells. Journal of Leukocyte Biology *98*, 913-922.

Cortés, M., Sanchez-Moral, L., de Barrios, O., Fernández-Aceñero, M.J., Martínez-Campanario, M., Esteve-Codina, A., Darling, D.S., Győrffy, B., Lawrence, T., Dean, D.C., and Postigo, A. (2017). Tumor-associated macrophages (TAMs) depend on ZEB1 for their cancer-promoting roles. The EMBO Journal *36*, 3336-3355.

Corzo, C.A., Condamine, T., Lu, L., Cotter, M.J., Youn, J.-I., Cheng, P., Cho, H.-I., Celis, E., Quiceno, D.G., Padhya, T.*, et al.* (2010). HIF-1α regulates function and differentiation of myeloid-derived suppressor cells in the tumor microenvironment. Journal of Experimental Medicine *207*, 2439-2453.

Corzo, C.A., Cotter, M.J., Cheng, P., Cheng, F., Kusmartsev, S., Sotomayor, E., Padhya, T., McCaffrey, T.V., McCaffrey, J.C., and Gabrilovich, D.I. (2009). Mechanism Regulating Reactive Oxygen Species in Tumor-Induced Myeloid-Derived Suppressor Cells. The Journal of Immunology *182*, 5693-5701.

Crawford, N. (1971). The Presence of Contractile Proteins in Platelet Microparticles Isolated from Human and Animal Platelet-free Plasma. British Journal of Haematology *21*, 53-69.

Curtale, G., Renzi, T.A., Mirolo, M., Drufuca, L., Albanese, M., De Luca, M., Rossato, M., Bazzoni, F., and Locati, M. (2018). Multi-Step Regulation of the TLR4 Pathway by the miR-125a~99b~let-7e Cluster. Frontiers in Immunology *9*.

Dasgupta, I., and Chatterjee, A. (2021). Recent Advances in miRNA Delivery Systems. Methods and Protocols *4*, 10.

Daveri, E., Vergani, E., Shahaj, E., Bergamaschi, L., La Magra, S., Dosi, M., Castelli, C., Rodolfo, M., Rivoltini, L., Vallacchi, V., and Huber, V. (2020). microRNAs Shape Myeloid Cell-Mediated Resistance to Cancer Immunotherapy. Frontiers in Immunology *11*.

de la Rica, L., García-Gómez, A., Comet, N.R., Rodríguez-Ubreva, J., Ciudad, L., Vento-Tormo, R., Company, C., Álvarez-Errico, D., García, M., Gómez-Vaquero, C., and Ballestar, E. (2015). NF-κB-direct activation of microRNAs with repressive effects on monocyte-specific genes is critical for osteoclast differentiation. Genome Biology *16*, 2.

Dollt, C., Michel, J., Kloss, L., Melchers, S., Schledzewski, K., Becker, K., Sauer, A., Krewer, A., Koll, F., and Schmieder, A. (2018). The novel immunoglobulin super family receptor SLAMF9 identified in TAM of murine and human melanoma influences pro-inflammatory cytokine secretion and migration. Cell Death & Disease *9*, 939.

Dror, S., Sander, L., Schwartz, H., Sheinboim, D., Barzilai, A., Dishon, Y., Apcher, S., Golan, T., Greenberger, S., Barshack, I.*, et al.* (2016). Melanoma miRNA trafficking controls tumour primary niche formation. Nature Cell Biology *18*, 1006-1017.

Duraiswamy, J., Freeman, G.J., and Coukos, G. (2013). Therapeutic PD-1 pathway blockade augments with other modalities of immunotherapy T-cell function to prevent immune decline in ovarian cancer. Cancer Res *73*, 6900-6912.

Duroux-Richard, I., Roubert, C., Ammari, M., Présumey, J., Grün, J.R., Häupl, T., Grützkau, A., Lecellier, C.-H., Boitez, V., Codogno, P.*, et al.* (2016). miR-125b controls monocyte adaptation to inflammation through mitochondrial metabolism and dynamics. Blood *128*, 3125-3136.

Dvorak, H.F., Quay, S.C., Orenstein, N.S., Dvorak, A.M., Hahn, P., Bitzer, A.M., and Carvalho, A.C. (1981). Tumor Shedding and Coagulation. Science *212*, 923-924.

Fabbri, M., Paone, A., Calore, F., Galli, R., Gaudio, E., Santhanam, R., Lovat, F., Fadda, P., Mao, C., Nuovo, G.J.*, et al.* (2012). MicroRNAs bind to Toll-like receptors to induce prometastatic inflammatory response. Proc Natl Acad Sci U S A *109*, E2110-2116.

Felicetti, F., De Feo, A., Coscia, C., Puglisi, R., Pedini, F., Pasquini, L., Bellenghi, M., Errico, M.C., Pagani, E., and Carè, A. (2016). Exosome-mediated transfer of miR-222 is sufficient to increase tumor malignancy in melanoma. Journal of Translational Medicine *14*, 56.

Feng, S., Cheng, X., Zhang, L., Lu, X., Chaudhary, S., Teng, R., Frederickson, C., Champion, M.M., Zhao, R., Cheng, L.*, et al.* (2018). Myeloid-derived suppressor cells inhibit T cell activation through nitrating LCK in mouse cancers. Proc Natl Acad Sci U S A *115*, 10094-10099.

Fiaschi, T., and Chiarugi, P. (2012). Oxidative Stress, Tumor Microenvironment, and Metabolic Reprogramming: A Diabolic Liaison. International Journal of Cell Biology *2012*, 762825.

Filipazzi, P., Valenti, R., Huber, V., Pilla, L., Canese, P., Iero, M., Castelli, C., Mariani, L., Parmiani, G., and Rivoltini, L. (2007). Identification of a New Subset of Myeloid Suppressor Cells in Peripheral Blood of Melanoma Patients With Modulation by a Granulocyte-Macrophage Colony-Stimulation Factor–Based Antitumor Vaccine. Journal of Clinical Oncology *25*, 2546-2553.

Flaherty, K.T., Robert, C., Hersey, P., Nathan, P., Garbe, C., Milhem, M., Demidov, L.V., Hassel, J.C., Rutkowski, P., Mohr, P.*, et al.* (2012). Improved Survival with MEK Inhibition in BRAF-Mutated Melanoma. New England Journal of Medicine *367*, 107-114.

Fleming, V. (2018). Immunosuppression in malignant melanoma induced by tumor-derived extracellular vesicles. Med. Dissertation. Medizinische Fakultät Mannheim, Universität Heidelberg.

Fleming, V., Hu, X., Weller, C., Weber, R., Groth, C., Riester, Z., Huser, L., Sun, Q., Nagibin, V., Kirschning, C.*, et al.* (2019). Melanoma Extracellular Vesicles Generate Immunosuppressive Myeloid Cells by Upregulating PD-L1 via TLR4 Signaling. Cancer Research *79*, 4715-4728.

Frumento, G., Rotondo , R., Tonetti , M., Damonte , G., Benatti , U., and Ferrara , G.B. (2002). Tryptophan-derived Catabolites Are Responsible for Inhibition of T and Natural Killer Cell Proliferation Induced by Indoleamine 2,3-Dioxygenase. Journal of Experimental Medicine *196*, 459-468.

Fu, G., Brkić, J., Hayder, H., and Peng, C. (2013). MicroRNAs in Human Placental Development and Pregnancy Complications. International Journal of Molecular Sciences *14*, 5519-5544.

Fu, Y., Chen, J., and Huang, Z. (2019). Recent progress in microRNA-based delivery systems for the treatment of human disease. ExRNA *1*, 24.

Gabrilovich, D., Ishida, T., Oyama, T., Ran, S., Kravtsov, V., Nadaf, S., and Carbone, D.P. (1998). Vascular Endothelial Growth Factor Inhibits the Development of Dendritic Cells and Dramatically Affects the Differentiation of Multiple Hematopoietic Lineages In Vivo: Presented in part at the Keystone Symposium “Cellular and Molecular Biology of Dendritic Cells,” Santa Fe, NM, March 3-9, 1998, and at the annual meeting of the American Association for Cancer Research, March 28-April 1, 1998. Blood *92*, 4150-4166.

Gabrilovich, D.I., Bronte, V., Chen, S.-H., Colombo, M.P., Ochoa, A., Ostrand-Rosenberg, S., and Schreiber, H. (2007). The Terminology Issue for Myeloid-Derived Suppressor Cells. Cancer Research *67*, 425-425.

Gabrilovich, D.I., Chen, H.L., Girgis, K.R., Cunningham, H.T., Meny, G.M., Nadaf, S., Kavanaugh, D., and Carbone, D.P. (1996). Production of vascular endothelial growth factor by human tumors inhibits the functional maturation of dendritic cells. Nature Medicine *2*, 1096-1103.

Gebhardt, C., Sevko, A., Jiang, H., Lichtenberger, R., Reith, M., Tarnanidis, K., Holland-Letz, T., Umansky, L., Beckhove, P., Sucker, A.*, et al.* (2015). Myeloid Cells

and Related Chronic Inflammatory Factors as Novel Predictive Markers in Melanoma Treatment with Ipilimumab. Clinical Cancer Research *21*, 5453-5459.

Gehad, A.E., Lichtman, M.K., Schmults, C.D., Teague, J.E., Calarese, A.W., Jiang, Y., Watanabe, R., and Clark, R.A. (2012). Nitric oxide-producing myeloid-derived suppressor cells inhibit vascular E-selectin expression in human squamous cell carcinomas. J Invest Dermatol *132*, 2642-2651.

George, J., Thoi, L., McManus, L., and Reimann, T. (1982). Isolation of human platelet membrane microparticles from plasma and serum. Blood *60*, 834-840.

Gerloff, D., Lützkendorf, J., Moritz, R.K.C., Wersig, T., Mäder, K., Müller, L.P., and Sunderkötter, C. (2020). Melanoma-Derived Exosomal miR-125b-5p Educates Tumor Associated Macrophages (TAMs) by Targeting Lysosomal Acid Lipase A (LIPA). Cancers *12*, 464.

Gerrits, A., Walasek, M.A., Olthof, S., Weersing, E., Ritsema, M., Zwart, E., van Os, R., Bystrykh, L.V., and de Haan, G. (2012). Genetic screen identifies microRNA cluster 99b/let-7e/125a as a regulator of primitive hematopoietic cells. Blood *119*, 377-387.

Ghafouri-Fard, S., Shoorei, H., Noferesti, L., Hussen, B.M., Moghadam, M.H.B., Taheri, M., and Rashnoo, F. (2023). Nanoparticle-mediated delivery of microRNAs-based therapies for treatment of disorders. Pathology - Research and Practice *248*, 154667.

Giesbrecht, K., Eberle, M.-E., Wölfle, S.J., Sahin, D., Sähr, A., Oberhardt, V., Menne, Z., Bode, K.A., Heeg, K., and Hildebrand, D. (2017). IL-1β As Mediator of Resolution That Reprograms Human Peripheral Monocytes toward a Suppressive Phenotype. Frontiers in Immunology *8*.

Gilmore, T.D. (2006). Introduction to NF-κB: players, pathways, perspectives. Oncogene *25*, 6680-6684.

Graff, J.W., Dickson, A.M., Clay, G., McCaffrey, A.P., and Wilson, M.E. (2012). Identifying Functional MicroRNAs in Macrophages with Polarized Phenotypes. Journal of Biological Chemistry *287*, 21816-21825.

Grishok, A., Pasquinelli, A.E., Conte, D., Li, N., Parrish, S., Ha, I., Baillie, D.L., Fire, A., Ruvkun, G., and Mello, C.C. (2001). Genes and Mechanisms Related to RNA Interference Regulate Expression of the Small Temporal RNAs that Control C. elegans Developmental Timing. Cell *106*, 23-34.

Grivennikov, S.I., and Karin, M. (2010). Dangerous liaisons: STAT3 and NF-κB collaboration and crosstalk in cancer. Cytokine & Growth Factor Reviews *21*, 11-19.

Groth, C., Arpinati, L., Shaul, M.E., Winkler, N., Diester, K., Gengenbacher, N., Weber, R., Arkhypov, I., Lasser, S., Petrova, V.*, et al.* (2021). Blocking Migration of Polymorphonuclear Myeloid-Derived Suppressor Cells Inhibits Mouse Melanoma Progression. Cancers *13*, 726.

Groth, C., Hu, X., Weber, R., Fleming, V., Altevogt, P., Utikal, J., and Umansky, V. (2019). Immunosuppression mediated by myeloid-derived suppressor cells (MDSCs) during tumour progression. British Journal of Cancer *120*, 16-25.

Guo, H., Ingolia, N.T., Weissman, J.S., and Bartel, D.P. (2010). Mammalian microRNAs predominantly act to decrease target mRNA levels. Nature *466*, 835-840.

Hald Albertsen, C., Kulkarni, J.A., Witzigmann, D., Lind, M., Petersson, K., and Simonsen, J.B. (2022). The role of lipid components in lipid nanoparticles for vaccines and gene therapy. Advanced Drug Delivery Reviews *188*, 114416.

Hart, K.M., Byrne, K.T., Molloy, M.J., Usherwood, E.M., and Berwin, B. (2011). IL-10 immunomodulation of myeloid cells regulates a murine model of ovarian cancer. Front Immunol *2*, 29.

Hayes, J., Peruzzi, P.P., and Lawler, S. (2014). MicroRNAs in cancer: biomarkers, functions and therapy. Trends in Molecular Medicine *20*, 460-469.

Helmbach, H., Rossmann, E., Kern, M.A., and Schadendorf, D. (2001). Drug-resistance in human melanoma. International Journal of Cancer *93*, 617-622.

Hildebrand, D., Eberle, M.E., Wolfle, S.M., Egler, F., Sahin, D., Sahr, A., Bode, K.A., and Heeg, K. (2018). Hsa-miR-99b/let-7e/miR-125a Cluster Regulates Pathogen Recognition Receptor-Stimulated Suppressive Antigen-Presenting Cells. Front Immunol *9*, 1224.

Hitotsumatsu, O., Ahmad, R.-C., Tavares, R., Wang, M., Philpott, D., Turer, E.E., Lee, B.L., Shiffin, N., Advincula, R., Malynn, B.A.*, et al.* (2008). The Ubiquitin-Editing Enzyme A20 Restricts Nucleotide-Binding Oligomerization Domain Containing 2-Triggered Signals. Immunity *28*, 381-390.

Hsu, A.C.Y., Dua, K., Starkey, M.R., Haw, T.-J., Nair, P.M., Nichol, K., Zammit, N., Grey, S.T., Baines, K.J., Foster, P.S.*, et al.* (2017). MicroRNA-125a and -b inhibit A20 and MAVS to promote inflammation and impair antiviral response in COPD. JCI Insight *2*.

Hsu, J., Hodgins, J.J., Marathe, M., Nicolai, C.J., Bourgeois-Daigneault, M.C., Trevino, T.N., Azimi, C.S., Scheer, A.K., Randolph, H.E., Thompson, T.W.*, et al.* (2018). Contribution of NK cells to immunotherapy mediated by PD-1/PD-L1 blockade. J Clin Invest *128*, 4654-4668.

Hu, C.-E., Gan, J., Zhang, R.-D., Cheng, Y.-R., and Huang, G.-J. (2011). Up-regulated myeloid-derived suppressor cell contributes to hepatocellular carcinoma development by impairing dendritic cell function. Scandinavian Journal of Gastroenterology *46*, 156-164.

Huang, B., Pan, P.-Y., Li, Q., Sato, A.I., Levy, D.E., Bromberg, J., Divino, C.M., and Chen, S.-H. (2006). Gr-1+CD115+ Immature Myeloid Suppressor Cells Mediate the Development of Tumor-Induced T Regulatory Cells and T-Cell Anergy in Tumor-Bearing Host. Cancer Research *66*, 1123-1131.

Huang, H.-C., Yu, H.-R., Huang, L.-T., Huang, H.-C., Chen, R.-F., Lin, I.-C., Ou, C.-Y., Hsu, T.-Y., and Yang, K.D. (2012). miRNA-125b regulates TNF-α production in CD14+ neonatal monocytes via post-transcriptional regulation. Journal of Leukocyte Biology *92*, 171-182.

Huber, V., Guardo, L.D., Lalli, L., Giardiello, D., Cova, A., Squarcina, P., Frati, P., Giacomo, A.M.D., Pilla, L., Tazzari, M.*, et al.* (2021). Back to simplicity: a four-marker blood cell score to quantify prognostically relevant myeloid cells in melanoma patients. Journal for ImmunoTherapy of Cancer *9*, e001167.

Huber, V., Vallacchi, V., Fleming, V., Hu, X., Cova, A., Dugo, M., Shahaj, E., Sulsenti, R., Vergani, E., Filipazzi, P.*, et al.* (2018). Tumor-derived microRNAs induce myeloid suppressor cells and predict immunotherapy resistance in melanoma. The Journal of Clinical Investigation *128*, 5505-5516.

Hutvágner, G., McLachlan, J., Pasquinelli, A.E., Bálint, É., Tuschl, T., and Zamore, P.D. (2001). A Cellular Function for the RNA-Interference Enzyme Dicer in the Maturation of the let-7 Small Temporal RNA. Science *293*, 834-838.

Hutvágner, G., and Zamore, P.D. (2002). A microRNA in a Multiple-Turnover RNAi Enzyme Complex. Science *297*, 2056-2060.

Iwata, T., Kondo, Y., Kimura, O., Morosawa, T., Fujisaka, Y., Umetsu, T., Kogure, T., Inoue, J., Nakagome, Y., and Shimosegawa, T. (2016). PD-L1(+)MDSCs are increased in HCC patients and induced by soluble factor in the tumor microenvironment. Sci Rep *6*, 39296.

Kanehisa, M., and Goto, S. (2000). KEGG: Kyoto Encyclopedia of Genes and Genomes. Nucleic Acids Research *28*, 27-30.

Kato, M., Takahashi, M., Akhand, A.A., Liu, W., Dai, Y., Shimizu, S., Iwamoto, T., Suzuki, H., and Nakashima, I. (1998). Transgenic mouse model for skin malignant melanoma. Oncogene *17*, 1885-1888.

Kaul, N., Gopalakrishna, R., Gundimeda, U., Choi, J., and Forman, H.J. (1998). Role of Protein Kinase C in Basal and Hydrogen Peroxide-Stimulated NF-κB Activation in the Murine Macrophage J774A.1 Cell Line. Archives of Biochemistry and Biophysics *350*, 79-86.

Kawamata, T., and Tomari, Y. (2010). Making RISC. Trends in Biochemical Sciences *35*, 368-376.

Kawasaki, T., and Kawai, T. (2014). Toll-Like Receptor Signaling Pathways. Frontiers in Immunology *5*.

Ketting, R.F., Fischer, S.E.J., Bernstein, E., Sijen, T., Hannon, G.J., and Plasterk, R.H.A. (2001). Dicer functions in RNA interference and in synthesis of small RNA involved in developmental timing in C. elegans. Genes & Development *15*, 2654-2659.

Kim, B.H., Roh, E., Lee, H.Y., Lee, I.-J., Ahn, B., Jung, S.-H., Lee, H., Han, S.-B., and Kim, Y. (2008). Benzoxathiole Derivative Blocks Lipopolysaccharide-Induced

Nuclear Factor-κB Activation and Nuclear Factor-κB-Regulated Gene Transcription through Inactivating Inhibitory κB Kinase β. Molecular Pharmacology *73*, 1309-1318.

Kim, S.-W., Ramasamy, K., Bouamar, H., Lin, A.-P., Jiang, D., and Aguiar, R.C.T. (2012). MicroRNAs miR-125a and miR-125b constitutively activate the NF-κB pathway by targeting the tumor necrosis factor alpha-induced protein 3 (TNFAIP3, A20). Proceedings of the National Academy of Sciences *109*, 7865-7870.

Kjeldsen, J.W., Lorentzen, C.L., Martinenaite, E., Ellebaek, E., Donia, M., Holmstroem, R.B., Klausen, T.W., Madsen, C.O., Ahmed, S.M., Weis-Banke, S.E.*, et al.* (2021). A phase 1/2 trial of an immune-modulatory vaccine against IDO/PD-L1 in combination with nivolumab in metastatic melanoma. Nature Medicine *27*, 2212-2223.

Knight, A., Karapetyan, L., and Kirkwood, J.M. (2023). Immunotherapy in Melanoma: Recent Advances and Future Directions. Cancers *15*, 1106.

Knight, S.W., and Bass, B.L. (2001). A Role for the RNase III Enzyme DCR-1 in RNA Interference and Germ Line Development in Caenorhabditis elegans. Science *293*, 2269-2271.

Kobie, J.J., Wu, R.S., Kurt, R.A., Lou, S., Adelman, M.K., Whitesell, L.J., Ramanathapuram, L.V., Arteaga, C.L., and Akporiaye, E.T. (2003). Transforming Growth Factor β Inhibits the Antigen-Presenting Functions and Antitumor Activity of Dendritic Cell Vaccines1. Cancer Research *63*, 1860-1864.

Kusmartsev, S., Cheng, F., Yu, B., Nefedova, Y., Sotomayor, E., Lush, R., and Gabrilovich, D. (2003). All-trans-retinoic acid eliminates immature myeloid cells from tumor-bearing mice and improves the effect of vaccination. Cancer Res *63*, 4441-4449.

Lagos-Quintana, M., Rauhut, R., Lendeckel, W., and Tuschl, T. (2001). Identification of Novel Genes Coding for Small Expressed RNAs. Science *294*, 853-858.

Lamprecht, A., Ubrich, N., Hombreiro Pérez, M., Lehr, C.M., Hoffman, M., and Maincent, P. (2000). Influences of process parameters on nanoparticle preparation performed by a double emulsion pressure homogenization technique. International Journal of Pharmaceutics *196*, 177-182.

Lasser, S.A., Ozbay Kurt, F.G., Arkhypov, I., Utikal, J., and Umansky, V. (2024). Myeloid-derived suppressor cells in cancer and cancer therapy. Nature Reviews Clinical Oncology.

Lau, N.C., Lim, L.P., Weinstein, E.G., and Bartel, D.P. (2001). An Abundant Class of Tiny RNAs with Probable Regulatory Roles in Caenorhabditis elegans. Science *294*, 858-862.

Lee, E.G., Boone, D.L., Chai, S., Libby, S.L., Chien, M., Lodolce, J.P., and Ma, A. (2000). Failure to Regulate TNF-Induced NF-κB and Cell Death Responses in A20-Deficient Mice. Science *289*, 2350-2354.

Lee, J., Rhee, M.H., Kim, E., and Cho, J.Y. (2012). BAY 11-7082 Is a Broad-Spectrum Inhibitor with Anti-Inflammatory Activity against Multiple Targets. Mediators of Inflammation *2012*, 416036.

Lee, R.C., and Ambros, V. (2001). An Extensive Class of Small RNAs in Caenorhabditis elegans. Science *294*, 862-864.

Lee, S.W.L., Paoletti, C., Campisi, M., Osaki, T., Adriani, G., Kamm, R.D., Mattu, C., and Chiono, V. (2019). MicroRNA delivery through nanoparticles. Journal of Controlled Release *313*, 80-95.

Lee, Y., Ahn, C., Han, J., Choi, H., Kim, J., Yim, J., Lee, J., Provost, P., Rådmark, O., Kim, S., and Kim, V.N. (2003). The nuclear RNase III Drosha initiates microRNA processing. Nature *425*, 415-419.

Lee, Y., Jeon, K., Lee, J.T., Kim, S., and Kim, V.N. (2002). MicroRNA maturation: stepwise processing and subcellular localization. The EMBO Journal *21*, 4663-4670.

Lee, Y., Kim, M., Han, J., Yeom, K.H., Lee, S., Baek, S.H., and Kim, V.N. (2004). MicroRNA genes are transcribed by RNA polymerase II. The EMBO Journal *23*, 4051-4060.

Leuschner, P.J.F., Ameres, S.L., Kueng, S., and Martinez, J. (2006). Cleavage of the siRNA passenger strand during RISC assembly in human cells. EMBO reports *7*, 314-320.

Li, H., Han, Y., Guo, Q., Zhang, M., and Cao, X. (2009). Cancer-Expanded Myeloid-Derived Suppressor Cells Induce Anergy of NK Cells through Membrane-Bound TGF-β11. The Journal of Immunology *182*, 240-249.

Li, J., Chen, J., Wang, S., Li, P., Zheng, C., Zhou, X., Tao, Y., Chen, X., Sun, L., Wang, A.*, et al.* (2019). Blockage of transferred exosome-shuttled miR-494 inhibits melanoma growth and metastasis. Journal of Cellular Physiology *234*, 15763-15774.

Li, J., Wang, L., Chen, X., Li, L., Li, Y., Ping, Y., Huang, L., Yue, D., Zhang, Z., Wang, F.*, et al.* (2017). CD39/CD73 upregulation on myeloid-derived suppressor cells via TGF-β-mTOR-HIF-1 signaling in patients with non-small cell lung cancer. Oncoimmunology *6*, e1320011.

Li, X., Liu, D., Chen, H., Zeng, B., Zhao, Q., Zhang, Y., Chen, Y., Wang, J., and Xing, H.R. (2022). Melanoma stem cells promote metastasis via exosomal miR-1268a inactivation of autophagy. Biological Research *55*, 29.

Liang, Y., Wang, W., Zhu, X., Yu, M., and Zhou, C. (2022). Inhibition of myeloid-derived suppressive cell function with all-trans retinoic acid enhanced anti-PD-L1 efficacy in cervical cancer. Scientific Reports *12*, 9619.

Libermann, T.A., and Baltimore, D. (1990). Activation of Interleukin-6 Gene Expression through the NF-κB Transcription Factor. Molecular and Cellular Biology *10*, 2327-2334.

Lim, H.X., Kim, T.S., and Poh, C.L. (2020). Understanding the Differentiation, Expansion, Recruitment and Suppressive Activities of Myeloid-Derived Suppressor Cells in Cancers. International Journal of Molecular Sciences *21*, 3599.

Liu, D., Li, X., Zeng, B., Zhao, Q., Chen, H., Zhang, Y., Chen, Y., Wang, J., and Xing, H.R. (2023). Exosomal microRNA-4535 of Melanoma Stem Cells Promotes Metastasis by Inhibiting Autophagy Pathway. Stem Cell Reviews and Reports *19*, 155-169.

Liu, Y., Wei, J., Guo, G., and Zhou, J. (2015). Norepinephrine-induced myeloid-derived suppressor cells block T-cell responses via generation of reactive oxygen species. Immunopharmacology and Immunotoxicology *37*, 359-365.

Liu, Y., Yu, Y., Yang, S., Zeng, B., Zhang, Z., Jiao, G., Zhang, Y., Cai, L., and Yang, R. (2009). Regulation of arginase I activity and expression by both PD-1 and CTLA-4 on the myeloid-derived suppressor cells. Cancer Immunology, Immunotherapy *58*, 687-697.

Loercher, A.E., Nash, M.A., Kavanagh, J.J., Platsoucas, C.D., and Freedman, R.S. (1999). Identification of an IL-10-producing HLA-DR-negative monocyte subset in the malignant ascites of patients with ovarian carcinoma that inhibits cytokine protein expression and proliferation of autologous T cells. J Immunol *163*, 6251-6260.

Luan, W., Ding, Y., Xi, H., Ruan, H., Lu, F., Ma, S., and Wang, J. (2021). Exosomal miR-106b-5p derived from melanoma cell promotes primary melanocytes epithelial-mesenchymal transition through targeting EphA4. Journal of Experimental & Clinical Cancer Research *40*, 107.

Ma, J., Zhan, Y., Xu, Z., Li, Y., Luo, A., Ding, F., Cao, X., Chen, H., and Liu, Z. (2017). ZEB1 induced miR-99b/let-7e/miR-125a cluster promotes invasion and metastasis in esophageal squamous cell carcinoma. Cancer Letters *398*, 37-45.

Mackensen, A., Carcelain, G., Viel, S., Raynal, M.C., Michalaki, H., Triebel, F., Bosq, J., and Hercend, T. (1994). Direct evidence to support the immunosurveillance concept in a human regressive melanoma. The Journal of Clinical Investigation *93*, 1397-1402.

Mackensen, A., Ferradini, L., Carcelain, G., Triebel, F., Faure, F., Viel, S., and Hercend, T. (1993). Evidence for in Situ Amplification of Cytotoxic T-Lymphocytes with Antitumor Activity in a Human Regressive Melanoma. Cancer Research *53*, 3569-3573.

Mahmoud, F., Shields, B., Makhoul, I., Avaritt, N., Wong, H.K., Hutchins, L.F., Shalin, S., and Tackett, A.J. (2017). Immune surveillance in melanoma: From immune attack to melanoma escape and even counterattack. Cancer Biology & Therapy *18*, 451-469.

Mao, Y., Sarhan, D., Steven, A., Seliger, B., Kiessling, R., and Lundqvist, A. (2014). Inhibition of tumor-derived prostaglandin-e2 blocks the induction of myeloid-derived suppressor cells and recovers natural killer cell activity. Clin Cancer Res *20*, 4096-4106.

Mariathasan, S., Turley, S.J., Nickles, D., Castiglioni, A., Yuen, K., Wang, Y., Kadel Iii, E.E., Koeppen, H., Astarita, J.L., Cubas, R.*, et al.* (2018). TGFβ attenuates tumour response to PD-L1 blockade by contributing to exclusion of T cells. Nature *554*, 544-548.

Mastio, J., Condamine, T., Dominguez, G., Kossenkov, A.V., Donthireddy, L., Veglia, F., Lin, C., Wang, F., Fu, S., Zhou, J.*, et al.* (2019). Identification of monocyte-like precursors of granulocytes in cancer as a mechanism for accumulation of PMN-MDSCs. J Exp Med *216*, 2150-2169.

Mastroianni, J., Stickel, N., Andrlova, H., Hanke, K., Melchinger, W., Duquesne, S., Schmidt, D., Falk, M., Andrieux, G., Pfeifer, D.*, et al.* (2019). miR-146a Controls Immune Response in the Melanoma Microenvironment. Cancer Research *79*, 183-195.

Matsusaka, T., Fujikawa, K., Nishio, Y., Mukaida, N., Matsushima, K., Kishimoto, T., and Akira, S. (1993). Transcription factors NF-IL6 and NF-kappa B synergistically activate transcription of the inflammatory cytokines, interleukin 6 and interleukin 8. Proceedings of the National Academy of Sciences *90*, 10193-10197.

McArthur, G.A., Chapman, P.B., Robert, C., Larkin, J., Haanen, J.B., Dummer, R., Ribas, A., Hogg, D., Hamid, O., Ascierto, P.A.*, et al.* (2014). Safety and efficacy of vemurafenib in BRAFV600E and BRAFV600K mutation-positive melanoma (BRIM-3): extended follow-up of a phase 3, randomised, open-label study. The Lancet Oncology *15*, 323-332.

Meng, Q., Duan, X., Yang, Q., Xue, D., Liu, Z., Li, Y., Jin, Q., Guo, F., Jia, S., Wang, Z.*, et al.* (2022). SLAMF6/Ly108 promotes the development of hepatocellular carcinoma via facilitating macrophage M2 polarization. Oncology Letters *23*, 83.

Mezrich, J.D., Fechner, J.H., Zhang, X., Johnson, B.P., Burlingham, W.J., and Bradfield, C.A. (2010). An Interaction between Kynurenine and the Aryl Hydrocarbon Receptor Can Generate Regulatory T Cells. The Journal of Immunology *185*, 3190-3198.

Mirza, N., Fishman, M., Fricke, I., Dunn, M., Neuger, A.M., Frost, T.J., Lush, R.M., Antonia, S., and Gabrilovich, D.I. (2006). All-trans-Retinoic Acid Improves Differentiation of Myeloid Cells and Immune Response in Cancer Patients. Cancer Research *66*, 9299-9307.

Mitchell, P.S., Parkin, R.K., Kroh, E.M., Fritz, B.R., Wyman, S.K., Pogosova-Agadjanyan, E.L., Peterson, A., Noteboom, J., O'Briant, K.C., Allen, A.*, et al.* (2008). Circulating microRNAs as stable blood-based markers for cancer detection. Proceedings of the National Academy of Sciences *105*, 10513-10518.

Miyoshi, K., Tsukumo, H., Nagami, T., Siomi, H., and Siomi, M.C. (2005). Slicer function of Drosophila Argonautes and its involvement in RISC formation. Genes & Development *19*, 2837-2848.

Molon, B., Ugel, S., Del Pozzo, F., Soldani, C., Zilio, S., Avella, D., De Palma, A., Mauri, P., Monegal, A., Rescigno, M.*, et al.* (2011). Chemokine nitration prevents

intratumoral infiltration of antigen-specific T cells. Journal of Experimental Medicine *208*, 1949-1962.

Morello, S., Pinto, A., Blandizzi, C., and Antonioli, L. (2016). Myeloid cells in the tumor microenvironment: Role of adenosine. OncoImmunology *5*, e1108515.

Movahedi, K., Guilliams, M., Van den Bossche, J., Van den Bergh, R., Gysemans, C., Beschin, A., De Baetselier, P., and Van Ginderachter, J.A. (2008). Identification of discrete tumor-induced myeloid-derived suppressor cell subpopulations with distinct T cell-suppressive activity. Blood *111*, 4233-4244.

Mukherji, B. (2013). Immunology of melanoma. Clinics in Dermatology *31*, 156-165.

Mulcahy, L.A., Pink, R.C., and Carter, D.R.F. (2014). Routes and mechanisms of extracellular vesicle uptake. Journal of Extracellular Vesicles *3*, 24641.

Munn, D.H., Sharma, M.D., Baban, B., Harding, H.P., Zhang, Y., Ron, D., and Mellor, A.L. (2005). GCN2 Kinase in T Cells Mediates Proliferative Arrest and Anergy Induction in Response to Indoleamine 2,3-Dioxygenase. Immunity *22*, 633-642.

Nagaraj, S., Gupta, K., Pisarev, V., Kinarsky, L., Sherman, S., Kang, L., Herber, D.L., Schneck, J., and Gabrilovich, D.I. (2007). Altered recognition of antigen is a mechanism of CD8+ T cell tolerance in cancer. Nat Med *13*, 828-835.

Nakajima, S., and Kitamura, M. (2013). Bidirectional regulation of NF-κB by reactive oxygen species: A role of unfolded protein response. Free Radical Biology and Medicine *65*, 162-174.

Nayerossadat, N., Maedeh, T., and Ali, P.A. (2012). Viral and nonviral delivery systems for gene delivery. Advanced Biomedical Research *1*, 27.

Ng, Y.S., Roca, H., Fuller, D., Sud, S., and Pienta, K.J. (2012). Chemical transfection of dye-conjugated microRNA precursors for microRNA functional analysis of M2 macrophages. Journal of Cellular Biochemistry *113*, 1714-1723.

Noman, M.Z., Desantis, G., Janji, B., Hasmim, M., Karray, S., Dessen, P., Bronte, V., and Chouaib, S. (2014). PD-L1 is a novel direct target of HIF-1alpha, and its blockade under hypoxia enhanced MDSC-mediated T cell activation. J Exp Med *211*, 781-790.

O'Brien, J., Hayder, H., Zayed, Y., and Peng, C. (2018). Overview of MicroRNA Biogenesis, Mechanisms of Actions, and Circulation. Frontiers in Endocrinology *9*.

Obermajer, N., and Kalinski, P. (2012). Key role of the positive feedback between PGE2 and COX2 in the biology of myeloid-derived suppressor cells. OncoImmunology *1*, 762-764.

Obermajer, N., Muthuswamy, R., Lesnock, J., Edwards, R.P., and Kalinski, P. (2011). Positive feedback between PGE2 and COX2 redirects the differentiation of human dendritic cells toward stable myeloid-derived suppressor cells. Blood *118*, 5498-5505.

Özbay Kurt, F.G. (2023). Targeting MDSC-mediated immunosuppression in melanoma. Med. Dissertation. Medizinische Fakultät Mannheim, Universität Heidelberg.

Parolini, I., Federici, C., Raggi, C., Lugini, L., Palleschi, S., De Milito, A., Coscia, C., Iessi, E., Logozzi, M., Molinari, A.*, et al.* (2009). Microenvironmental pH Is a Key Factor for Exosome Traffic in Tumor Cells *. Journal of Biological Chemistry *284*, 34211-34222.

Passarelli, A., Mannavola, F., Stefania Stucci, L., Tucci, M., and Silvestris, F. (2017). Immune system and melanoma biology: a balance between immunosurveillance and immune escape. Oncotarget *8*.

Paul, P., Chakraborty, A., Sarkar, D., Langthasa, M., Rahman, M., Bari, M., Singha, R.S., Malakar, A.K., and Chakraborty, S. (2018). Interplay between miRNAs and human diseases. Journal of Cellular Physiology *233*, 2007-2018.

Pedroso de Lima, M.C., Simões, S., Pires, P., Faneca, H., and Düzgüneş, N. (2001). Cationic lipid–DNA complexes in gene delivery: from biophysics to biological applications. Advanced Drug Delivery Reviews *47*, 277-294.

Pegoraro, A., De Marchi, E., Ferracin, M., Orioli, E., Zanoni, M., Bassi, C., Tesei, A., Capece, M., Dika, E., Negrini, M.*, et al.* (2021). P2X7 promotes metastatic spreading and triggers release of miRNA-containing exosomes and microvesicles from melanoma cells. Cell Death & Disease *12*, 1088.

Peng, L., Zhang, H., Hao, Y., Xu, F., Yang, J., Zhang, R., Lu, G., Zheng, Z., Cui, M., Qi, C.-F.*, et al.* (2016). Reprogramming macrophage orientation by microRNA 146b targeting transcription factor IRF5. eBioMedicine *14*, 83-96.

Pico de Coaña, Y., Wolodarski, M., van der Haar Àvila, I., Nakajima, T., Rentouli, S., Lundqvist, A., Masucci, G., Hansson, J., and Kiessling, R. (2020). PD-1 checkpoint blockade in advanced melanoma patients: NK cells, monocytic subsets and host PD-L1 expression as predictive biomarker candidates. OncoImmunology *9*, 1786888.

Pillai, R.S., Bhattacharyya, S.N., Artus, C.G., Zoller, T., Cougot, N., Basyuk, E., Bertrand, E., and Filipowicz, W. (2005). Inhibition of Translational Initiation by Let-7 MicroRNA in Human Cells. Science *309*, 1573-1576.

Pop, M.A., and Almquist, B.D. (2021). Controlled Delivery of MicroRNAs into Primary Cells Using Nanostraw Technology. Advanced NanoBiomed Research *1*, 2000061.

Potenza, N., Panella, M., Castiello, F., Mosca, N., Amendola, E., and Russo, A. (2017). Molecular mechanisms governing microRNA-125a expression in human hepatocellular carcinoma cells. Scientific Reports *7*, 10712.

Prima, V., Kaliberova, L.N., Kaliberov, S., Curiel, D.T., and Kusmartsev, S. (2017). COX2/mPGES1/PGE2 pathway regulates PD-L1 expression in tumor-associated macrophages and myeloid-derived suppressor cells. Proc Natl Acad Sci U S A *114*, 1117-1122.

Qian, B.-Z., Li, J., Zhang, H., Kitamura, T., Zhang, J., Campion, L.R., Kaiser, E.A., Snyder, L.A., and Pollard, J.W. (2011). CCL2 recruits inflammatory monocytes to facilitate breast-tumour metastasis. Nature *475*, 222-225.

Raber, P.L., Thevenot, P., Sierra, R., Wyczechowska, D., Halle, D., Ramirez, M.E., Ochoa, A.C., Fletcher, M., Velasco, C., Wilk, A.*, et al.* (2014). Subpopulations of myeloid-derived suppressor cells impair T cell responses through independent nitric oxide-related pathways. Int J Cancer *134*, 2853-2864.

Rajaram, M.V.S., Ni, B., Morris, J.D., Brooks, M.N., Carlson, T.K., Bakthavachalu, B., Schoenberg, D.R., Torrelles, J.B., and Schlesinger, L.S. (2011). Mycobacterium tuberculosis lipomannan blocks TNF biosynthesis by regulating macrophage MAPK-activated protein kinase 2 (MK2) and microRNA miR-125b. Proceedings of the National Academy of Sciences *108*, 17408-17413.

Raposo, G., Nijman, H.W., Stoorvogel, W., Liejendekker, R., Harding, C.V., Melief, C.J., and Geuze, H.J. (1996). B lymphocytes secrete antigen-presenting vesicles. Journal of Experimental Medicine *183*, 1161-1172.

Ritchie, M.E., Phipson, B., Wu, D., Hu, Y., Law, C.W., Shi, W., and Smyth, G.K. (2015). limma powers differential expression analyses for RNA-sequencing and microarray studies. Nucleic Acids Research *43*, e47-e47.

Rivera, L.B., and Bergers, G. (2015). Intertwined regulation of angiogenesis and immunity by myeloid cells. Trends in Immunology *36*, 240-249.

Rodriguez, A., Griffiths-Jones, S., Ashurst, J.L., and Bradley, A. (2004a). Identification of Mammalian microRNA Host Genes and Transcription Units. Genome Research *14*, 1902-1910.

Rodríguez, P.C., and Ochoa, A.C. (2008). Arginine regulation by myeloid derived suppressor cells and tolerance in cancer: mechanisms and therapeutic perspectives. Immunological Reviews *222*, 180-191.

Rodriguez, P.C., Quiceno, D.G., and Ochoa, A.C. (2006). l-arginine availability regulates T-lymphocyte cell-cycle progression. Blood *109*, 1568-1573.

Rodriguez, P.C., Quiceno, D.G., Zabaleta, J., Ortiz, B., Zea, A.H., Piazuelo, M.B., Delgado, A., Correa, P., Brayer, J., Sotomayor, E.M.*, et al.* (2004b). Arginase I Production in the Tumor Microenvironment by Mature Myeloid Cells Inhibits T-Cell Receptor Expression and Antigen-Specific T-Cell Responses. Cancer Research *64*, 5839-5849.

Santovito, D., and Weber, C. (2022). Non-canonical features of microRNAs: paradigms emerging from cardiovascular disease. Nature Reviews Cardiology *19*, 620-638.

Saraiva, M., Christensen, J.R., Tsytsykova, A.V., Goldfeld, A.E., Ley, S.C., Kioussis, D., and O′Garra, A. (2005). Identification of a Macrophage-Specific Chromatin Signature in the IL-10 Locus1. The Journal of Immunology *175*, 1041-1046.

Sato, Y., Shimizu, K., Shinga, J., Hidaka, M., Kawano, F., Kakimi, K., Yamasaki, S., Asakura, M., and Fujii, S.I. (2015). Characterization of the myeloid-derived suppressor cell subset regulated by NK cells in malignant lymphoma. Oncoimmunology *4*, e995541.

Serafini, P., Borrello, I., and Bronte, V. (2006). Myeloid suppressor cells in cancer: Recruitment, phenotype, properties, and mechanisms of immune suppression. Seminars in Cancer Biology *16*, 53-65.

Shen, Y., Guo, D., Weng, L., Wang, S., Ma, Z., Yang, Y., Wang, P., Wang, J., and Cai, Z. (2017). Tumor-derived exosomes educate dendritic cells to promote tumor metastasis via HSP72/HSP105-TLR2/TLR4 pathway. OncoImmunology *6*, e1362527.

Shu, S.L., Yang, Y., Allen, C.L., Maguire, O., Minderman, H., Sen, A., Ciesielski, M.J., Collins, K.A., Bush, P.J., Singh, P.*, et al.* (2018). Metabolic reprogramming of stromal fibroblasts by melanoma exosome microRNA favours a pre-metastatic microenvironment. Scientific Reports *8*, 12905.

Simon, P.S., Sharman, S.K., Lu, C., Yang, D., Paschall, A.V., Tulachan, S.S., and Liu, K. (2015). The NF-κB p65 and p50 homodimer cooperate with IRF8 to activate iNOS transcription. BMC Cancer *15*, 770.

Sinha, P., Clements, V.K., Bunt, S.K., Albelda, S.M., and Ostrand-Rosenberg, S. (2007). Cross-Talk between Myeloid-Derived Suppressor Cells and Macrophages Subverts Tumor Immunity toward a Type 2 Response1. The Journal of Immunology *179*, 977-983.

Smyth, G.K. (2004). Linear Models and Empirical Bayes Methods for Assessing Differential Expression in Microarray Experiments. Statistical Applications in Genetics and Molecular Biology *3*.

Stavast, C.J., and Erkeland, S.J. (2019). The Non-Canonical Aspects of MicroRNAs: Many Roads to Gene Regulation. Cells *8*, 1465.

Steele, C.W., Karim, S.A., Leach, J.D.G., Bailey, P., Upstill-Goddard, R., Rishi, L., Foth, M., Bryson, S., McDaid, K., Wilson, Z.*, et al.* (2016). CXCR2 Inhibition Profoundly Suppresses Metastases and Augments Immunotherapy in Pancreatic Ductal Adenocarcinoma. Cancer Cell *29*, 832-845.

Steinbrink, K., Graulich, E., Kubsch, S., Knop, J., and Enk, A.H. (2002). CD4+ and CD8+ anergic T cells induced by interleukin-10–treated human dendritic cells display antigen-specific suppressor activity. Blood *99*, 2468-2476.

Steinbrink, K., Wölfl, M., Jonuleit, H., Knop, J., and Enk, A.H. (1997). Induction of tolerance by IL-10-treated dendritic cells. The Journal of Immunology *159*, 4772-4780.

Stiff, A., Trikha, P., Mundy-Bosse, B., McMichael, E., Mace, T.A., Benner, B., Kendra, K., Campbell, A., Gautam, S., Abood, D.*, et al.* (2018). Nitric Oxide Production by Myeloid-Derived Suppressor Cells Plays a Role in Impairing Fc

Receptor–Mediated Natural Killer Cell Function. Clinical Cancer Research *24*, 1891-1904.

Strauss, L., Mahmoud, M.A.A., Weaver, J.D., Tijaro-Ovalle, N.M., Christofides, A., Wang, Q., Pal, R., Yuan, M., Asara, J., Patsoukis, N., and Boussiotis, V.A. (2020). Targeted deletion of PD-1 in myeloid cells induces antitumor immunity. Science Immunology *5*, eaay1863.

Subramanian, A., Tamayo, P., Mootha, V.K., Mukherjee, S., Ebert, B.L., Gillette, M.A., Paulovich, A., Pomeroy, S.L., Golub, T.R., Lander, E.S., and Mesirov, J.P. (2005). Gene set enrichment analysis: A knowledge-based approach for interpreting genome-wide expression profiles. Proceedings of the National Academy of Sciences *102*, 15545-15550.

Sun, C., Wang, L., Huang, S., Heynen, G.J.J.E., Prahallad, A., Robert, C., Haanen, J., Blank, C., Wesseling, J., Willems, S.M.*, et al.* (2014). Reversible and adaptive resistance to BRAF(V600E) inhibition in melanoma. Nature *508*, 118-122.

Sun, R., Xiong, Y., Liu, H., Gao, C., Su, L., Weng, J., Yuan, X., Zhang, D., and Feng, J. (2020). Tumor-associated neutrophils suppress antitumor immunity of NK cells through the PD-L1/PD-1 axis. Translational Oncology *13*, 100825.

Taganov, K.D., Boldin, M.P., Chang, K.-J., and Baltimore, D. (2006). NF-κB-dependent induction of microRNA miR-146, an inhibitor targeted to signaling proteins of innate immune responses. Proceedings of the National Academy of Sciences *103*, 12481-12486.

Takada, Y., Mukhopadhyay, A., Kundu, G.C., Mahabeleshwar, G.H., Singh, S., and Aggarwal, B.B. (2003). Hydrogen peroxide activates NF-kappa B through tyrosine phosphorylation of I kappa B alpha and serine phosphorylation of p65: evidence for the involvement of I kappa B alpha kinase and Syk protein-tyrosine kinase. Journal of Biological Chemistry *278*, 24233-24241.

Tcyganov, E.N., Sanseviero, E., Marvel, D., Beer, T., Tang, H.Y., Hembach, P., Speicher, D.W., Zhang, Q., Donthireddy, L.R., Mostafa, A.*, et al.* (2022). Peroxynitrite in the tumor microenvironment changes the profile of antigens allowing escape from cancer immunotherapy. Cancer Cell *40*, 1173-1189 e1176.

Théry, C., Zitvogel, L., and Amigorena, S. (2002). Exosomes: composition, biogenesis and function. Nature Reviews Immunology *2*, 569-579.

Thomas, D.A., and Massagué, J. (2005). TGF-β directly targets cytotoxic T cell functions during tumor evasion of immune surveillance. Cancer Cell *8*, 369-380.

Tian, T., Wang, Y., Wang, H., Zhu, Z., and Xiao, Z. (2010). Visualizing of the cellular uptake and intracellular trafficking of exosomes by live-cell microscopy. Journal of Cellular Biochemistry *111*, 488-496.

Tili, E., Michaille, J.-J., Cimino, A., Costinean, S., Dumitru, C.D., Adair, B., Fabbri, M., Alder, H., Liu, C.G., Calin, G.A., and Croce, C.M. (2007). Modulation of miR-155 and miR-125b Levels following Lipopolysaccharide/TNF-α Stimulation and Their

Possible Roles in Regulating the Response to Endotoxin Shock1. The Journal of Immunology *179*, 5082-5089.

Tkach, M., and Théry, C. (2016). Communication by Extracellular Vesicles: Where We Are and Where We Need to Go. Cell *164*, 1226-1232.

Tobin, R.P., Jordan, K.R., Kapoor, P., Spongberg, E., Davis, D., Vorwald, V.M., Couts, K.L., Gao, D., Smith, D.E., Borgers, J.S.W.*, et al.* (2019). IL-6 and IL-8 Are Linked With Myeloid-Derived Suppressor Cell Accumulation and Correlate With Poor Clinical Outcomes in Melanoma Patients. Frontiers in Oncology *9*.

Trikha, P., and Carson, W.E. (2014). Signaling pathways involved in MDSC regulation. Biochimica et Biophysica Acta (BBA) - Reviews on Cancer *1846*, 55-65.

Tumino, N., Besi, F., Martini, S., Di Pace, A.L., Munari, E., Quatrini, L., Pelosi, A., Fiore, P.F., Fiscon, G., Paci, P.*, et al.* (2022). Polymorphonuclear Myeloid-Derived Suppressor Cells Are Abundant in Peripheral Blood of Cancer Patients and Suppress Natural Killer Cell Anti-Tumor Activity. Frontiers in Immunology *12*.

Umansky, V., Blattner, C., Gebhardt, C., and Utikal, J. (2016). The Role of Myeloid-Derived Suppressor Cells (MDSC) in Cancer Progression. Vaccines *4*, 36.

Valadi, H., Ekström, K., Bossios, A., Sjöstrand, M., Lee, J.J., and Lötvall, J.O. (2007). Exosome-mediated transfer of mRNAs and microRNAs is a novel mechanism of genetic exchange between cells. Nature Cell Biology *9*, 654-659.

van Niel, G., Carter, D.R.F., Clayton, A., Lambert, D.W., Raposo, G., and Vader, P. (2022). Challenges and directions in studying cell–cell communication by extracellular vesicles. Nature Reviews Molecular Cell Biology *23*, 369-382.

van Niel, G., D'Angelo, G., and Raposo, G. (2018). Shedding light on the cell biology of extracellular vesicles. Nature Reviews Molecular Cell Biology *19*, 213-228.

Vasquez-Dunddel, D., Pan, F., Zeng, Q., Gorbounov, M., Albesiano, E., Fu, J., Blosser, R.L., Tam, A.J., Bruno, T., Zhang, H.*, et al.* (2013). STAT3 regulates arginase-I in myeloid-derived suppressor cells from cancer patients. The Journal of Clinical Investigation *123*, 1580-1589.

Veglia, F., Sanseviero, E., and Gabrilovich, D.I. (2021). Myeloid-derived suppressor cells in the era of increasing myeloid cell diversity. Nature Reviews Immunology *21*, 485-498.

Veglia, F., Tyurin, V.A., Blasi, M., De Leo, A., Kossenkov, A.V., Donthireddy, L., To, T.K.J., Schug, Z., Basu, S., Wang, F.*, et al.* (2019). Fatty acid transport protein 2 reprograms neutrophils in cancer. Nature *569*, 73-78.

Vence, L., Palucka, A.K., Fay, J.W., Ito, T., Liu, Y.-J., Banchereau, J., and Ueno, H. (2007). Circulating tumor antigen-specific regulatory T cells in patients with metastatic melanoma. Proceedings of the National Academy of Sciences *104*, 20884-20889.

Vignard, V., Labbé, M., Marec, N., André-Grégoire, G., Jouand, N., Fonteneau, J.-F., Labarrière, N., and Fradin, D. (2020). MicroRNAs in Tumor Exosomes Drive Immune Escape in Melanoma. Cancer Immunology Research *8*, 255-267.

Vuk-Pavlović, S., Bulur, P.A., Lin, Y., Qin, R., Szumlanski, C.L., Zhao, X., and Dietz, A.B. (2010). Immunosuppressive CD14+HLA-DRlow/− monocytes in prostate cancer. The Prostate *70*, 443-455.

Wang, Y., Luo, J., Zhang, H., and Lu, J. (2016). microRNAs in the Same Clusters Evolve to Coordinately Regulate Functionally Related Genes. Molecular Biology and Evolution *33*, 2232-2247.

Wang, Z., Jiang, J., Li, Z., Zhang, J., Wang, H., and Qin, Z. (2010). A myeloid cell population induced by Freund adjuvant suppresses T-cell-mediated antitumor immunity. J Immunother *33*, 167-177.

Weber, R. (2020). Regulation of CCR5 expression and immunosuppressive phenotype of MDSC in melanoma. Med. Dissertation. Medizinische Fakultät Mannheim, Universität Heidelberg.

Weber, R., Groth, C., Lasser, S., Arkhypov, I., Petrova, V., Altevogt, P., Utikal, J., and Umansky, V. (2021). IL-6 as a major regulator of MDSC activity and possible target for cancer immunotherapy. Cellular Immunology *359*, 104254.

Weber, R., Riester, Z., Hüser, L., Sticht, C., Siebenmorgen, A., Groth, C., Hu, X., Altevogt, P., Utikal, J.S., and Umansky, V. (2020). IL-6 regulates CCR5 expression and immunosuppressive capacity of MDSC in murine melanoma. Journal for ImmunoTherapy of Cancer *8*, e000949.

Weisman, S., Hirsch-Lerner, D., Barenholz, Y., and Talmon, Y. (2004). Nanostructure of Cationic Lipid-Oligonucleotide Complexes. Biophysical Journal *87*, 609-614.

Welte, T., Kim, I.S., Tian, L., Gao, X., Wang, H., Li, J., Holdman, X.B., Herschkowitz, J.I., Pond, A., Xie, G.*, et al.* (2016). Oncogenic mTOR signalling recruits myeloid-derived suppressor cells to promote tumour initiation. Nature Cell Biology *18*, 632-644.

Wölfle, S.J., Strebovsky, J., Bartz, H., Sähr, A., Arnold, C., Kaiser, C., Dalpke, A.H., and Heeg, K. (2011). PD-L1 expression on tolerogenic APCs is controlled by STAT-3. European Journal of Immunology *41*, 413-424.

Xiao, D., Barry, S., Kmetz, D., Egger, M., Pan, J., Rai, S.N., Qu, J., McMasters, K.M., and Hao, H. (2016). Melanoma cell–derived exosomes promote epithelial–mesenchymal transition in primary melanocytes through paracrine/autocrine signaling in the tumor microenvironment. Cancer Letters *376*, 318-327.

Xie, Q.W., Kashiwabara, Y., and Nathan, C. (1994). Role of transcription factor NF-kappa B/Rel in induction of nitric oxide synthase. Journal of Biological Chemistry *269*, 4705-4708.

Yang, N. (2015). An overview of viral and nonviral delivery systems for microRNA. International Journal of Pharmaceutical Investigation *5*, 179-181.

Ye, Q., Li, Z., Li, Y., Li, Y., Zhang, Y., Gui, R., Cui, Y., Zhang, Q., Qian, L., Xiong, Y., and Yu, Y. (2023). Exosome-Derived microRNA: Implications in Melanoma Progression, Diagnosis and Treatment. Cancers *15*, 80.

Ying, S.-Y., Chang, D.C., and Lin, S.-L. (2008). The MicroRNA (miRNA): Overview of the RNA Genes that Modulate Gene Function. Molecular Biotechnology *38*, 257-268.

Yoda, M., Kawamata, T., Paroo, Z., Ye, X., Iwasaki, S., Liu, Q., and Tomari, Y. (2010). ATP-dependent human RISC assembly pathways. Nature Structural & Molecular Biology *17*, 17-23.

Zaborowski, M.P., Balaj, L., Breakefield, X.O., and Lai, C.P. (2015). Extracellular Vesicles: Composition, Biological Relevance, and Methods of Study. BioScience *65*, 783-797.

Zhang, B., Wang, Z., Wu, L., Zhang, M., Li, W., Ding, J., Zhu, J., Wei, H., and Zhao, K. (2013). Circulating and tumor-infiltrating myeloid-derived suppressor cells in patients with colorectal carcinoma. PLoS One *8*, e57114.

Zhao, J.-L., Huang, F., He, F., Gao, C.-C., Liang, S.-Q., Ma, P.-F., Dong, G.-Y., Han, H., and Qin, H.-Y. (2016). Forced Activation of Notch in Macrophages Represses Tumor Growth by Upregulating miR-125a and Disabling Tumor-Associated Macrophages. Cancer Research *76*, 1403-1415.

Zhou, X., Yan, T., Huang, C., Xu, Z., Wang, L., Jiang, E., Wang, H., Chen, Y., Liu, K., Shao, Z., and Shang, Z. (2018a). Melanoma cell-secreted exosomal miR-155-5p induce proangiogenic switch of cancer-associated fibroblasts via SOCS1/JAK2/STAT3 signaling pathway. Journal of Experimental & Clinical Cancer Research *37*, 242.

Zhou, Y.-x., Zhao, W., Mao, L.-w., Wang, Y.-l., Xia, L.-q., Cao, M., Shen, J., and Chen, J. (2018b). Long non-coding RNA NIFK-AS1 inhibits M2 polarization of macrophages in endometrial cancer through targeting miR-146a. The International Journal of Biochemistry & Cell Biology *104*, 25-33.

Zhuang, G., Wu, X., Jiang, Z., Kasman, I., Yao, J., Guan, Y., Oeh, J., Modrusan, Z., Bais, C., Sampath, D., and Ferrara, N. (2012). Tumour-secreted miR-9 promotes endothelial cell migration and angiogenesis by activating the JAK-STAT pathway. The EMBO Journal *31*, 3513-3523.

Zitvogel, L., Regnault, A., Lozier, A., Wolfers, J., Flament, C., Tenza, D., Ricciardi-Castagnoli, P., Raposo, G., and Amigorena, S. (1998). Eradication of established murine tumors using a novel cell-free vaccine: dendritic cell derived exosomes. Nature Medicine *4*, 594-600.

Zuhorn, I.S., and Hoekstra, D. (2002). On the Mechanism of Cationic Amphiphile-mediated Transfection. To Fuse or not to Fuse: Is that the Question? The Journal of Membrane Biology *189*, 167-179.

ACKNOWLEDGEMENT

I would like to express my sincere gratitude to Prof. Dr. Viktor Umansky for supervising my doctoral studies, providing valuable advice and suggestions throughout the process, as well as for proofreading my thesis and being the first reviewer. Thank you for all your support, encouragement, and guidance.

I would also like to express my appreciation and thanks to the other members of the examination committee, namely Prof. Dr. Ana Martin-Villalba, Prof. Dr. Rienk Offringa, and Prof. Dr. Stefan Wiemann. Special thanks to Prof. Dr. Rienk Offringa for being the second reviewer and for sharing his scientific expertise as a member of my thesis advisory committee. Many thanks to Prof. Dr. Karen Bieback and Prof. Dr. Peter Altevogt, who were also members of my thesis advisory committee. Having the opportunity to meet with you and get your feedback on my research project was an absolute pleasure.

With special thanks to Prof. Dr. Sergij Goerdt and Martina Nolte-Bohres, I would like to thank the Research Training Group 2099 "Hallmarks of Skin Cancer" for financial support, inspiring lectures, courses, and conferences. I'm also very grateful for the chance to participate in a research stay at the Fondazione IRCCS Istituto Nazionale dei Tumori in Milan. I would like to extend my sincere thanks to Prof. Dr. Licia Rivoltini and her whole research group for this. I would like to thank Nicola Cerioli, Alessandro Mereu, and Agata Cova for their help and for the enjoyable time we shared.

I am deeply grateful to all present and previous members of the Umansky lab for their invaluable support throughout our time in the lab and beyond: Prof. Dr. Peter Altevogt, Ihor Arkhypov, Rebekka Bitsch, Feyza Gul Özbay Kurt, Alissa Lepper, Vera Petrova, Christopher Groth, and Ece Tavukcuoglu. I'm sincerely grateful to Prof. Dr. Peter Altevogt for his unwavering support and enthusiasm for science. I would also like to thank Lennart Fritz, Nina Gutzeit, and Nina Lemmen for their contribution to the project and for trusting me with the responsibility of supervising.

I would like to extend my appreciation to Prof. Dr. Jochen Utikal and the entire Utikal lab for their valuable scientific input during our collaborative lab meetings. Additionally, I am grateful to Sayran Arif-Said, Yvonne Nowak, Ludmila Umansky, and Camela Jost for their technical assistance.

I would like to acknowledge the Microarray Core Facility at the DKFZ Heidelberg for performing the microarrays, as well as Dr. Carolina De La Torre for helping with the analysis.

I am also grateful to Prof. Dr. Martina Seiffert, Dr. Lena Alexopolou, Dr. Carsten Kirschning, and Dr. Dagmar Hildebrand for generously providing valuable materials.

It is with deep appreciation that I conclude by thanking my parents, my brother, and my friends. Without their tremendous understanding and encouragement in the past few years, it would be impossible for me to complete my study.